UCTEA Turkish Chamber of Civil Engineers

Teknik Dergi

Technical Journal

Volume 29 Issue 4 July 2018

Teknik Dergi is indexed by

- Science Citation Index Expanded
- Scopus
- Journal Citation Reports / Science Edition
- Engineering Index
- Concrete Abstracts (American Concrete Institute)
- National Technical Information Service (US NTIS)
- CITIS
- Ulrich's International Periodical's Directory
- TÜBİTAK / ULAKBİM

TEKNİK DERGİ PUBLICATION PRINCIPLES

Teknik Dergi is a scientific and technical journal indexed by the Science Citation Index Expanded. Annually six issues are published, three in Turkish in the months of January, May and September, three in English in March, July and November. Its main principles of publication are summarized below:

1. Articles reporting original scientific research and those reflecting interesting engineering applications are accepted for publication. To be classified as original, the work should either produce new scientific knowledge or add a genuinely new dimension to the existing knowledge or develop a totally new method or substantially improve an existing method.
2. Articles reporting preliminary results of scientific studies and those which do not qualify as full articles but provide useful information for the reader can be considered for publication as technical notes.
3. Discussions received from the readers of the published articles within three months from publication are reviewed by the Editorial Board and then published together with the closing remarks of the author.
4. Manuscripts submitted for publication are evaluated by two or three reviewers unknown to the authors. In the light of their reports, final decision to accept or decline is taken by the Editorial Board. General policy of the Board is to get the insufficient manuscripts improved in line with the reviewers' proposals. Articles that fail to reach the desired level are declined. Reasons behind decisions are not declared.
5. A signed statement is taken from the authors, declaring that the article has not been published as a "journal article or book chapter". In case the Editorial Board is in the opinion that the article has already been published elsewhere with minor changes or suspects plagiarism or a similar violation of ethics, then not only that article, but none of the articles of the same authors are published.
6. Papers reporting works presented as conference papers and developed further may be considered for publication. The conference it was presented to is given as a footnote in the first page.
7. Additionally, a document signed by all authors, transferring the copyright to UCTEA Chamber of Civil Engineers is submitted together with the manuscript.

Printed by: Yorum Basın Yayın Sanayi Ltd. Şti.
Başkent Org. Sanayi Bölgesi No: 12 Malıköy - Sincan / Ankara - Tel: 0.312.395 21 12

Date of Print: 01 July 2018 / Number of copies: 2.000

Distributed to İMO members free of charge. / Local periodical.

UCTEA Turkish Chamber of Civil Engineers

Teknik Dergi

Technical Journal

Volume 29 Issue 4 July 2018

UCTEA Turkish Chamber of Civil Engineers

Teknik Dergi *Technical Journal*

Publisher:
Cemal GÖKÇE
On behalf of UCTEA Turkish Chamber of Civil Engineers

Administrative Officer:
Bahaettin SARI

Correspondence:
Teknik Dergi
Chamber of Civil Engineers
Necatibey Cad. No:57
Kızılay 06440 Ankara, Turkey
Tel : +90 (312) 294 30 00
Faks: +90 (312) 294 30 88
Web: www.imo.org.tr
E-mail:teknikdergi@imo.org.tr

Publication Frequency:
Bimonthly

ISSN : 1300-3453

Reviewers:

This list is renewed each year and includes reviewers who served in the last two years of publication.

Emine AĞAR
Sami Oğuzhan AKBAŞ
Özge AKBOĞA KALE
M. Vefa AKPINAR
Zuhal AKYÜREK
Hilmi Doğan ALTINBİLEK
Davit ARDITI
Deniz ARTAN İLTER
Cem AYDEMİR
Yusuf AYVAZ
Selim BARADAN
Bekir Oğuz BARTIN
Bilge BAŞ
Zerrin BAYRAKDAR
İdris BEDİRHANOĞLU
Serkan BEKİROĞLU
Niyazi Özgür BEZGİN
İlknur BOZBEY
Zafer BOZKUŞ
Zekai CELEP
Halim CEYLAN
Barlas Özden ÇAĞLAYAN
Özgür ÇAKIR
Necati ÇATBAŞ
Erkan ÇELEBİ
Kutay ÇELEBİOĞLU
Oğuz Cem ÇELİK
Hilmi Berk ÇELİKOĞLU
Ender DEMİREL
Fatih DİKBAŞ
Seyyit Ümit DİKMEN
Ahmet Anıl DİNDAR
Emrah DOĞAN
Nilay ELGİNÖZ KANAT
Murat Altuğ ERBERİK
E. Mete ERDEMGİL
Ercan ERDİŞ
Esin ERGEN PEHLEVAN
Ayşen ERGİN
Gökmen ERGÜN
Güngör EVREN
Ergun GEDİZLİOĞLU
Haluk GERÇEK
Mustafa GÖĞÜŞ
Ilgın GÖKAŞAR
M. Halis GÜNEL
Mehmet Şükrü GÜNEY
Aslı Pelin GÜRGÜN
Soner HALDENBİLEN
Zeki HASGÜR
Zeynep IŞIK
Recep İYİSAN
Murat KARACASU
Engin KARAESMEN
Erhan KARAESMEN
Halil KARAHAN
Mustafa KARAŞAHİN
C. Melek KAZEZYILMAZ ALHAN
Engin KEYDER
Veysel Şadan Özgür KIRCA
Niyazi Uğur KOÇKAL
Özgür KURÇ
Hilmi LUŞ
Yetiş Şazi MURAT
Sepanta NAIMI
Dilek OKUYUCU
Mehmet Hakkı OMURTAG
Engin ORAKDÖĞEN
Akın ÖNALP
Aybike ÖNGEL
Bihrat ÖNÖZ
Halit ÖZEN
Hakkı Oral ÖZHAN
Hulusi ÖZKUL
Beliz ÖZORHON ORAKÇAL
Turan ÖZTURAN
Gül POLAT TATAR
Altuğ SAYGILI
Hasan SAYGIN
Serdar SELAMET
Osman SİVRİKAYA
Serdar SOYÖZ
İbrahim SÖNMEZ
Ayşe Filiz SUNAR
Özkan ŞENGÜL
Aykut ŞENOL
Ali Ünal ŞORMAN
Ergin TARI
Erhan TEKİN
H. Onur TEZCAN
Onur Behzat TOKDEMİR
Nabi Kartal TOKER
Mustafa TOKYAY
Tamer TOPAL
Cem TOPKAYA
Ahmet TORTUM
Ahmet TÜRER
Handan TÜRKOĞLU
Mehmet UTKU
Alper ÜNLÜ
Tanvir WASTI
Mert Yücel YARDIMCI
Ufuk YAZGAN
Emine Beyhan YEĞEN
Osman YILDIZ
Koray Kamil YILMAZ
M. Tuğrul YILMAZ
M. Semih YÜCEMEN
Yeliz YÜKSELEN AKSOY
Nabi YÜZER

Teknik Dergi is a peer reviewed periodical publishing papers of original research and interesting practice. It addresses both the research community and the practicing engineers.

UCTEA Turkish Chamber of Civil Engineers

Teknik Dergi

Technical Journal

Volume: 29 Issue: 4 July 2018

CONTENTS

Teknik Dergi, 2018 8469-8496, Paper 508

Bending of Super-Elliptical Mindlin Plates by Finite Element Method

Murat ALTEKİN[1]

ABSTRACT

Bending of shear deformable super-elliptical plates under transverse load was investigated using the Mindlin plate theory by means of the finite element method. Four-noded isoparametric quadrilateral plate bending element with three degrees of freedom per node was used. Parametric results for the maximum deflections were presented via sensitivity analysis for several geometric characteristics such as thickness, aspect ratio, and super-elliptical power. Good agreement with the solutions of elliptical and rectangular plates was obtained using fine mesh. The results revealed that the deflections of clamped and point supported super-elliptical plates lie in the range bounded by elliptical and rectangular plates. However, the bending response of simply supported plates was observed to be entirely different. It was shown that high rate of convergence is required to obtain such a relation and using insufficient number of degrees of freedom results in finding a totally different trend for the clamped case.

Keywords: Plate, bending, deflection, finite element method.

1. INTRODUCTION

Plates are basic structural members which are used extensively in many disciplines like mechanical, civil, aerospace, and marine engineering, and in offshore structures. Because of their practical importance, the analysis of plates has always received significant interest, and thousands of studies have been published [1-12]. These studies may be categorized into various ways with regard to (i) the shape of the plate, (ii) the plate theory, (iii) the solution method, (iv) the material properties, (v) the boundary conditions, (vi) the scope of research (bending, buckling, or vibration), (vii) the type of analysis (theoretical, experimental or computational), and (viii) the classifications based on the thickness (membrane, thin, moderately thick or thick [13].

Since dealing with 2-D equations is relatively simple than 3-D equations, and 3-D equations inevitably involve numerical errors of experimental nature as well as 2-D equations do [14], the extensive literature mostly involves solutions using 2-D equations. The publications on

Note:
- This paper has been received on August 03, 2017 and accepted for publication by the Editorial Board on May 16, 2018.
- Discussions on this paper will be accepted by September 30, 2018.
- DOI: 10.18400/tekderg.332384

1 Yildiz Technical University, Department of Civil Engineering, İstanbul, Turkey - altekin@yildiz.edu.tr

plates are basically focused on the analysis of thin and moderately thick plates based on Kirchhoff and Mindlin plate theories, respectively [15-76]. These plate theories have been two of the most applied models on the analysis of plates [37]. This is partly because these theories have been widely accepted among researchers [38], and partly because these models produce results with acceptable accuracy with less computational effort in comparison with three-dimensional elasticity solutions or higher order plate theories. Since closed form solutions are only available for a limited number of cases depending on (i) the geometry of the plate, (ii) the loading, (iii) the boundary conditions, and (iv) the plate model, numerical methods have almost always been employed in the solution of plate problems.

Bending is one of the most common and important mechanical behaviors of plates, which is often crucial for safety and performance of the structures [39]. Due to their geometrical simplicity rectangular plates have been widely studied in the literature. However, from the engineering point of view, sharp corners may be critical due to stress concentrations. Besides, plates with curved boundaries have been used in many industrial applications (e.g, platforms, wings of aircrafts, components of machines).

Despite their common practical importance, there is still lack of data on plates with curved perimeters. Furthermore, notwithstanding their prevalent usage in engineering applications (e.g., slabs supported by columns, solar panels, printed circuit boards, and telescope mirrors) the investigations on point supported plates are less common than those involving simply supported or clamped boundaries owing to mathematical difficulties.

Super-elliptical plates include a large variety of plate shapes ranging from an ellipse to a rectangle with rounded corners. Unlike plates with sharp corners, rectangular plates with rounded corners enable to diffuse and dilute stress concentrations [40]. Despite the recently published papers, the studies on the analysis of super-elliptical plates have mostly been made for the dynamic behavior, and generally thin plates have been investigated [41-59]. To the best of the author's knowledge, there are only nine published papers on the bending of super-elliptical plates all of which focused on thin plates only [60-68]. Thus, the current work was motivated by the lack of contributions on the bending analysis of shear deformable super-elliptical plates. As far as the author knows, in the literature devoted to the bending analysis of super-elliptical plates under transverse load, this is the first study solved by the finite element method, and also the first paper in which the Mindlin plate model was used to examine simply supported, clamped, and point supported super-elliptical plates. In the current study sensitivity analysis was made to determine the influence of the thickness, the super-elliptical power, the aspect ratio, and the boundary conditions on the maximum deflection of moderately thick super-elliptical plates. Convergence studies were performed for h-refinement (i.e., more of the same kind of elements [69]), and the results were checked with the solutions of the limiting cases which are elliptical (e) and rectangular (r) plates.

2. FORMULATION

The boundary of the homogeneous and isotropic plate with uniform thickness is defined by

$$\left(\frac{x}{a}\right)^{2k}+\left(\frac{y}{b}\right)^{2k}=1, \qquad k=1,2,...,\infty \tag{1}$$

As k is raised, the shape becomes a rectangle with rounded corners, and therefore, the area of the middle surface of the plate increases with increasing k (Fig. 1). Four-noded isoparametric quadrilateral plate bending element with straight boundaries developed by Hughes et al. (1977) [70] was used in discretiziting the plate domain. The geometry of the element is identified by [71].

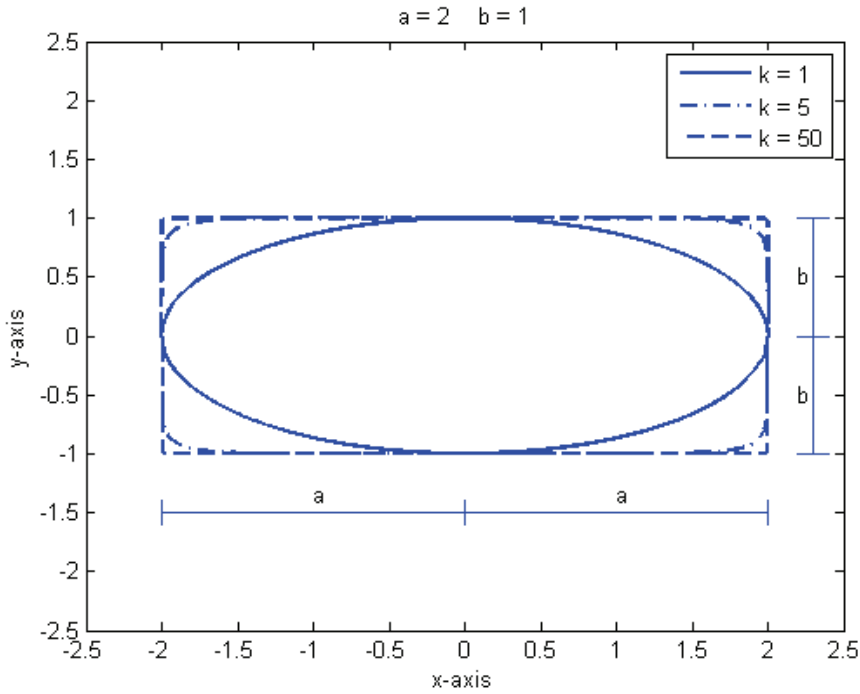

Figure 1. Geometry of a super-elliptical plate (c=2)

$$x = \sum_{i=1}^{4} N_i x_i, \qquad y = \sum_{i=1}^{4} N_i y_i, \qquad N_i = \frac{1}{4}(1+rr_i)(1+ss_i) \tag{2}$$

Each element has three field variables (i.e., degrees of freedom) per node. These field variables involve the deflection, and the rotations denoted by w, θ_x and θ_y, respectively.

$$w = \sum_{i=1}^{4} N_i w_i, \qquad \theta_x = \sum_{i=1}^{4} N_i \theta_{xi}, \qquad \theta_y = \sum_{i=1}^{4} N_i \theta_{yi} \tag{3}$$

The element shape functions are bilinear for transverse displacement and rotations. C^0 continuity for the displacement model was ensured based on the Mindlin's plate theory. The

shear locking was prevented by separating the shear and bending energy terms and using selective integration procedure. The curvature and shear deformation vector $\{\varepsilon\}$ and the nodal displacement vector $\{d_i\}$ are related by [71]

$$\{d_i\}^T = \{w_i \quad \theta_{xi} \quad \theta_{yi}\}, \qquad \{\varepsilon\} = \sum_{i=1}^{4} [B_i]\{d_i\} \tag{4}$$

$$[B_i] = \begin{bmatrix} 0 & 0 & \dfrac{\partial N_i}{\partial x} \\ 0 & -\dfrac{\partial N_i}{\partial y} & 0 \\ 0 & -\dfrac{\partial N_i}{\partial x} & \dfrac{\partial N_i}{\partial y} \\ \dfrac{\partial N_i}{\partial x} & 0 & N_i \\ \dfrac{\partial N_i}{\partial y} & -N_i & 0 \end{bmatrix}, \qquad \{\varepsilon\} = \begin{Bmatrix} k_x = \sum_{i=1}^{4} \theta_{yi} \dfrac{\partial N_i}{\partial x} \\ k_y = -\sum_{i=1}^{4} \theta_{xi} \dfrac{\partial N_i}{\partial y} \\ k_{xy} = \sum_{i=1}^{4} \theta_{yi} \dfrac{\partial N_i}{\partial y} - \sum_{i=1}^{4} \theta_{xi} \dfrac{\partial N_i}{\partial x} \\ \phi_x = \sum_{i=1}^{4} w_i \dfrac{\partial N_i}{\partial x} + \sum_{i=1}^{4} \theta_{yi} N_i \\ \phi_y = \sum_{i=1}^{4} w_i \dfrac{\partial N_i}{\partial y} - \sum_{i=1}^{4} \theta_{xi} N_i \end{Bmatrix} \tag{5}$$

The element stiffness matrix is given by

$$[k_e] = \iint_A [B]^T [C][B]\,dx\,dy, \qquad [k_e] = [k_B] + [k_S] \tag{6}$$

where [71]

$$[B] = [[B_1] \quad [B_2] \quad [B_3] \quad [B_4]]_{5\times 12}, \qquad [C] = \begin{bmatrix} [C_B]_{3\times 3} & [0]_{3\times 2} \\ [0]_{2\times 3} & [C_S]_{2\times 2} \end{bmatrix}_{5\times 5} \tag{7}$$

$$D = \frac{Eh^3}{12(1-\nu^2)}, \qquad [C_B] = D \begin{bmatrix} 1 & \nu & 0 \\ \nu & 1 & 0 \\ 0 & 0 & \dfrac{(1-\nu)}{2} \end{bmatrix}, \qquad G = \frac{E}{2(1+\nu)} \tag{8}$$

$$[C_S] = D_S \begin{bmatrix} 1 & 0 \\ 0 & 1 \end{bmatrix}, \qquad D_s = Gh\kappa \tag{9}$$

The element stiffness matrix $[k_e]$ shown in Eq. (6) is composed of the bending stiffness $[k_B]$ and the shear stiffness $[k_S]$ parts for which numerical integrations are performed using Gauss quadrature with 2x2 [8] and 1x1 schemes, respectively [71].

The strain-displacement matrix [B] shown in Eq. (7) is formed by the matrix $[B_i]$ where i=1,2,3,4 such that the first three rows of $[B_i]$ relate the curvatures to displacements, and the last two rows of $[B_i]$ relate the shear deformations to displacements [73]. $[C_B]$ and $[C_S]$ are the bending and shear parts of the constitutive matrix [C] which represents rigidity.

3. ANALYSIS

Due to the two fold symmetry with respect to x and y axes the quarter of the plate was considered in the solution. The mesh pattern used in the paper is composed of nonuniform quadrilateral elements. The process of automatic mesh generation was executed by an algorithm which was coded in Python by the author (Fig. 2), and the figures were plotted using Matlab. Six cases including clamped (C), simply supported (S), and point-supported (PS) plates were investigated in the paper (Tables 1-2). For cases 1-2, the plate was considered to be resting on symmetrically distributed four point supports located on the plate contour and on the diagonals defined by $y = \pm(b/a)x$ such that for a large value of the super-elliptical power (such as k=200) the plate approximates to a corner supported rectangular plate. The transverse displacement was prevented at the point supports each of which was modelled by a line support of length $\Delta = 0.5/(3p)$ on the above mentioned diagonal lines.

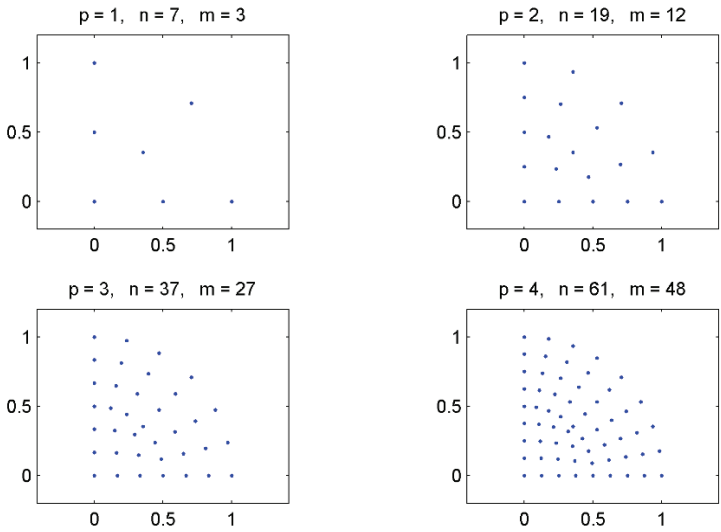

Figure 2. Location of the nodes in a quarter of the plate (k=1, c=1)

Two types of loading were considered: (i) uniformly distributed transverse pressure q, and (ii) a transverse central point load Q. The geometrical boundary conditions were satisfied exactly. The global nodal displacements were obtained by

$$[K]\{U\} = \{F\} \tag{10}$$

The simulation was carried out using the parameters defined by

$$c = \frac{a}{b}, \qquad \eta = \frac{h}{b}, \qquad \kappa = \frac{5}{6}, \qquad \nu = 0.3, \qquad W = w\frac{D}{qa^4}, \qquad \lambda = w\frac{D}{Qa^2} \tag{11}$$

$$\mu = \frac{W_{(PS)}}{W_{(C)}}\frac{1}{c}, \qquad \beta = \frac{\lambda_{(PS)}}{\lambda_{(C)}}\frac{1}{c}, \qquad \Omega = Wa^4 \tag{12}$$

Table 1. Details of the numerical investigations

Support configuration	(PS)	(PS)	(C)	(C)	(S)	(S)
Type of loading	q	Q	q	Q	q	Q
Case number	1	2	3	4	5	6

Table 2. Number of meshes and nodes in a quarter of the plate

Support configuration	(PS)	(C)	(S)
Case number	1-2	3-4	5-6
m	4332	2028	2028
n	4447	2107	2107
p	38	26	26

4. NUMERICAL RESULTS

Convergence studies by h-refinement showed that the use of fine mesh is required for admissable accuracy. The accuracy of the results was validated by comparing the nondimensional maximum deflection with those of elliptical, rectangular, and super-elliptical plates (Tables 3-6). Some of the results cited in Tables 3-6 were scaled by the author, and some of them were computed by the author using the formulations given in the cited references. Good agreement was obtained in the comparison tests which were made for thin and moderately thick plates.

Basic information such as the method of solution and the range of the super-elliptical power used in the previous studies on the bending of super-elliptical plates was shown in Table 7.

Table 3. Comparison of nondimensional maximum deflection of thin elliptical and rectangular plates (η=0.002)

		Case 3	Case 3	Case 5	Case 5	Case 4	Case 6	
		(C)	(C)	(S)	(S)	(C)	(S)	
p	2k	W (c=1)	W (c=2)	W (c=1)	W (c=2)	λ (c=1)	λ (c=1)	Reference
	(e)	0.015625		0.063702		0.019894	0.050501	[27]
	(e)	0.015625		0.064103	0.009043			[72]
26	2	0.0156202	0.00211820	0.0636745	0.0088940	0.0198863	0.0504901	
25	2	0.0156198	0.00211820	0.0636723	0.0088937	0.0198855	0.0504891	
24	2	0.0156193	0.00211820	0.0636697	0.0088934	0.0198846	0.0504879	
	(r)	0.02016					0.0464	[72]
	(r)	0.02032						[2]
	(r)			0.064992	0.01013		0.0464	[27]
26	400	0.0202462	0.0025333	0.0650483	0.0101323	0.0224422	0.0464279	
25	400	0.0202463	0.00253330	0.0650475	0.0101322	0.0224415	0.0464270	
24	400	0.0202463	0.00253330	0.0650469	0.0101322	0.0224408	0.0464265	

Table 4. Comparison of nondimensional maximum deflection W of shear deformable elliptical and rectangular plates

p	c	2k	η=0.010	η=0.020	η=0.050	η=0.100	Reference	Case
	1	(e)			0.01578		[21]	3
	1	(e)	0.01561	0.01564	0.01578	0.01633	[29]	3
26	1	2	0.0156271	0.0156485	0.0157985	0.0163341		3
25	1	2	0.0156266	0.0156481	0.0157981	0.0163337		3
24	1	2	0.0156262	0.0156476	0.0157976	0.0163332		3
	1	(r)	0.020256	0.0202864		0.0212368	[26]	3
26	1	400	0.020256	0.0202865	0.0204978	0.0212373		3
25	1	400	0.0202561	0.0202865	0.0204978	0.0212374		3
24	1	400	0.0202561	0.0202866	0.0204979	0.0212375		3
	2	(r)	0.0025339	0.0025366		0.0026236	[26]	3
26	2	400	0.0025342	0.0025369	0.0025560	0.0026239		3
25	2	400	0.0025342	0.0025369	0.0025560	0.0026239		3
24	2	400	0.0025342	0.0025370	0.0025560	0.0026239		3
	1	(e)				0.06442	[22]	5
26	1	2	0.0636814	0.0637028	0.0638528	0.0643885		5
25	1	2	0.0636791	0.0637005	0.0638505	0.0643862		5
24	1	2	0.0636766	0.0636980	0.0638480	0.0643836		5
	1	(r)		0.06496		0.06576	[24]	5
	1	(r)		0.065031		0.06584	[20]	5

Table 4. Comparison of nondimensional maximum deflection W of shear deformable elliptical and rectangular plates (continue)

p	c	2k	η=0.010	η=0.020	η=0.050	η=0.100	Reference	Case
26	1	400	0.0652761	0.0655787	0.0665933	0.0686209		5
25	1	400	0.0652752	0.0655777	0.0665922	0.0686198		5
24	1	400	0.0652743	0.0655766	0.0665909	0.0686184		5
	2	(r)		0.01013		0.01020	[24]	5
26	2	400	0.0101487	0.0101708	0.0102472	0.0104068		5
25	2	400	0.0101486	0.0101707	0.0102471	0.0104067		5
24	2	400	0.0101485	0.0101706	0.0102470	0.0104065		5
	1	(r)		0.40928			[25]	1
38	1	400	0.403840	0.405156	0.410184	0.422200		1
36	1	400	0.403740	0.405052	0.410063	0.422025		1
34	1	400	0.403629	0.404935	0.409928	0.421832		1
32	1	400	0.403503	0.404804	0.409776	0.421618		1

Table 5. Comparison of nondimensional maximum deflection of (PS) thin super-elliptical plates (η=0.002)

p	c	2k	W (Case 1)	λ (Case 2)	Reference
	1	2	0.0828		[60]
	1	2	0.0831	0.0564	[65]
	1	2	0.084		[19]
38	1	2	0.0828439	0.0567861	
36	1	2	0.0828088	0.0567855	
34	1	2	0.0827695	0.0567847	
	1	40	0.3739		[60]
38	1	40	0.372567	0.147073	
36	1	40	0.372474	0.147074	
34	1	40	0.372370	0.147076	
	1	100	0.3939	0.1522	[65]
38	1	100	0.392393	0.152677	
36	1	100	0.392299	0.152680	
34	1	100	0.392193	0.152683	
	1	(r)	0.3984		[72]
	1	(r)	0.4052		[18]
	1	(r)	0.40799	0.15654	[17]
	1	(r)	0.4081		[31, 28]

Table 5. Comparison of nondimensional maximum deflection of (PS) thin super-elliptical plates (η=0.002) (continue)

p	c	2k	W (Case 1)	λ (Case 2)	Reference
	1	(r)	0.4171		[15]
	1	(r)	0.4208		[16]
	1	(r)		0.15657	[36]
38	1	400	0.402925	0.155642	
36	1	400	0.402828	0.155645	
34	1	400	0.402720	0.155649	
	2	2	0.0497		[60]
38	2	2	0.0496860	0.0650117	
36	2	2	0.0496704	0.0650103	
34	2	2	0.0496531	0.0650088	
	2	40	0.2140		[60]
38	2	40	0.213463	0.170878	
36	2	40	0.213428	0.170876	
34	2	40	0.213388	0.170873	

Table 6. Comparison of the central deflection Ω of thin (C) super-elliptical plates under q (η=0.002)

c	d	k=1	k=2	k=4	k=6	k=8	k=10	Reference
1	2	0.01563	0.01375	0.00696	0.00335	0.00172	0.00096	[68]
1	2	0.01563	0.01375	0.00696	0.00335	0.00172	0.00096	[61]
1	4	0.01563	0.01817	0.01683	0.01404	0.01129	0.00900	[61]
1	6	0.01563	0.01945	0.02009	0.01991	0.01964	0.01934	[61]
1	8	0.01563	0.01971	0.02027	0.02024	0.02019	0.02017	[61]
1							0.02017	[63]
1			0.01971	0.02027			0.02017	[64]
1		0.0156202	0.0197669	0.0202216	0.0202425	0.0202450	0.0202456	p=26
1		0.0156198	0.0197666	0.0202215	0.0202425	0.0202450	0.0202456	p=25
1		0.0156193	0.0197662	0.0202214	0.0202425	0.0202450	0.0202456	p=24
2	2	0.03390	0.02783	0.01531	0.00864	0.00512	0.00319	[68]
2	2	0.03390	0.02783	0.01531	0.00864	0.00512	0.00319	[61]
2	4	0.03390	0.03682	0.03562	0.03198	0.02785	0.02391	[61]
2	6	0.03390	0.03927	0.04073	0.04101	0.04110	0.04102	[61]
2	8	0.03390	0.03973	0.04063	0.04063	0.04062	0.04064	[61]
2		0.03390	0.03973	0.04063			0.04064	[64]
2		0.0338912	0.039824	0.0404944	0.0405264	0.0405312	0.0405312	p=26
2		0.0338912	0.039824	0.0404944	0.0405264	0.0405312	0.0405312	p=25
2		0.0338912	0.039824	0.0404944	0.040528	0.0405312	0.0405328	p=24
3	2	0.03835	0.02983	0.01778	0.01167	0.00813	0.00587	[61]

Table 6. Comparison of the central deflection Ω of thin (C) super-elliptical plates under q (η=0.002) (continue)

c	d	k=1	k=2	k=4	k=6	k=8	k=10	Reference
3	4	0.03835	0.03891	0.03919	0.03747	0.03460	0.03139	[61]
3	6	0.03835	0.04116	0.04251	0.04338	0.04411	0.04462	[61]
3	8	0.03835	0.04157	0.04198	0.04191	0.04124	0.04189	[61]
3		0.0383535	0.0416583	0.0418777	0.0418851	0.0418851	0.0418851	p=26
3		0.0383535	0.0416583	0.0418851	0.0418851	0.0418851	0.0418851	p=25
3		0.0383535	0.0416583	0.0418851	0.0418851	0.0418851	0.0418851	p=24

Table 7. Publications on the bending of isotropic super-elliptical plates

Reference	k considered	Method	d	Support configuration
[60]	1, 2, 3, .., 19, 20, 300	Ritz	12	(PS)
[61]	1, 2, 4, 6, 8, 10	Galerkin	8	(C)
[65]	1, 2, 3, .., 19, 20, 50, 250	Ritz	18	(PS)
[62]	1, 2, 4, 6	New Double Side Approach		(C)
[63]	10	Galerkin	8	(C)
[64]	1, 2, 4, 10	Ritz	8	(S), (C)
[66]	1, 2, 3, .., 19, 20, 50, 200	Ritz	8	(PS)
[67]	2, 4, 6	Galerkin, Double Side Approach		(C)
[68]	1, 2, 4, 6, 8, 10	Ritz	2	(C)

Since the maximum deflection develops at the center of the plate, the numerical investigations for the cases presented in Table 1 regarding the nondimensional central deflection of shear deformable super-elliptical plates were made for several values of the parameter of thickness from η=0.002 to η=0.100 in Appendix A (Tables A1-A15). Each table was constructed to observe how the deflection trend -from an elliptical to a rectangular plate- is affected with the shape (the shape of the plate is defined by the super-elliptical power which controls the roundness of the corner) and with the aspect ratio. The deflection trend corresponding to two types of loading was depicted in the same table (Tables A1-A15). Clamped (C), simply supported (S), and point-supported (PS) super-elliptical plates were analyzed in Tables A1-A5, A6-A10, and A11-A15, respectively. A decreasing incrementation in the nondimensional central deflection of clamped (C) and point-supported (PS) plates with increasing super-elliptical power was identified in Tables A1-A5 and A11-A15. The bending behavior of simply supported (S) super-elliptical plates was examined in Tables A6-A10, and it was shown that for k>3 the nondimensional central deflection decreases with increasing super-elliptical power. It was detected that the deflection trend is not affected by the thickness of the plate.

5. CONCLUSIONS

Bending of moderately thick super-elliptical plates was examined based on the first order shear deformation theory (FSDT). The numerical simulation was made using the finite element method. Influence of the geometric properties of the plate on the maximum

deflection was investigated via sensitivity analysis. Three support configurations were considered within the scope of the paper.

The bending results obtained for clamped super-elliptical plates under transverse uniform pressure in the current study were compared with those presented by Ceribasi et al. (2008) [61], Ceribasi (2012) [63], Zhang (2013) [64], and Altunsaray (2017) [68] (Table 7). In these publications, the trial function was constructed as the product of the basic function and a complete two dimensional polynomial function of degree d. Since the results corresponding to k>10 have not been presented in these publications, a relation between the maximum deflection of super-elliptical plates and that of rectangular plates is not available in the literature. Relatively fewer terms in the trial function were considered in these studies, and therefore the deflection parameter in the studies [61, 68] was found to be decreasing for c=1 and k>4 (Table 6).

However, the results in the current study reveal that the central deflection of a clamped super-elliptical plate lies in the range bounded by elliptical and rectangular plates as expected because the maximum deflection of a clamped square plate is larger than the central deflection of a clamped circular plate. This statement was also verified for super-elliptical plates under a transverse central point load (Tables A1-A5). Therefore, for both types of loading, W and λ increase with increasing k. It is worth noting that slight discrepancies which may possibly arise from truncation or rounding-off errors may be neglected for c=3 (Table A4, Case 3).

However, the case is different for a simply supported super-elliptical plate (Tables A6-A10). The answer may be found in the fact that "the central deflection of the circular plate is larger than that of the corresponding square plate. This result may be attributed to the action of the reactive forces concentrated at the corners of the square plate which have the tendency to produce deflection of the plate convex upward" [72]. Therefore, based on the results of this study, it can be stated that interpolation may be used for the prediction of the deflection of clamped super-elliptical plates, but it should not be used for simply supported super-elliptical plates. The super-elliptical power corresponding to the maximum deflection increases with increasing aspect ratio. Beyond these specific value of k as k is raised, W and λ decrease.

As far as the author knows there has been no published paper on point-supported shear deformable super-elliptical plates. Therefore, the accuracy of the results in the current study was validated through comparison with the results of thin plates, and good agreement was obtained (Tables 4-5). The maximum deflection of a corner-supported super-elliptical plate lies in the range bounded by elliptical and rectangular plates (Table A11-A15). Consequently, interpolation may be used. Compared to simply supported plates, the transverse displacement of corner supported plates is larger, but the difference gets smaller with decreasing super-elliptical power.

The numerical simulations reveal that for the loadings and for the support configurations considered in the study, the linear bending response of (C) and (PS) super-elliptical plates is similar to each other (Figs. 3-4).

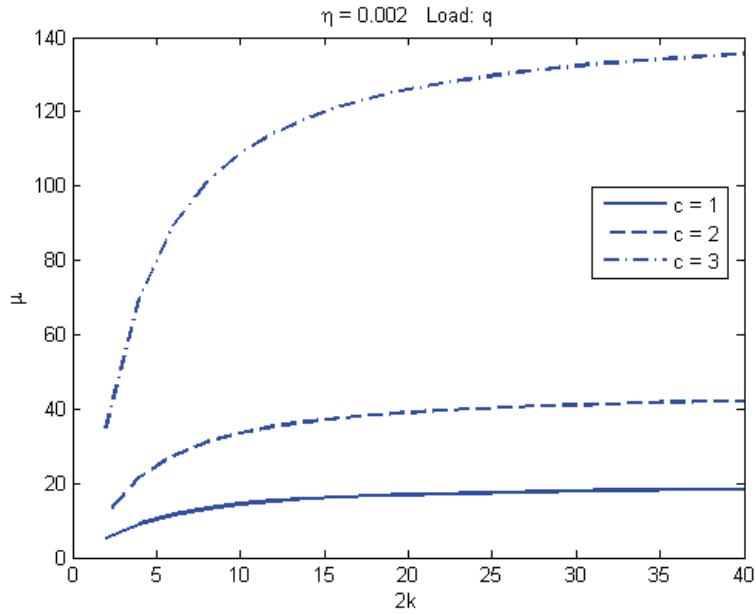

Figure 3. Bending response of (PS) and (C) super-elliptical plates under q

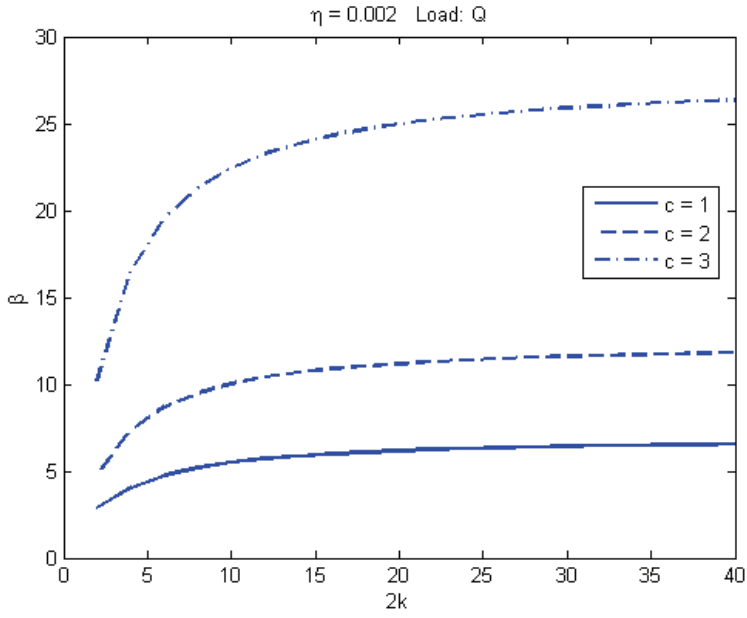

Figure 4. Bending response of (PS) and (C) super-elliptical plates under Q

It was shown that computation with high rate of convergence is required to determine the trend of the relation between the maximum deflection and the super-elliptical power (Tables 2-4). Especially for (S) and (C) plates, considering relatively fewer terms in the trial function, may lead to loss of precision due to low rate of convergence, and therefore the aforementioned trend may not be obtained with admissible accuracy.

The quadrilateral element and the mesh pattern used in the study are capable of simulating the bending response of super-elliptical plates efficiently. The boundary conditions have considerable importance on the results. The results reveal that super-elliptical plates require extensive computational effort in comparison with elliptical and rectangular plates.

Symbols

a, b, c	: semi-major, and semi-minor axes of the plate, aspect ratio
d	: degree of the complete two dimensional polynomial function
h	: thickness of the plate
k, m	: super-elliptical power, number of meshes in the quarter of the plate
n, p	: number of nodes and number of partitions in the quarter of the plate
q, w	: uniform transverse pressure, deflection
D, E, G, Q	: flexural rigidity, Young's modulus, shear modulus, transverse point load
W	: nondimensional deflection under uniform transverse pressure q
k_x , k_y, k_{xy}	: curvatures, twist
r_i, s_i	: local coordinates of the i-th node (i=1, 2, 3, 4)
D_s, N_i	: shear rigidity, shape function (i=1, 2, 3, 4)
κ, η, ν	: shear correction factor , parameter of thickness, Poisson's ratio
θ_x, θ_y	: rotations
λ	: nondimensional deflection under central point load Q
ϕ_x, ϕ_y	: average shear deformations
$[k_e]$, [K]	: element, and global stiffness matrices
[B], [C]	: strain-displacement matrix, constitutive matrix
{F}, {U}	: global nodal load vector, global displacement vector
$[k_B]$, $[k_S]$	: bending, and shear stiffness part of $[k_e]$
$[C_B]$, $[C_S]$	: bending, and shear deformation part of [C]
$W_{(PS)}$, $W_{(C)}$	: nondimensional deflection of (PS) and (C) plates under q
$\lambda_{(PS)}$, $\lambda_{(C)}$	: nondimensional deflection of (PS) and (C) plates under Q
$\{\varepsilon\}$, $\{d_i\}$	: curvature and shear deformation vector, nodal displacement vector

References

[1] Reddy, J.N., Chao, W.C., Large-deflection and large-amplitude free vibrations of laminated composite-material plates, Computers and Structures, 13 (1-3), 341-347, 1981.

[2] Mbakogu, F.C., Pavlovic, M.N., Bending of clamped orthotropic rectangular plates: a variational symbolic solution, Computers and Structures, 77 (2), 117-128, 2000.

[3] Bayer, I., Guven, U., Altay, G., A parametric study on vibrating clamped elliptical plates with variable thickness, Journal of Sound and Vibration, 254 (1), 179-188, 2002.

[4] Ozkul, T.A., Ture, U., The transition from thin plates to moderately thick plates by using finite element analysis and the shear locking problem, Thin-Walled Structures, 42 (10), 1405-1430, 2004.

[5] Setoodeh, A.R., Karami, G., Static, free vibration and buckling analysis of anisotropic thick laminated composite plates on distributed and point elastic supports using a 3-D layer-wise FEM, Engineering Structures, 26 (2), 211-220, 2004.

[6] Algazin, S.D., Vibrations of a free-edge variable-thickness plate of arbitrary shape in plan, Journal of Applied Mechanics and Technical Physics, 52 (1), 126-131, 2011.

[7] Cai, Y.C., Tian, L.G., Atluri, S.N., A simple locking-free discrete shear triangular plate element, CMES, 77 (4), 221-238, 2011.

[8] Kutlu, A., Omurtag, M.H., Large deflection bending analysis of elliptic plates on orthotropic elastic foundation with mixed finite element method, International Journal of Mechanical Sciences, 65 (1), 64-74, 2012.

[9] Sapountzakis, E.J., Dikaros, I.C., Large deflection analysis of plates stiffened by parallel beams, Engineering Structures, 35, 254-271, 2012.

[10] Thai, H.-T., Choi, D.-H., Analytical solutions of refined plate theory for bending, buckling and vibration analyses of thick plates, Applied Mathematical Modelling, 37 (18-19), 8310-8323, 2013.

[11] Rao, L.B., Rao, C.K., Buckling of annular plates with elastically restrained external and internal edges, Mechanics Based Design of Structures and Machines, 41 (2), 222-235, 2013.

[12] Sanusei, S., Mazhari, E., Shahidi, A., Analysis of buckling behavior of elliptical plate with non-concentric elliptic hole, International Journal of Materials Engineering and Technology, 13 (1), 81-108, 2015.

[13] Szilard, R., Theories and Applications of Plate Analysis, USA, John Wiley & Sons Inc.,2004.

[14] Altay, G., Dokmeci, M.C., A polar theory for vibrations of thin elastic shells, International Journal of Solids and Structures, 43 (9), 2578–2601, 2006.

[15] Lee, S.L., Ballesteros, P., Uniformly loaded rectangular plate supported at the corners, International Journal of Mechanical Sciences, 2 (3), 206-211, 1960.

[16] Szilard, R., Theory and Analysis of Plates, Englewood Cliffs, USA, Prentice Hall, 1974.

[17] Rajaiah, K., Rao, A.K., Collocation solution for point-supported square plates, Journal of Applied Mechanics, 45 (2), 424-425, 1978.

[18] Shanmugam, N.E., Huang, R., Yu, C.H., Lee, S.L., Uniformly loaded rhombic orthotropic plates supported at corners, Computers & Structures, 30 (5), 1037-1045, 1988.

[19] Nong, L., Bao-lian, F., The symmetrical bending of an elastic circular plate supported at K internal points, Applied Mathematics and Mechanics, 12 (11), 1091-1096, 1991.

[20] Liew, K.M., Han, J.B., Bending analysis of simply supported shear deformable skew plates, Journal of Engineering Mechanics, 123 (3), 214-221, 1997.

[21] Han, J.B., Liew, K.M., An eight-node curvilinear differential quadrature formulation for Reissner/Mindlin plates, Computer Methods in Applied Mechanics and Engineering, 141 (3-4), 265-280, 1997a.

[22] Han, J.B., Liew, K.M., Analysis of moderately thick circular plates using differential quadrature method, Computer Methods in Applied Mechanics and Engineering, 123 (12), 1247-1252, 1997b.

[23] Wang, C.M., Lim, G.T., Bending solutions of sectorial Mindlin plates from Kirchhoff plates, Journal of Engineering Mechanics, 126 (4), 367-372, 2000.

[24] Wang, C.M., Lim, G.T., Reddy, J.N., Lee, K.H., Relationships between bending solutions of Reissner and Mindlin plate theories, Engineering Structures, 23 (7), 838-849, 2001.

[25] Wang, C.M., Wang, Y.C., Reddy, J.N., Problems and remedy for the Ritz method in determining stress resultants of corner supported rectangular plates, Computers and Structures, 80 (2), 145-154, 2002.

[26] Lim, G.T., Reddy, J.N., On canonical bending relationships for plates, International Journal of Solids and Structures, 40 (12), 3039-3067, 2003.

[27] Reddy, J.N., Theory and Analysis of Elastic Plates and Shells, Second Edition, Boca Raton, CRC Press, 2007.

[28] Lim, C.W., Yao, W.A., Cui, S., Benchmark symplectic solutions for bending of corner-supported rectangular thin plates, The IES Journal Part A: Civil & Structural Engineering, 1 (2), 106-115, 2008.

[29] Civalek, O., Ersoy, H., Free vibration and bending analysis of circular Mindlin plates using singular convolution method, Communications in Numerical Methods in Engineering, 25 (8), 907-922, 2009.

[30] Batista, M., An elementary derivation of basic equations of the Reissner and Mindlin plate theories, Engineering Structures, 32 (3), 906-909, 2010a.

[31] Batista, M., New analytical solution for bending problem of uniformly loaded rectangular plate supported on corners, The IES Journal Part A: Civil & Structural Engineering, 3 (2), 75-84, 2010b.

[32] Nguyen-Xuan, H., Tran, L.V., Thai, C.H., Nguyen-Thoi, T., Analysis of functionally graded plates by an efficient finite element method with node-based strain smoothing, Thin-Walled Structures, 54, 1-18, 2012.

[33] Asemi, K., Ashrafi, H., Salehi, M., Shariyat, M., Three-dimensional static and dynamic analysis of functionally graded elliptical plates, employing graded finite elements, Acta Mechanica, 224 (8), 1849-1864, 2013.

[34] Wang, C. Y., Vibrations of completely free rounded rectangular plates, Journal of Vibration and Acoustics, 137 (2), doi:10.1115/1.4029159, 2015a.

[35] Wang, C. Y., Vibrations of completely free rounded regular polygonal plates, International Journal of Acoustics and Vibration, 20 (2), 107-112, 2015b.

[36] Li, R., Wang, P., Tian, Y., Wang, B., Li, G., A unified analytic solution approach to static bending and free vibration problems of rectangular thin plates, Scientific Reports DOI: 10.1038/srep17054, 2016.

[37] Falsone, G., Settineri, D., A Kirchhoff-like solution for the Mindlin plate model: A new finite element Approach, Mechanics Research Communications, 40, 1– 10, 2012.

[38] Endo, M., Study on an alternative deformation concept for the Timoshenko beam and Mindlin plate models, International Journal of Engineering Science, 87, 32–46, 2015.

[39] Li, R., Wang, B., Li G., Benchmark bending solutions of rectangular thin plates point-supported at two adjacent corners, Applied Mathematics Letters, 40, 53-58, 2015.

[40] Liew, K.M., Kitipornchai, S., Lim, C.W., Free vibration analysis of thick superelliptical plates, Journal of Engineering Mechanics, 124 (2), 137-145, 1998.

[41] DeCapua, N.J., Sun, B.C., Transverse vibration of a class of orthotropic plates, Journal of Applied Mechanics, 39 (2), 613-615, 1972.

[42] Irie, T., Yamada, G., Sonoda, M., Natural frequencies of square membrane and square plate with rounded corners, Journal of Sound and Vibration, 86 (3), 442-448, 1983.

[43] Wang, C.M., Wang, L., Vibration and buckling of super elliptical plates. Journal of Sound and Vibration, 171 (3), 301-314, 1994.

[44] Lim, C.W., Liew, K.M., Vibrations of perforated plates with rounded corners, Journal of Engineering Mechanics, 121 (2), 203-213, 1995.

[45] Lim, C.W., Kitipornchai, S., Liew, K.M., A free-vibration analysis of doubly connected super-elliptical laminated composite plates, Composites Science and Technology, 58 (3-4), 435-445, 1998.

[46] Chen, C.C., Lim, C.W., Kitipornchai, S., Liew, K.M., Vibration of symmetrically laminated thick super elliptical plates, Journal of Sound and Vibration, 220 (4), 659-682, 1999.

[47] Chen, C.C., Kitipornchai, S.,Free vibration of symmetrically laminated thick perforated plates, Journal of Sound and Vibration, 230 (1), 111-132, 2000.

[48] Liew, K.M., Feng, Z.C., Three-dimensional free vibration analysis of perforated superelliptical plates via the p-Ritz method, International Journal of Mechanical Sciences, 43 (11), 2613-2630, 2001.

[49] Zhou, D., Lo, S.H., Cheung, Y.K., Au, F.T.K., 3-D vibration analysis of generalized super elliptical plates using Chebyshev-Ritz method, International Journal of Solids and Structures, 41 (16-17), 4697-4712, 2004.

[50] Wu, L., Liu, J., Free vibration analysis of arbitrary shaped thick plates by differential cubature method. International Journal of Mechanical Sciences, 47 (1), 63-81, 2005.

[51] Altekin, M., Free linear vibration and buckling of super-elliptical plates resting on symmetrically distributed point-supports on the diagonals, Thin-Walled Structures, 46 (10), 1066-1086, 2008.

[52] Altekin, M., Free vibration of orthotropic super-elliptical plates on intermediate supports, Nuclear Engineering and Design, 239 (6), 981-999, 2009.

[53] Altekin, M., Free in-plane vibration of super-elliptical plates, Shock and Vibration, 18 (3), 471-484, 2010b.

[54] Altekin, M., Free transverse vibration of shear deformable super-elliptical plates, Wind and Structures, 24 (4), 307-331, 2017.

[55] Ceribasi, S., Altay, G., Free vibration of super elliptical plates with constant and variable thickness by Ritz method, Journal of Sound and Vibration, 319 (1-2), 668-680, 2009.

[56] Jazi, S.R., Farhatnia, F., Buckling analysis of functionally graded super elliptical plate using pb-2 Ritz method, Advanced Materials Research, 383-390, 5387-5391, 2012.

[57] Zhang, D.G., Zhou, H.M., Nonlinear symmetric free vibration analysis of super elliptical isotropic thin plates, CMC: Computers, Materials & Continua, 40 (1), 21-34, 2014. (the author does not have access to this paper)

[58] Hasheminejad, S.M., Keshvari, M.M., Ashory, M.R., Dynamic stability of super elliptical plates resting on elastic foundations under periodic in-plane loads, Journal of Engineering Mechanics, 140 (1), 172-181, 2014.

[59] Ghaheri, A., Nosier, A., Keshmiri, A., Parametric stability of symmetrically laminated composite super-elliptical plates, Journal of Composite Materials DOI: 10.1177/0021998316629481, 2016.

[60] Altekin, M., Altay, G., Static analysis of point-supported super-elliptical plates, Archive of Applied Mechanics, 78 (4), 259-266, 2008.

[61] Ceribasi, S., Altay, G., Dökmeci, M.C., Static analysis of super elliptical clamped plates by Galerkin's method, Thin-Walled Structures, 46 (2), 122-127, 2008.

[62] Tang, H.W., Yang, Y.T., Chen, C.K., Application of new double side approach method to the solution of super-elliptical plate problems, Acta Mechanica, 223 (4), 745-753, 2012.

[63] Ceribasi, S., Static and dynamic analysis of thin uniformly loaded super elliptical FGM plates, Mechanics of Advanced Materials and Structures, 19 (5), 325-335, 2012.

[64] Zhang, D.G., Non-linear bending analysis of super-elliptical thin plates, International Journal of Non-Linear Mechanics, 55, 180-185, 2013.

[65] Altekin, M., Bending of orthotropic super-elliptical plates on intermediate point supports, Ocean Engineering, 37 (11-12), 1048-1060, 2010a.

[66] Altekin, M., Large deflection analysis of point supported super-elliptical plates, Structural Engineering and Mechanics, 51 (2), 333-347, 2014.

[67] Tang, H.W., Lo, C.Y., Application of double side approach method on super elliptical Winkler plate, International Journal of Mechanical, Aerospace, Industrial, Mechatronic and Manufacturing Engineering, 8 (8), 1472-1476, 2014.

[68] Altunsaray, E., Static deflections of symmetrically laminated quasi-isotropic super-elliptical thin plates, Ocean Engineering, 141, 337-350, 2017.

[69] Reddy, J.N., An Introduction to the Finite Element Method, Second Edition, Singapore, McGraw-Hill International editions, 1993.

[70] Hughes, T.J.R., Taylor, R.L., Kanoknukulchai, W., A simple and efficient finite element for plate bending, International Journal for Numerical Methods in Engineering, 11 (10), 1529-1543, 1977.

[71] Krishnamoorthy, C.S., Finite Element Analysis: Theory and Programming, (Second Edition), New Delhi, Tata McGraw-Hill Publishing Company Limited, 1994.

[72] Timoshenko, S. P., Woinowsky-Krieger, S., Theory of Plates and Shells, Singapore, McGraw-Hill International Editions, 1959.

[73] Ozgan, K., Daloglu, A.T., Shear locking free finite elements for thick plates on elastic foundations, Teknik Dergi/Technical Journal of Turkish Chamber of Civil Engineers, 22 (107), 5341-5358, 2011 (in Turkish).

[74] Kumbasar, N., A generalized finite difference method for plates and rotational shells using Betti's theorem, Teknik Dergi/Technical Journal of Turkish Chamber of Civil Engineers, 28 (4), 8129-8142, 2017 (in Turkish).

[75] Aksoylar, C., Omurtag, M.H., Mixed finite element analysis of composite plates under blast loading, Teknik Dergi/Technical Journal of Turkish Chamber of Civil Engineers, 22 (109), 5689-5711, 2011 (in Turkish).

[76] Karasin, A.H., Gulkan, P. An approximate finite grid solution for plates on elastic foundations, Teknik Dergi/Technical Journal of Turkish Chamber of Civil Engineers, 19 (93), 4445-4454, 2008 (in Turkish).

Appendix A

Table A1. Nondimensional central deflection of (C) super-elliptical plates (p=26, η=0.002)

	W	W	W	λ	λ	λ
2k	c=1	c=2	c=3	c=1	c=2	c=3
2	0.0156202	0.0021182	0.0004735	0.0198863	0.0068442	0.0031454
4	0.0197669	0.002489	0.0005143	0.0222393	0.0072021	0.0032137
6	0.0201555	0.0025246	0.0005168	0.0224094	0.0072232	0.0032157
8	0.0202216	0.0025309	0.0005170	0.0224342	0.007226	0.0032159
10	0.0202377	0.0025324	0.0005171	0.0224396	0.0072265	0.0032159
12	0.0202425	0.0025329	0.0005171	0.0224411	0.0072267	0.0032159
14	0.0202443	0.0025331	0.0005171	0.0224416	0.0072267	0.0032159
16	0.020245	0.0025332	0.0005171	0.0224418	0.0072267	0.0032159
18	0.0202454	0.0025332	0.0005171	0.0224419	0.0072267	0.0032159
20	0.0202456	0.0025332	0.0005171	0.0224419	0.0072267	0.0032159
22	0.0202457	0.0025332	0.0005171	0.0224419	0.0072267	0.0032159
24	0.0202457	0.0025332	0.0005171	0.022442	0.0072267	0.0032159
26	0.0202458	0.0025332	0.0005171	0.022442	0.0072267	0.0032159
28	0.0202458	0.0025332	0.0005171	0.022442	0.0072267	0.0032159
30	0.0202458	0.0025332	0.0005171	0.022442	0.0072267	0.0032159
32	0.0202459	0.0025333	0.0005171	0.022442	0.0072267	0.0032159
34	0.0202459	0.0025333	0.0005171	0.022442	0.0072267	0.0032159
36	0.0202459	0.0025333	0.0005171	0.022442	0.0072267	0.0032159
38	0.0202459	0.0025333	0.0005171	0.022442	0.0072267	0.0032159
40	0.020246	0.0025333	0.0005171	0.022442	0.0072267	0.0032159
100	0.0202461	0.0025333	0.0005171	0.0224421	0.0072268	0.0032159
400	0.0202462	0.0025333	0.0005171	0.0224422	0.0072268	0.0032159

Table A2. Nondimensional central deflection of (C) super-elliptical plates (p=26, η=0.010)

	W	W	W	λ	λ	λ
2k	c=1	c=2	c=3	c=1	c=2	c=3
2	0.0156271	0.002119	0.0004736	0.0199322	0.0068554	0.0031502
4	0.0197758	0.0024899	0.0005145	0.0222873	0.0072138	0.0032187
6	0.0201651	0.0025255	0.0005169	0.0224581	0.007235	0.0032207
8	0.0202314	0.0025318	0.0005172	0.0224833	0.0072378	0.0032209
10	0.0202475	0.0025333	0.0005173	0.0224888	0.0072384	0.0032209
12	0.0202524	0.0025338	0.0005173	0.0224904	0.0072385	0.0032209
14	0.0202541	0.002534	0.0005173	0.022491	0.0072386	0.0032209
16	0.0202549	0.002534	0.0005173	0.0224912	0.0072386	0.0032209
18	0.0202552	0.0025341	0.0005173	0.0224914	0.0072386	0.0032209
20	0.0202554	0.0025341	0.0005173	0.0224914	0.0072386	0.0032209

Table A2. Nondimensional central deflection of (C) super-elliptical plates (p=26, η=0.010) (continue)

	W	W	W	λ	λ	λ
2k	c=1	c=2	c=3	c=1	c=2	c=3
22	0.0202555	0.0025341	0.0005173	0.0224915	0.0072386	0.0032209
24	0.0202556	0.0025341	0.0005173	0.0224915	0.0072386	0.0032209
26	0.0202556	0.0025341	0.0005173	0.0224916	0.0072386	0.0032209
28	0.0202557	0.0025341	0.0005173	0.0224916	0.0072386	0.0032209
30	0.0202557	0.0025341	0.0005173	0.0224916	0.0072386	0.0032209
32	0.0202557	0.0025341	0.0005173	0.0224916	0.0072387	0.0032209
34	0.0202557	0.0025341	0.0005173	0.0224916	0.0072387	0.0032209
36	0.0202557	0.0025341	0.0005173	0.0224917	0.0072387	0.0032209
38	0.0202558	0.0025341	0.0005173	0.0224917	0.0072387	0.0032209
40	0.0202558	0.0025341	0.0005173	0.0224917	0.0072387	0.0032209
100	0.0202559	0.0025342	0.0005173	0.0224918	0.0072387	0.0032209
400	0.020256	0.0025342	0.0005173	0.0224919	0.0072387	0.0032209

Table A3. Nondimensional central deflection of (C) super-elliptical plates (p=26, η=0.020)

	W	W	W	λ	λ	λ
2k	c=1	c=2	c=3	c=1	c=2	c=3
2	0.0156485	0.0021213	0.0004741	0.0200758	0.0068904	0.0031651
4	0.0198036	0.0024925	0.0005150	0.0224373	0.007250	0.0032341
6	0.0201946	0.0025282	0.0005175	0.0226103	0.0072716	0.0032363
8	0.0202615	0.0025345	0.0005178	0.0226363	0.0072745	0.0032365
10	0.0202778	0.002536	0.0005178	0.0226423	0.0072752	0.0032366
12	0.0202828	0.0025365	0.0005178	0.0226442	0.0072754	0.0032366
14	0.0202846	0.0025367	0.0005178	0.022645	0.0072755	0.0032366
16	0.0202853	0.0025368	0.0005178	0.0226454	0.0072756	0.0032366
18	0.0202857	0.0025368	0.0005178	0.0226457	0.0072756	0.0032366
20	0.0202859	0.0025368	0.0005178	0.0226458	0.0072756	0.0032366
22	0.020286	0.0025369	0.0005178	0.022646	0.0072756	0.0032367
24	0.020286	0.0025369	0.0005178	0.0226461	0.0072757	0.0032367
26	0.0202861	0.0025369	0.0005178	0.0226461	0.0072757	0.0032367
28	0.0202861	0.0025369	0.0005178	0.0226462	0.0072757	0.0032367
30	0.0202862	0.0025369	0.0005178	0.0226463	0.0072757	0.0032367
32	0.0202862	0.0025369	0.0005178	0.0226463	0.0072757	0.0032367
34	0.0202862	0.0025369	0.0005178	0.0226464	0.0072757	0.0032367
36	0.0202862	0.0025369	0.0005178	0.0226464	0.0072757	0.0032367
38	0.0202862	0.0025369	0.0005178	0.0226465	0.0072757	0.0032367
40	0.0202863	0.0025369	0.0005178	0.0226465	0.0072757	0.0032367
100	0.0202864	0.0025369	0.0005178	0.0226469	0.0072758	0.0032367
400	0.0202865	0.0025369	0.0005178	0.0226471	0.0072758	0.0032367

Table A4. Nondimensional central deflection of (C) super-elliptical plates (p=26, η=0.050)

	W	W	W	λ	λ	λ
2k	c=1	c=2	c=3	c=1	c=2	c=3
2	0.0157985	0.0021374	0.0004776	0.0210805	0.007135	0.0032692
4	0.0199967	0.002511	0.0005188	0.0234863	0.0075038	0.0033422
6	0.0203998	0.0025472	0.0005212	0.023674	0.0075277	0.0033453
8	0.0204702	0.0025535	0.0005215	0.0237062	0.0075316	0.0033459
10	0.0204879	0.0025551	0.0005215	0.0237155	0.0075329	0.0033461
12	0.0204934	0.0025556	0.0005216	0.0237195	0.0075335	0.0033463
14	0.0204955	0.0025558	0.0005216	0.0237218	0.0075338	0.0033464
16	0.0204964	0.0025559	0.0005215	0.0237232	0.0075341	0.0033465
18	0.0204968	0.0025559	0.0005215	0.0237243	0.0075343	0.0033465
20	0.0204971	0.0025559	0.0005215	0.0237251	0.0075344	0.0033466
22	0.0204972	0.002556	0.0005215	0.0237258	0.0075346	0.0033466
24	0.0204973	0.002556	0.0005215	0.0237264	0.0075347	0.0033467
26	0.0204974	0.002556	0.0005215	0.0237268	0.0075347	0.0033467
28	0.0204974	0.002556	0.0005215	0.0237272	0.0075348	0.0033467
30	0.0204974	0.002556	0.0005215	0.0237276	0.0075349	0.0033467
32	0.0204975	0.002556	0.0005215	0.0237279	0.0075349	0.0033467
34	0.0204975	0.002556	0.0005215	0.0237282	0.007535	0.0033467
36	0.0204975	0.002556	0.0005215	0.0237284	0.007535	0.0033468
38	0.0204975	0.002556	0.0005215	0.0237286	0.0075351	0.0033468
40	0.0204975	0.002556	0.0005215	0.0237288	0.0075351	0.0033468
100	0.0204977	0.002556	0.0005215	0.0237311	0.0075355	0.0033469
400	0.0204978	0.002556	0.0005215	0.0237324	0.0075357	0.003347

Table A5. Nondimensional central deflection of (C) super-elliptical plates (p=26, η=0.100)

	W	W	W	λ	λ	λ
2k	c=1	c=2	c=3	c=1	c=2	c=3
2	0.0163341	0.002195	0.0004902	0.0246689	0.0080081	0.0036407
4	0.0206759	0.0025769	0.0005322	0.0272251	0.0084088	0.0037277
6	0.0211185	0.0026145	0.0005347	0.027463	0.008441	0.003734
8	0.021201	0.0026212	0.0005349	0.0275167	0.0084486	0.0037359
10	0.0212231	0.0026229	0.0005350	0.0275379	0.008452	0.0037369
12	0.0212306	0.0026235	0.0005350	0.0275494	0.0084539	0.0037375
14	0.0212337	0.0026237	0.0005350	0.0275568	0.0084553	0.0037379
16	0.0212351	0.0026238	0.0005350	0.0275622	0.0084563	0.0037382
18	0.0212358	0.0026238	0.0005350	0.0275662	0.008457	0.0037385
20	0.0212362	0.0026238	0.0005350	0.0275694	0.0084576	0.0037387
22	0.0212365	0.0026239	0.0005350	0.027572	0.0084581	0.0037388
24	0.0212366	0.0026239	0.0005350	0.0275742	0.0084585	0.003739

Table A5. Nondimensional central deflection of (C) super-elliptical plates (p=26, η=0.100) (continue)

	W	W	W	λ	λ	λ
2k	c=1	c=2	c=3	c=1	c=2	c=3
26	0.0212367	0.0026239	0.0005350	0.0275761	0.0084588	0.0037391
28	0.0212368	0.0026239	0.0005350	0.0275776	0.0084591	0.0037392
30	0.0212369	0.0026239	0.0005350	0.027579	0.0084593	0.0037393
32	0.0212369	0.0026239	0.0005350	0.0275802	0.0084596	0.0037393
34	0.021237	0.0026239	0.0005350	0.0275812	0.0084598	0.0037394
36	0.021237	0.0026239	0.0005350	0.0275822	0.0084599	0.0037394
38	0.021237	0.0026239	0.0005350	0.027583	0.0084601	0.0037395
40	0.021237	0.0026239	0.0005350	0.0275838	0.0084602	0.0037395
100	0.0212372	0.0026239	0.0005350	0.0275928	0.0084617	0.003740
400	0.0212373	0.0026239	0.0005350	0.0275979	0.0084627	0.0037403

Table A6. Nondimensional central deflection of (S) super-elliptical plates (p=26, η=0.002)

	W	W	W	W	λ	λ	λ	λ
2k	c=1	c=2	c=3	c=5	c=1	c=2	c=3	c=5
2	0.0636745	0.008894	0.0021009	0.0003069	0.0504901	0.0165024	0.0074299	0.0026975
4	0.0729315	0.0105591	0.0024185	0.0003301	0.0514505	0.0170786	0.0075629	0.0027121
6	0.0702026	0.0104952	0.0024387	0.0003319	0.0493006	0.0168586	0.0075473	0.0027114
8	0.0684491	0.0103899	0.0024357	0.0003322	0.048222	0.016735	0.0075382	0.0027111
10	0.0674217	0.0103182	0.0024315	0.0003322	0.0476429	0.0166673	0.0075333	0.002711
12	0.0667878	0.0102711	0.0024282	0.0003322	0.0473018	0.0166272	0.0075306	0.002711
14	0.0663739	0.0102393	0.0024258	0.0003322	0.0470854	0.0166018	0.0075289	0.0027109
16	0.0660904	0.0102171	0.0024241	0.0003322	0.0469402	0.0165847	0.0075277	0.0027109
18	0.0658883	0.0102011	0.0024228	0.0003322	0.0468381	0.0165727	0.0075269	0.0027109
20	0.0657395	0.0101892	0.0024218	0.0003322	0.0467637	0.016564	0.0075264	0.0027109
22	0.0656269	0.0101801	0.0024211	0.0003322	0.0467079	0.0165574	0.0075259	0.0027108
24	0.0655398	0.010173	0.0024205	0.0003322	0.0466649	0.0165524	0.0075256	0.0027108
26	0.0654709	0.0101674	0.002420	0.0003322	0.0466312	0.0165485	0.0075254	0.0027108
28	0.0654157	0.0101629	0.0024196	0.0003322	0.0466043	0.0165453	0.0075252	0.0027108
30	0.0653707	0.0101592	0.0024193	0.0003322	0.0465824	0.0165427	0.007525	0.0027108
32	0.0653335	0.0101561	0.002419	0.0003322	0.0465644	0.0165406	0.0075248	0.0027108
34	0.0653025	0.0101536	0.0024188	0.0003322	0.0465494	0.0165389	0.0075247	0.0027108
36	0.0652763	0.0101514	0.0024186	0.0003322	0.0465368	0.0165374	0.0075246	0.0027108
38	0.0652541	0.0101496	0.0024185	0.0003322	0.0465261	0.0165362	0.0075246	0.0027108
40	0.065235	0.010148	0.0024183	0.0003322	0.0465169	0.0165351	0.0075245	0.0027108
100	0.0650823	0.0101352	0.0024172	0.0003321	0.046444	0.0165265	0.0075239	0.0027108
400	0.0650483	0.0101323	0.002417	0.0003321	0.0464279	0.0165246	0.0075238	0.0027108

Table A7. Nondimensional central deflection of (S) super-elliptical plates (p=26, η=0.010)

	W	W	W	W	λ	λ	λ	λ
2k	c=1	c=2	c=3	c=5	c=1	c=2	c=3	c=5
2	0.0636814	0.0088986	0.002102	0.0003070	0.0505361	0.0165219	0.0074394	0.002701
4	0.0730054	0.0105663	0.0024195	0.0003301	0.0515375	0.0171014	0.0075729	0.0027157
6	0.0703163	0.0105047	0.0024398	0.0003320	0.0494094	0.0168836	0.0075575	0.0027149
8	0.0685856	0.0104007	0.0024369	0.0003323	0.0483427	0.0167611	0.0075484	0.0027147
10	0.0675735	0.0103299	0.0024328	0.0003323	0.0477714	0.0166941	0.0075437	0.0027146
12	0.0669505	0.0102835	0.0024296	0.0003323	0.0474359	0.0166546	0.0075409	0.0027145
14	0.066545	0.0102523	0.0024273	0.0003323	0.0472238	0.0166295	0.0075392	0.0027145
16	0.0662681	0.0102305	0.0024255	0.0003323	0.0470818	0.0166128	0.0075381	0.0027145
18	0.0660714	0.0102148	0.0024243	0.0003323	0.0469823	0.016601	0.0075374	0.0027144
20	0.0659271	0.0102031	0.0024233	0.0003322	0.0469101	0.0165925	0.0075368	0.0027144
22	0.0658182	0.0101942	0.0024226	0.0003322	0.0468562	0.0165861	0.0075364	0.0027144
24	0.0657343	0.0101874	0.002422	0.0003322	0.0468148	0.0165812	0.0075361	0.0027144
26	0.0656682	0.0101819	0.0024216	0.0003322	0.0467824	0.0165774	0.0075358	0.0027144
28	0.0656154	0.0101775	0.0024212	0.0003322	0.0467566	0.0165743	0.0075356	0.0027144
30	0.0655725	0.010174	0.0024209	0.0003322	0.0467358	0.0165719	0.0075355	0.0027144
32	0.0655372	0.010171	0.0024206	0.0003322	0.0467187	0.0165699	0.0075353	0.0027144
34	0.0655078	0.0101686	0.0024204	0.0003322	0.0467045	0.0165682	0.0075352	0.0027144
36	0.0654832	0.0101665	0.0024202	0.0003322	0.0466926	0.0165668	0.0075352	0.0027144
38	0.0654623	0.0101647	0.0024201	0.0003322	0.0466825	0.0165656	0.0075351	0.0027144
40	0.0654444	0.0101632	0.0024199	0.0003322	0.046674	0.0165645	0.007535	0.0027144
100	0.0653053	0.0101513	0.0024189	0.0003322	0.0466076	0.0165566	0.0075345	0.0027143
400	0.0652761	0.0101487	0.0024187	0.0003322	0.0465938	0.0165548	0.0075344	0.0027143

Table A8. Nondimensional central deflection of (S) super-elliptical plates (p=26, η=0.020)

	W	W	W	W	λ	λ	λ	λ
2k	c=1	c=2	c=3	c=5	c=1	c=2	c=3	c=5
2	0.0637028	0.0089057	0.0021037	0.0003072	0.0506796	0.0165669	0.007460	0.0027082
4	0.0731182	0.010577	0.0024212	0.0003302	0.0517381	0.0171516	0.0075944	0.0027232
6	0.0704814	0.0105183	0.0024416	0.0003321	0.0496391	0.0169366	0.0075793	0.0027225
8	0.0687806	0.0104162	0.0024389	0.0003324	0.0485882	0.0168157	0.0075704	0.0027222
10	0.0677882	0.0103466	0.0024348	0.0003324	0.0480272	0.0167497	0.0075658	0.0027221
12	0.0671794	0.010301	0.0024317	0.0003324	0.0476989	0.0167109	0.0075631	0.0027221
14	0.0667846	0.0102705	0.0024294	0.0003324	0.0474922	0.0166863	0.0075615	0.0027221
16	0.066516	0.0102492	0.0024277	0.0003324	0.0473544	0.01667	0.0075604	0.002722
18	0.0663261	0.0102339	0.0024265	0.0003324	0.0472584	0.0166585	0.0075597	0.002722
20	0.0661872	0.0102225	0.0024256	0.0003323	0.0471889	0.0166503	0.0075591	0.002722
22	0.066083	0.010214	0.0024249	0.0003323	0.0471372	0.0166441	0.0075587	0.002722
24	0.0660029	0.0102073	0.0024243	0.0003323	0.0470978	0.0166394	0.0075584	0.002722
26	0.0659401	0.0102021	0.0024239	0.0003323	0.0470671	0.0166357	0.0075582	0.002722
28	0.0658901	0.0101979	0.0024235	0.0003323	0.0470427	0.0166328	0.007558	0.002722
30	0.0658497	0.0101945	0.0024232	0.0003323	0.0470231	0.0166304	0.0075578	0.002722
32	0.0658166	0.0101916	0.002423	0.0003323	0.047007	0.0166285	0.0075577	0.002722
34	0.0657891	0.0101893	0.0024228	0.0003323	0.0469938	0.0166269	0.0075576	0.002722
36	0.0657662	0.0101873	0.0024226	0.0003323	0.0469827	0.0166255	0.0075575	0.002722
38	0.0657467	0.0101857	0.0024224	0.0003323	0.0469734	0.0166244	0.0075575	0.002722
40	0.0657302	0.0101842	0.0024223	0.0003323	0.0469655	0.0166234	0.0075574	0.002722
100	0.0656044	0.0101732	0.0024213	0.0003323	0.0469057	0.0166161	0.0075569	0.0027219
400	0.0655787	0.0101708	0.0024211	0.0003323	0.0468937	0.0166146	0.0075568	0.0027219

Table A9. Nondimensional central deflection of (S) super-elliptical plates (p=26, η=0.050)

	W	W	W	W	λ	λ	λ	λ
2k	c=1	c=2	c=3	c=5	c=1	c=2	c=3	c=5
2	0.0638528	0.0089362	0.0021108	0.0003079	0.0516844	0.01684	0.0075802	0.0027496
4	0.0735879	0.0106203	0.0024283	0.0003308	0.0529488	0.0174451	0.0077195	0.0027663
6	0.0711233	0.0105711	0.0024492	0.0003327	0.0509485	0.0172402	0.0077058	0.0027658
8	0.0695174	0.0104746	0.0024469	0.0003329	0.0499498	0.0171247	0.0076976	0.0027657
10	0.0685858	0.0104087	0.0024431	0.0003330	0.0494214	0.0170621	0.0076934	0.0027657
12	0.0680194	0.0103658	0.0024402	0.0003330	0.0491157	0.0170255	0.007691	0.0027657
14	0.0676557	0.0103372	0.002438	0.0003329	0.0489254	0.0170026	0.0076895	0.0027657
16	0.0674107	0.0103174	0.0024365	0.0003329	0.04880	0.0169875	0.0076886	0.0027657
18	0.0672392	0.0103032	0.0024353	0.0003329	0.0487136	0.0169771	0.0076879	0.0027657
20	0.067115	0.0102929	0.0024345	0.0003329	0.0486518	0.0169696	0.0076875	0.0027657
22	0.0670225	0.010285	0.0024338	0.0003329	0.0486064	0.016964	0.0076871	0.0027657
24	0.0669521	0.010279	0.0024333	0.0003329	0.048572	0.0169598	0.0076869	0.0027657
26	0.0668974	0.0102743	0.0024329	0.0003329	0.0485455	0.0169566	0.0076867	0.0027657
28	0.0668542	0.0102706	0.0024326	0.0003329	0.0485246	0.016954	0.0076865	0.0027657
30	0.0668194	0.0102675	0.0024323	0.0003329	0.048508	0.016952	0.0076864	0.0027657
32	0.0667911	0.010265	0.0024321	0.0003329	0.0484945	0.0169503	0.0076863	0.0027657
34	0.0667678	0.010263	0.0024319	0.0003329	0.0484834	0.0169489	0.0076863	0.0027657
36	0.0667484	0.0102613	0.0024318	0.0003329	0.0484743	0.0169478	0.0076862	0.0027657
38	0.0667321	0.0102598	0.0024317	0.0003329	0.0484666	0.0169468	0.0076861	0.0027657
40	0.0667183	0.0102586	0.0024315	0.0003329	0.0484601	0.016946	0.0076861	0.0027657
100	0.0666152	0.0102492	0.0024307	0.0003329	0.048413	0.0169401	0.0076858	0.0027657
400	0.0665933	0.0102472	0.0024305	0.0003329	0.0484038	0.016939	0.0076857	0.0027657

Table A10. Nondimensional central deflection of (S) super-elliptical plates (p=26, η=0.100)

	W	W	W	W	λ	λ	λ	λ
2k	c=1	c=2	c=3	c=5	c=1	c=2	c=3	c=5
2	0.0643885	0.009017	0.002129	0.0003101	0.0552728	0.017755	0.0079749	0.0028843
4	0.0747886	0.010729	0.0024473	0.0003328	0.0569857	0.0184107	0.0081293	0.0029066
6	0.0726465	0.0106973	0.0024692	0.0003345	0.0551806	0.0182273	0.0081196	0.0029072
8	0.071204	0.0106105	0.0024675	0.0003348	0.054278	0.0181226	0.0081132	0.0029074
10	0.0703689	0.0105507	0.0024642	0.0003348	0.0538061	0.0180664	0.008110	0.0029076
12	0.0698649	0.0105118	0.0024615	0.0003348	0.0535368	0.018034	0.0081083	0.0029077
14	0.0695437	0.010486	0.0024596	0.0003348	0.0533716	0.0180141	0.0081073	0.0029078
16	0.069329	0.0104683	0.0024582	0.0003348	0.0532641	0.0180011	0.0081067	0.0029079
18	0.0691795	0.0104557	0.0024572	0.0003348	0.053191	0.0179923	0.0081063	0.0029079
20	0.0690719	0.0104466	0.0024565	0.0003348	0.0531394	0.0179861	0.008106	0.002908
22	0.0689921	0.0104397	0.0024559	0.0003348	0.0531018	0.0179815	0.0081058	0.002908
24	0.0689316	0.0104344	0.0024555	0.0003348	0.0530736	0.0179781	0.0081057	0.002908
26	0.0688847	0.0104303	0.0024551	0.0003348	0.0530521	0.0179755	0.0081056	0.002908
28	0.0688476	0.010427	0.0024548	0.0003348	0.0530353	0.0179735	0.0081056	0.0029081
30	0.0688179	0.0104244	0.0024546	0.0003348	0.0530221	0.0179719	0.0081055	0.0029081
32	0.0687938	0.0104223	0.0024544	0.0003348	0.0530114	0.0179707	0.0081055	0.0029081
34	0.0687739	0.0104205	0.0024542	0.0003348	0.0530027	0.0179696	0.0081055	0.0029081
36	0.0687573	0.010419	0.0024541	0.0003348	0.0529956	0.0179688	0.0081055	0.0029081
38	0.0687434	0.0104177	0.002454	0.0003348	0.0529896	0.0179681	0.0081055	0.0029081
40	0.0687316	0.0104167	0.0024539	0.0003348	0.0529846	0.0179675	0.0081055	0.0029081
100	0.0686419	0.0104086	0.0024531	0.0003348	0.0529503	0.0179636	0.0081055	0.0029082
400	0.0686209	0.0104068	0.002453	0.0003348	0.0529454	0.0179633	0.0081057	0.0029083

Table A11. Nondimensional central deflection of (PS) super-elliptical plates (p=38, η=0.002)

	W	W	W	λ	λ	λ
2k	c=1	c=2	c=3	c=1	c=2	c=3
2	0.0828439	0.0496860	0.0498087	0.0567861	0.0650117	0.0965172
4	0.180261	0.107651	0.107750	0.0900652	0.105834	0.158468
6	0.234681	0.138874	0.138519	0.106860	0.125763	0.188297
8	0.268146	0.157613	0.156803	0.116866	0.137362	0.205496
10	0.290677	0.170016	0.168817	0.123500	0.144927	0.216637
12	0.306864	0.178814	0.177292	0.128222	0.150247	0.224432
14	0.319056	0.185377	0.183586	0.131756	0.154192	0.230189
16	0.328572	0.190458	0.188441	0.134503	0.157234	0.234613
18	0.336207	0.194510	0.192301	0.136699	0.159652	0.238120
20	0.342471	0.197816	0.195442	0.138496	0.161620	0.240968
22	0.347704	0.200565	0.198049	0.139994	0.163254	0.243327
24	0.352142	0.202888	0.200246	0.141262	0.164631	0.245313
26	0.355953	0.204875	0.202124	0.142349	0.165808	0.247007
28	0.359263	0.206596	0.203747	0.143293	0.166826	0.248471
30	0.362163	0.208100	0.205164	0.144118	0.167716	0.249747
32	0.364727	0.209426	0.206412	0.144847	0.168499	0.250870
34	0.367010	0.210605	0.207519	0.145496	0.169194	0.251865
36	0.369055	0.211658	0.208508	0.146077	0.169815	0.252754
38	0.370898	0.212606	0.209397	0.146600	0.170373	0.253553
40	0.372567	0.213463	0.210200	0.147073	0.170878	0.254275
100	0.392393	0.223530	0.219583	0.152677	0.176788	0.262675
400	0.402925	0.228789	0.224440	0.155642	0.179862	0.267007

Table A12. Nondimensional central deflection of (PS) super-elliptical plates (p=38, η=0.010)

	W	W	W	λ	λ	λ
2k	c=1	c=2	c=3	c=1	c=2	c=3
2	0.0829997	0.0497447	0.0498487	0.0568923	0.0650605	0.0965594
4	0.180465	0.107733	0.107802	0.0901769	0.105890	0.158516
6	0.234941	0.138966	0.138575	0.106984	0.125824	0.188348
8	0.268461	0.157711	0.156859	0.117003	0.137427	0.205548
10	0.291041	0.170118	0.168873	0.123649	0.144994	0.216689
12	0.307270	0.178920	0.177348	0.128382	0.150316	0.224484
14	0.319500	0.185485	0.183640	0.131926	0.154262	0.230240
16	0.329048	0.190569	0.188495	0.134680	0.157305	0.234664
18	0.336712	0.194622	0.192354	0.136884	0.159725	0.238170
20	0.343002	0.197930	0.195495	0.138687	0.161694	0.241018
22	0.348258	0.200681	0.198101	0.140191	0.163328	0.243376

Table A12. Nondimensional central deflection of (PS) super-elliptical plates (p=38, η=0.010) (continue)

	W	W	W	λ	λ	λ
2k	c=1	c=2	c=3	c=1	c=2	c=3
24	0.352716	0.203004	0.200298	0.141464	0.164706	0.245362
26	0.356545	0.204994	0.202175	0.142556	0.165884	0.247056
28	0.359871	0.206716	0.203798	0.143504	0.166903	0.248519
30	0.362788	0.208221	0.205214	0.144333	0.167793	0.249795
32	0.365365	0.209548	0.206462	0.145066	0.168577	0.250918
34	0.367660	0.210728	0.207569	0.145718	0.169273	0.251914
36	0.369717	0.211782	0.208558	0.146302	0.169894	0.252803
38	0.371571	0.212731	0.209447	0.146827	0.170453	0.253602
40	0.373250	0.213589	0.210250	0.147303	0.170959	0.254323
100	0.393214	0.223675	0.219638	0.152944	0.176880	0.262729
400	0.403840	0.228952	0.224505	0.155935	0.179965	0.267071

Table A13. Nondimensional central deflection of (PS) super-elliptical plates (p=38, η=0.020)

	W	W	W	λ	λ	λ
2k	c=1	c=2	c=3	c=1	c=2	c=3
2	0.0832763	0.0498034	0.0498795	0.0571537	0.0651435	0.0966129
4	0.180826	0.107809	0.107842	0.0904526	0.105978	0.158572
6	0.235381	0.139054	0.138618	0.107279	0.125918	0.188407
8	0.268975	0.157810	0.156906	0.117317	0.137526	0.205609
10	0.291620	0.170227	0.168922	0.123980	0.145098	0.216753
12	0.307907	0.179036	0.177398	0.128728	0.150424	0.224548
14	0.320186	0.185608	0.183692	0.132285	0.154374	0.230306
16	0.329778	0.190699	0.188548	0.135051	0.157421	0.234731
18	0.337480	0.194758	0.192408	0.137264	0.159843	0.238238
20	0.343803	0.198070	0.195550	0.139077	0.161815	0.241087
22	0.349089	0.200826	0.198157	0.140589	0.163452	0.243446
24	0.353573	0.203153	0.200355	0.141869	0.164832	0.245432
26	0.357427	0.205146	0.202233	0.142968	0.166013	0.247127
28	0.360775	0.206871	0.203857	0.143921	0.167033	0.248591
30	0.363711	0.208380	0.205274	0.144756	0.167925	0.249868
32	0.366306	0.209710	0.206522	0.145493	0.168710	0.250992
34	0.368618	0.210892	0.207630	0.146150	0.169407	0.251988
36	0.370690	0.211949	0.208620	0.146737	0.170030	0.252878
38	0.372558	0.212900	0.209509	0.147267	0.170591	0.253677
40	0.374251	0.213760	0.210313	0.147747	0.171097	0.254399
100	0.394398	0.223877	0.219711	0.153439	0.177036	0.262814
400	0.405156	0.229177	0.224587	0.156469	0.180135	0.267164

Table A14. Nondimensional central deflection of (PS) super-elliptical plates (p=38, η=0.050)

	W	W	W	λ	λ	λ
2k	c=1	c=2	c=3	c=1	c=2	c=3
2	0.0846261	0.0500438	0.0499834	0.0587831	0.0656061	0.0968665
4	0.182576	0.108113	0.107970	0.0921728	0.106465	0.158835
6	0.237433	0.139403	0.138760	0.109082	0.126428	0.188681
8	0.271287	0.158197	0.157059	0.119194	0.138058	0.205892
10	0.294156	0.170647	0.169084	0.125921	0.145650	0.217044
12	0.310634	0.179485	0.177568	0.130723	0.150992	0.224847
14	0.323076	0.186082	0.183869	0.134327	0.154957	0.230611
16	0.332810	0.191194	0.188732	0.137134	0.158017	0.235042
18	0.340636	0.195273	0.192598	0.139383	0.160450	0.238554
20	0.347068	0.198603	0.195745	0.141227	0.162432	0.241407
22	0.352449	0.201373	0.198356	0.142767	0.164077	0.243770
24	0.357020	0.203715	0.200559	0.144073	0.165466	0.245760
26	0.360952	0.205720	0.202441	0.145194	0.166653	0.247459
28	0.364370	0.207457	0.204068	0.146168	0.167680	0.248926
30	0.367369	0.208976	0.205488	0.147022	0.168578	0.250206
32	0.370023	0.210315	0.206740	0.147777	0.169369	0.251332
34	0.372388	0.211506	0.207850	0.148449	0.170071	0.252331
36	0.374510	0.212571	0.208842	0.149052	0.170699	0.253223
38	0.376423	0.213529	0.209734	0.149595	0.171264	0.254024
40	0.378159	0.214397	0.210540	0.150087	0.171775	0.254748
100	0.398929	0.224617	0.219973	0.155971	0.177776	0.263196
400	0.410184	0.230003	0.224883	0.159160	0.180932	0.267580

Table A15. Nondimensional central deflection of (PS) super-elliptical plates (p=38, η=0.100)

	W	W	W	λ	λ	λ
2k	c=1	c=2	c=3	c=1	c=2	c=3
2	0.0885912	0.0506813	0.0502333	0.0643120	0.0670971	0.0976216
4	0.187676	0.108918	0.108279	0.0980058	0.108040	0.159629
6	0.243230	0.140307	0.139099	0.115132	0.128065	0.189502
8	0.277631	0.159180	0.157421	0.125419	0.139745	0.206736
10	0.300946	0.171696	0.169466	0.132289	0.147378	0.217907
12	0.317795	0.180590	0.177967	0.137211	0.152757	0.225727
14	0.330551	0.187235	0.184282	0.140918	0.156752	0.231505
16	0.340554	0.192389	0.189157	0.143813	0.159838	0.235948
18	0.348613	0.196503	0.193034	0.146139	0.162295	0.239471
20	0.355251	0.199865	0.196191	0.148051	0.164297	0.242334

Table A15. Nondimensional central deflection of (PS) super-elliptical plates (p=38, η=0.100) (continue)

	W	W	W	λ	λ	λ
2k	c=1	c=2	c=3	c=1	c=2	c=3
22	0.360815	0.202664	0.198812	0.149651	0.165961	0.244706
24	0.365549	0.205031	0.201022	0.151012	0.167366	0.246704
26	0.369628	0.207060	0.202911	0.152182	0.168569	0.248410
28	0.373180	0.208817	0.204545	0.153201	0.169610	0.249883
30	0.376302	0.210355	0.205972	0.154097	0.170520	0.251169
32	0.379069	0.211712	0.207228	0.154890	0.171323	0.252301
34	0.381539	0.212919	0.208344	0.155598	0.172036	0.253305
36	0.383758	0.213999	0.209341	0.156233	0.172674	0.254202
38	0.385763	0.214972	0.210238	0.156808	0.173248	0.255008
40	0.387583	0.215852	0.211048	0.157329	0.173768	0.255736
100	0.409704	0.226284	0.220552	0.163679	0.179914	0.264261
400	0.422200	0.231875	0.225540	0.167300	0.183214	0.268733

Teknik Dergi, 2018 8497-8513, Paper 509

A Numerical Approach for Modeling of Turbulent Newtonian Fluid Flow in Eccentric Annulus

Erman ÜLKER[1]
Sıla Övgü KORKUT[2]
Mehmet SORGUN[3]

ABSTRACT

Turbulent flow is a complicated process that frequently appears not only in nature but also in engineering applications. Numerical methods frequently are used to solve turbulent flow problems due to the difficulty of solving Navier-Stokes equations. In this study, Navier-Stokes equations including inner pipe rotation effect are solved via two different techniques. A semi-analytical technique is described and applied to turbulent Newtonian fluid flow in an eccentric annulus with pipe rotation. The accuracy of the semi-analytical method is compared with the obtained numerical results of the Newton-Raphson method. The semi-analytical method is computationally time consuming, however, it may allow tackling the non-linearity of challenging problems in hydraulics. A mechanistic model including the semi-analytical method is developed in order to predict pressure gradient for turbulent flow through eccentric horizontal annulus with pipe rotation. The mechanistic model is discretisized using central difference approximation and then solved analytically in each iteration by freezing the non-linear terms. Computational frameworks are developed in MATLAB. The mathematical model is confirmed by the experimental study, which is conducted in Izmir Katip Celebi University. Results show that computational fluid model is capable of estimating pressure gradient with an error of less than 14 %.

Keywords: Eccentric annular flow, finite difference method, mechanistic modeling, Newtonian fluid, pipe rotation, turbulent flow.

1. INTRODUCTION

Most of the water flow problems related to civil engineering are mostly turbulent. Turbulent flow is a complex and chaotic process encountered in many engineering disciplines. The main reason is complexity and difficulties of turbulent solutions of Navier- Stokes equations

Note:
- This paper has been received on September 05, 2017 and accepted for publication by the Editorial Board on April 17, 2018.
- Discussions on this paper will be accepted by September 30, 2018.
- DOI: 10.18400/tekderg.336801

1 Izmir Katip Celebi University, Dep. of Civil Engineering, İzmir, Turkey - erman.ulker@ikc.edu.tr
2 Izmir Katip Celebi University, Engineering Sciences, İzmir, Turkey - silaovgu.korkut@ikc.edu.tr
3 Izmir Katip Celebi University, Dep. of Civil Engineering, İzmir, Turkey - mehmetsorgun@gmail.com

which hinder analytical demonstration. Even a simple problem in turbulent fluid flow is of concern regarding existence and uniqueness of the solution.

In applications of fluid flow through the annulus, the geometry is rarely concentric. Most of them lose the alignment of the center body and become eccentric due to gravity, bending etc. Fluid flow in an eccentric annulus has attracted great attention of researchers over the years. Deissler [1] investigated an analytical model for turbulent heat and mass transfer in smooth tubes. He took into account the effect of kinematic viscosity in the region close to the wall and obtained good agreement with experimental results. After his previous work, Deissler and Taylor [2] conducted an analytical study to describe the velocity profile of turbulent flow through eccentric annular geometries. Wolffe and Clump [3] conducted an experimental study determining velocity lines and locus of maximum velocity for turbulent flow of air. They compared their experimental results with the calculated solution of Navier-Stokes equation with Heyda's assumption [4] for analytical solution of laminar flow in annuli containing eccentricity. Johnson and Sparrow [5] [6] conducted experimental work on turbulent flow in eccentric annulus and they reported that circumferential pressure gradient is larger than that of concentric annulus. Also, they observed that friction factor decreases with increasing eccentricity. Rehme [7] proposed a correlation of friction factor prediction for turbulent flow in channels with non-circular cross-sections. He concluded that this prediction method is better than all previous attempts and it can be used on other shapes of channels such as eccentric annulus. Kacker [8] conducted an experimental study of fully turbulent flow in a circular pipe containing one or two eccentrically located rods. He developed a correlation to estimate friction factor. The correlation predicts the experimental data with 2% error margin for both one and two rod geometries. Usui and Tsuruta [9] analyzed the equation of motion for fully turbulent flow in an eccentric annulus using Kirchoff transformation. They explained the dependence of eccentricity on friction factor at high Reynolds number ranges. Tosun [10] proposed an approximate solution axial laminar flow through the eccentric annulus and he compared his results with previously published experimental works. The approximate solution is relatively in good agreement with the data in the literature. He and his group [11] [12] expanded the study of non-Newtonian fluids applying the Power law, Bingham plastic and Sutterby models. Those studies concluded that proposed approximate solution is in good agreement with previous experimental studies. Ogino et al. [13] also investigated the momentum equation for fully developed turbulent flow in the eccentric annulus. They used the bipolar coordinate transform in order to model the eccentric annulus geometry. Haciislamoglu and Langlinais [14] investigated the effect of eccentricity on frictional pressure losses without inner pipe rotation and obtained pressure losses reduction as high as 60%. Nouri et al. [15] conducted an experimental study on Newtonian and non-Newtonian fluids in both concentric and eccentric annulus. They concluded that the flow resistance decreases as the eccentricity is increased as compared with smooth pipe flow. One year later, Nouri and Whitelaw [16] introduced rotational effect in the same study and their results showed that the effect of rotation on frictional pressure losses decreases with increase in Reynolds number after the flow is in transition. Decreasing of rotational effect on frictional pressure losses continues until they are equal to the non rotation case. Numerical and analytical approaches have been performed for modelling turbulent flow. The study of Haciislamoglu and Langlinais [14] was conducted under the laminar flow regime. Corresponding to this study, Erge et al. [17] conducted another experimental study of turbulent flow in the eccentric annulus. They concluded that eccentricity significantly

reduces the frictional pressure loss in turbulent flow as well. Mossa [18] conducted an experimental study of turbulent flow, which averaged Reynolds number in the range of [10,000 ; 30,000]. He applied statistical analysis to find velocity fluctuations around the local averaged value. Erge et al. [19] conducted an experimental, analytical and numerical study of the effect of eccentricity on frictional pressure loss. They concluded that frictional pressure loss in fully eccentric annulus has up to 50% discrepancy than the results which is calculated with Narrow Slot approach. Recently, Rushd et al [20] investigated eccentricity, roughness and rotation effects on frictional pressure loss. They conducted an experimental study and developed a CFD model in ANSYS validated by experimental results. Their CFD analysis showed that effect of roughness and eccentricity are more prominent than the effect of inner pipe rotation.

This study aims to develop a mechanistic model including a semi-analytical method for determining accurate pressure gradient of turbulent flow through the fully eccentric annulus, including the effect of pipe rotation. The semi-analytical method presents the discretization of the equation with finite difference method and solved iteratively by fixing the non-linear terms.

2. EXPERIMENTAL METHOD

A flow loop was constructed at Izmir Katip Celebi University, Civil Engineering, Fluid Mechanics & Hydraulics Laboratory. A Newtonian fluid, water, has been used in the experiment. Flow loop, 10 m long, has been formed using 80 mm diameter outer pipe and 40 mm diameter inner pipe. The inner pipe is chromium plated and the outer pipe is made of plexiglass. In this study, both pipes are assumed smooth. In the present experimental study, Newtonian fluid flows through the annulus that is between inner and outer pipes. The inner pipe has been fixed concentrically at both ends and full eccentric annulus has been obtained at the test section. The test section is 0.5 m long and 7 m away from the upstream due to obtaining a fully developed section. A picture of the flow loop is shown in Fig. 1 and the specifications of the experimental setup are given in Table 1.

Figure 1. Izmir Katip Celebi University Civil Engineering (IKCU-CE) Flow Loop

Table 1. Test Parameter Values During Experiments

Experiment Specifications	Values
Inner - Outer Pipe Diameter	40 – 80 mm
Flow Loop length	10 m
Flow velocity	0.7 – 3.6 m/s
Inner pipe rotation speed	0 – 120 rpm

The following procedure is used for the tests:

- Fill the feeding tank with water
- Start the thermostatic heater for increasing the temperature of the fluid in the feeding tank
- Set the heater to desired value by digital controller
- Start 230 V DC motor on the tank for stirring the fluid in the tank in order to have homogenous temperature distribution in the fluid
- Open the butterfly valve to release the fluid to the system
- Start 10 HP pump
- Wait till the flow is steady and isothermal in the entire system
- Set flow rate to desired value
- Start 230 V DC motor for rotating inner pipe
- Set inner pipe rotation rate to desired value
- Start data acquisition system
- Start 0-50V / 0-20 A switching power supply
- Connect ETRANS-M 210 electromagnetic flowmeter to the power supply
- Connect ETRANS-DP pressure transmitter to the power supply
- Start recording data
- As soon as the readings are stable, change one of the input parameters (flow rate, inner pipe rotation rate, temperature)
- Repeat the previous step until data is collected for all desired parameters.
- Stop recording data
- Disconnect flowmeter and pressure transmitter
- Stop power supply
- Stop the motor for inner pipe rotation
- Stop the pump
- Stop the motor for stirring the fluid inside the feeding tank
- Stop the heater

The detail of experimental tools and complete data set can be seen by interested readers in the previous work [21]. When the system is completely filled with the fluid, a motor pump of 10 HP is switched on. To make rotation pipes ready for rotating, 230 V DC motor is turned

on as well. Furthermore, a 0-50V / 0-20 A switching power supply is used in order to switch on ETRANS-M 210 electromagnetic flowmeter and ETRANS-DP pressure transmitter which are connected to a desktop PC via a DT80 data logger. Data logger retrieves the data each 5 seconds from the system and the data is stored in 5 minutes intervals for each flow condition. The pressure gradient and flow rate are recorded by taking their average during 5 minutes. The fluid is arranged to attain the desired flow value in the system by using the butterfly valve. Reynolds number of the system is between $3.8x10^4 - 1.08x10^5$. Then, the digital controller of the inner pipe rotation motor is set to the desired value of rotational speed as well. The fluid is allowed to run through the system for a certain time till the flow becomes steady and isothermal in the entire system. As soon as the readings are stable, experimental data recording is started. Input parameters are changed accordingly and repeated as in previous steps until data is collected for all desired parameters.

3. MECHANISTIC MODEL

Navier-Stokes equations for turbulent flow including pipe rotation in Cartesian Coordinate in an open form is formulated without assumptions as; (Bird et al. [22])

For the x-direction;

$$\rho\left(\frac{\partial u}{\partial t}+u\frac{\partial u}{\partial x}+v\frac{\partial u}{\partial y}+w\frac{\partial u}{\partial z}\right)=$$

$$-\frac{\partial P}{\partial x}+\left[\frac{\partial}{\partial x}\tau_{xx}+\frac{\partial}{\partial y}\tau_{yx}+\frac{\partial}{\partial z}\tau_{zx}\right]+\rho g_x-\frac{\partial\left(\rho u'^2\right)}{\partial x}-\frac{\partial(\rho u'v')}{\partial y}-\frac{\partial(\rho u'w')}{\partial z}+\rho\omega^2 y. \quad (1)$$

For the y-direction;

$$\rho\left(\frac{\partial v}{\partial t}+u\frac{\partial v}{\partial x}+v\frac{\partial v}{\partial y}+w\frac{\partial v}{\partial z}\right)=$$

$$-\frac{\partial P}{\partial y}+\left[\frac{\partial}{\partial x}\tau_{xy}+\frac{\partial}{\partial y}\tau_{yy}+\frac{\partial}{\partial z}\tau_{zy}\right]+\rho g_y-\frac{\partial(\rho u'v')}{\partial x}-\frac{\partial\left(\rho v'^2\right)}{\partial y}-\frac{\partial(\rho v'w')}{\partial z}. \quad (2)$$

For the z-direction;

$$\rho\left(\frac{\partial w}{\partial t}+u\frac{\partial w}{\partial x}+v\frac{\partial w}{\partial y}+w\frac{\partial w}{\partial z}\right)=$$

$$-\frac{\partial P}{\partial z}+\left[\frac{\partial}{\partial x}\tau_{xz}+\frac{\partial}{\partial y}\tau_{yz}+\frac{\partial}{\partial z}\tau_{zz}\right]+\rho g_z-\frac{\partial(\rho u'w')}{\partial x}-\frac{\partial(\rho v'w')}{\partial y}-\frac{\partial\left(\rho w'^2\right)}{\partial z}. \quad (3)$$

Necessary assumptions are assigned to simplify Navier-Stokes equations. The following assumptions are taken into account;

- fully developed turbulent flow
- steady state

- incompressible fluid

Moreover, Erge et al. [23] take into account other assumptions, which are no gravitational effects and an isothermal system. So, Navier-Stokes equations for Newtonian fluids in a narrow slot can be written as;

$$\frac{\partial}{\partial y}\left[(\mu+\mu_t)\frac{\partial u}{\partial y}\right]=\frac{\partial P}{\partial x}+\rho\omega^2 y. \tag{4}$$

In order to define turbulent viscosity, Prandtl's Mixing Length Hypothesis has been used in the literature [24]. Turbulent viscosity can be formulated as;

$$\mu_t=\rho l_m^2\left|\frac{\partial u}{\partial y}\right| \tag{5}$$

The mixing length can be expressed in the van Driest formula;

$$l_m=\kappa y \tag{6}$$

where κ is von Karman constant and its value is 0.4. The viscous effect is significant close to the wall and mixing length approaches zero at the wall. In order to account for this behavior, the viscous damping function could be added to the van Driest's formula;

$$l_m=\kappa y\left(1-e^{-\frac{y^+}{A}}\right) \tag{7}$$

where $y^+=\frac{y\sqrt{\tau_w\rho}}{\mu}$ and $\tau_w=-H\frac{\partial P}{\partial x}$. Here A represents van Driest's damping constant and it has been assumed to be 26 for smooth surfaces without suction or blowing. H is the half height of the annulus.

It is now obvious that both l_m and μ_t are the function of y. Chain rule method will be applied step by step to the final version of momentum equation for slot flow approximation. It can be seen in Eq. (8). Then, to solve the obtained equation, the finite difference algorithm is used.

$$(\mu+\mu_t)\frac{\partial^2 u}{\partial y^2}+2\rho l_m\frac{\partial l_m}{\partial y}\left(\frac{\partial u}{\partial y}\right)^2=\frac{\partial P}{\partial x}+\rho\omega^2 y \tag{8}$$

On both inner and outer pipe surfaces ($y=0\ or\ y=2H$) , it is assumed to exist a non-slip boundary condition. Due to symmetrical geometry of fluid flow, the boundary condition is taken only at the bottom of the channel as $u(y=0)=0$. On the other hand, there is no shear stress at the center of the flow in the annulus. In other words, the maximum velocity of the flow is reached at the center of the flow profile. In mathematical representation of this boundary condition is $\frac{du}{dy}(y=H)=0$.

In the present study, experiments were conducted for flow through the fully eccentric annulus. Therefore, the height of the annulus should be determined in view of the eccentric

annulus. Previous researchers used complex coordinates transformation, conformal mapping or computational iterations. Iyoho and Azar [25] proposed a model for determining height of eccentric annulus with a simple formula;

$$2H = \sqrt{r_o^2 - \varepsilon^2 c^2 sin^2\theta} - r_i + \varepsilon c cos\theta \tag{9}$$

3.1. Numerical Methods

In order to discretisize derivatives of the Eq. (8), the central difference scheme is used;

$$\frac{\partial u}{\partial y} = \frac{u_{i+1} - u_{i-1}}{2\Delta y} \tag{10}$$

$$\frac{\partial^2 u}{\partial y^2} = \frac{u_{i+1} - 2u_i + u_{i-1}}{(\Delta y)^2} \tag{11}$$

To proceed with the computer programming, derivative operators are needed to be put into matrix form by using the above formulas with accounting boundary conditions. Then, it leads to

$$\frac{\partial}{\partial y} = D_1 = \frac{1}{2\Delta y}\begin{pmatrix} 0 & 1 & 0 & \cdots & \cdots & 0 \\ -1 & 0 & 1 & 0 & \cdots & 0 \\ 0 & -1 & 0 & \ddots & \ddots & \vdots \\ \vdots & 0 & \ddots & \ddots & 1 & 0 \\ \vdots & \vdots & \ddots & -1 & 0 & 1 \\ 0 & 0 & \cdots & 0 & -1 & 0 \end{pmatrix} \tag{12}$$

$$\frac{\partial^2}{\partial y^2} = D_2 = \frac{1}{(\Delta y)^2}\begin{pmatrix} -2 & 1 & 0 & \cdots & \cdots & 0 \\ 1 & -2 & 1 & 0 & \cdots & 0 \\ 0 & 1 & -2 & \ddots & \ddots & \vdots \\ \vdots & 0 & \ddots & \ddots & 1 & 0 \\ \vdots & \vdots & \ddots & 1 & -2 & 1 \\ 0 & 0 & \cdots & 0 & 1 & -2 \end{pmatrix} \tag{13}$$

where D_1 and D_2 are $(N-1) \times (N-1)$ matrices in which N represents the number of discretization in the numerical solution. Therefore, the final version of the discretisized momentum equation for slot flow is as follows;

$$(\vec{\mu} + 2\vec{\mu}_t) D_2 \vec{u} + 2\rho \vec{l}_m D_1 \vec{l}_m (D_2 \vec{u})^2 = \vec{P}_x \tag{14}$$

Due to the symmetricity of the computational domain, Eq. (14) has been solved by using two approaches on the interval $[0, H]$ by dividing N equal sub-intervals.

3.2. A Semi-Analytical Method

The main idea of the semi-analytical method is based on frozen non-linear term. After getting rid of the non-linearity and embedding the matrices defined in Eq. (12) and (13) into Eq. (8), it is transformed into an algebraic equation such that

$$A\vec{U} = B$$

which is solved analytically. In literature Vidts and White [26] proposed a semi-analytical method for solving a linear partial differential equation. The authors also discretisized the space by considering central difference approximation and then an ordinary differential

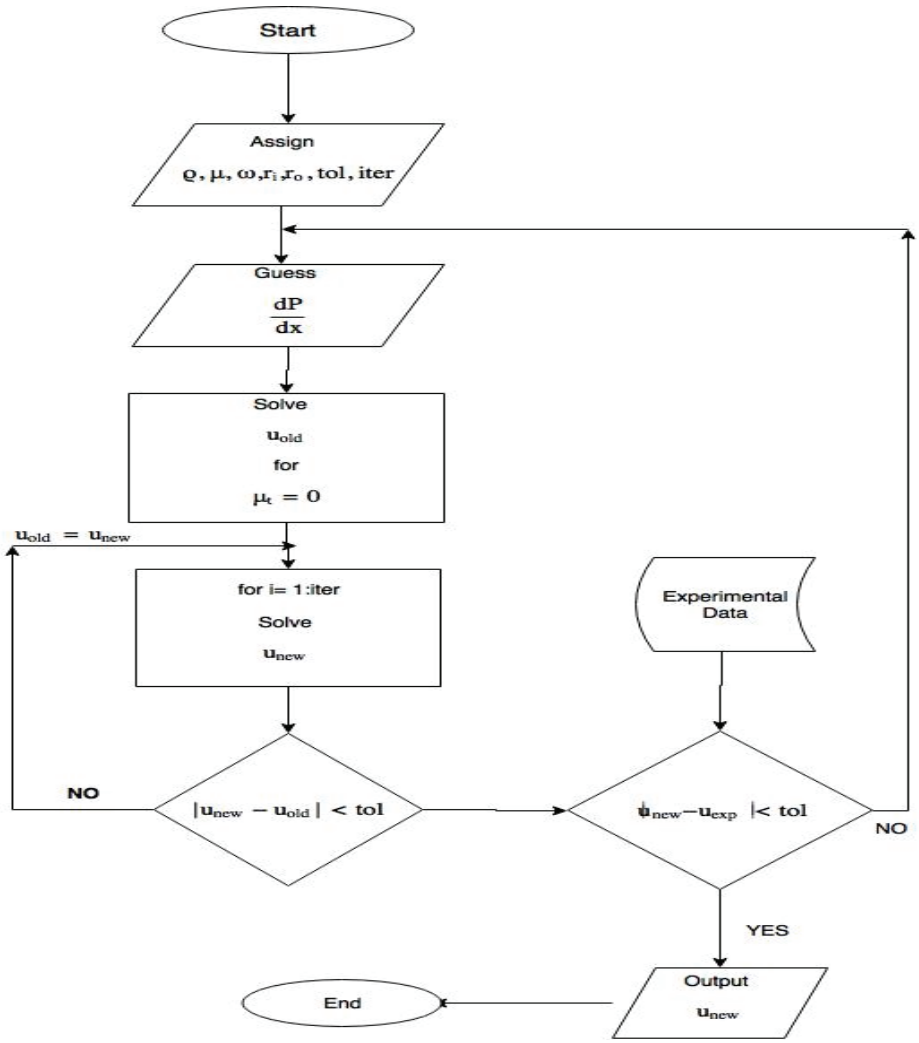

Figure 2. Flowchart of the computer code with new approach

equation is obtained which is solved analytically. Moreover, detailed discussion on the applications of semi-analytical methods for fluid flows can be found in [27]. One of the famous techniques for the semi-analytical solution is Adomian decomposition method. However, to obtain a series expansion the technique has tedious calculations therein. In the present study, an alternative semi-analytical method is suggested.

The process of the semi-analytical method is organized as follows: The initial assumption of the velocity profile is obtained by considering it laminar where the turbulent viscosity is assigned the value of zero. This assumption is taken as an old value of the velocity. In the iterative process, obtaining the new solution the non-linear term is frozen by using the old solution. After freezing the non-linear term the solution is obtained analytically. In order to obtain the final solution, the accuracy of the solution is checked by a given tolerance. If the tolerance is not attained, then it is returned back to the iterative loop by assigning the new solution as an old solution. Otherwise, the new solution is assigned as the pre-final solution. Then, the pre-final solution is compared with experimental data. If the error between the pre-final solution and experimental data is less than the given tolerance then the pre-final solution is assigned as the final solution. Otherwise, the program returns to assign initial assumptions of the pressure gradient. The flow chart of this program can be seen in Fig. 2.

3.3. Newton-Raphson Method

After getting an algebraic non-linear equation the question leads to finding the root instead of the solution. Thus, Newton-Raphson method is the well-known and accurate non-linear solver among engineers and scientists for finding the root of $F(\vec{u}) = 0$. Thus, Newton-Rapson method is used to check the validity of the solutions obtained via the semi-analytical method. The process of Newton's algorithms is defined as

$$\vec{u}_{n+1} = u_n - (F'(\vec{u}_n))^{-1} F(\vec{u}_n) \tag{15}$$

where $F: \mathbb{R}^n \to \mathbb{R}^n$ and $F(\vec{u}) \in C^2(\mathbb{R}^n)$. By fixing $\vec{u}_n$ the above equation becomes a linear equation even though $F(.)$ is non-linear. It is worth mentioning that the choice of the initial assumption, $\vec{u}_0 \in \mathbb{R}^n$, is a key point for both avoiding the singularity problem of $(F'(\vec{u}_n))^{-1}$ and also the convergence of the method. After doing tedious calculations we obtain

$$F(\vec{u}_n) = (\mu + 2\mu_t) D_2 \vec{u}_n + 2\rho l_m D_1 l_m (D_1 \vec{u})^2 - \vec{P}_x. \tag{16}$$

Here, $F'(\vec{u})$ denotes the derivative of $F(\vec{u})$ with respect to $\vec{u}$. Thus, the derivative of $F(\vec{u})$ in operator form is as follows:

$$F'(\vec{u}) = (\mu + 2\mu_t) D_2 + 2\rho l_m (D_1 l_m (2 D_1 \vec{u}) + l_m D_2 \vec{u}). \tag{17}$$

The operator forms defined in Eq. (16) and Eq. (17) are substituted into Newton-Raphson method given in Eq. (15). This equation is solved for $\vec{u}_{n+1}$. In the computational process of this approach, the initialization of the velocity, $\vec{u}_0$, is assigned as zero vector and this initialization vector is called the old solution. In the iterative process, solve Eq. (15) for getting the new solution for the velocity. Then, check the error of the solutions between the

new and the old solutions by a given tolerance. If the tolerance is not attained, then return to the iterative loop by assigning the new solution as an old solution. Otherwise, the new solution is assigned as the pre-final solution. Then, the pre-final solution is compared with experimental data. If the error between the pre-final solution and experimental data is less than the given tolerance then the pre-final solution is assigned as the final one. Otherwise, the program returns to assignation of the initial assumption of the pressure gradient.

3.4. Comparison of Both Methods

The computer codes are tested for 60 rpm inner pipe rotation and random pressure gradient. In Table 2, it can be seen that the discrepancy between Newton's method and the semi-analytical method is insignificant. Therefore, other important parameter-computational cost-is checked for the same procedure. Table 3 shows time elapsed values for each method for

Table 2. Comparison of Two Numerical Approches

Average Fluid Velocity (m/s)	Pressure Gradient (Pa/m)	Pressure Gradient (Pa/m)	Pressure Gradient (Pa/m)
	Newton's Method	Semi-Analytical Method	Experimental Result
1.09	354.112	354.108	312.074
1.41	526.893	526.881	510.901
1.74	732.615	732.622	731.447
2.44	1254.433	1254.456	1258.121
2.71	1539.298	1539.32	1578.124
3.37	2236.169	2236.179	2239.762

Table 3. Computational Cost For Two Models Used In The Present Study For Calculating Frictional Pressure Losses At Same Input Parameters

Elapsed Time (second)	
Newton's Method	Semi-Analytical Method
8.8	20
8.6	28
8.7	34
9.3	39
9.4	43
9.5	56
10.6	69

predicting average velocity at the same input parameters. It is seen that the semi-analytical method takes relatively longer time than the Newton's method. The mathematical content of hydraulics applications is far from trivial. Comprehensive understanding of the physical behavior of fluid flow is required for getting accurate solutions. Just recently, methods have been eventually available to predict all features of annular flow including its affecting parameters such as flow velocity, rotating cylinder, eccentricity while numerical approaches have been developing with technological enhancement.

4. RESULTS AND DISCUSSION

In the present study, a semi-analytical method is applied to fully developed turbulent Newtonian fluid flow in the eccentric annulus with pipe rotation. Because of the non-availability of the exact solution, the solutions obtained via the semi-analytical method is compared with a well-known numerical method, Newton-Raphson method, in terms of applicability and accuracy. However, the semi-analytical method takes relatively longer time than Newton's method. It is observed that increasing step size over 1000 makes no difference in pressure gradient for all cases. In other words, the step size is formulated as $\Delta y = \frac{H}{1000}$. Although the semi-analytical method is computationally expensive, it may help researchers to overcome the non-linearity of challenging problems in order to have the semi-analytical solution. The momentum equation of fully developed turbulent flow including inner pipe rotation in curvilinear coordinates, such as Bipolar coordinate that is one of the adequate coordinate systems for eccentric annulus geometry, is a good example of this challenging problem.

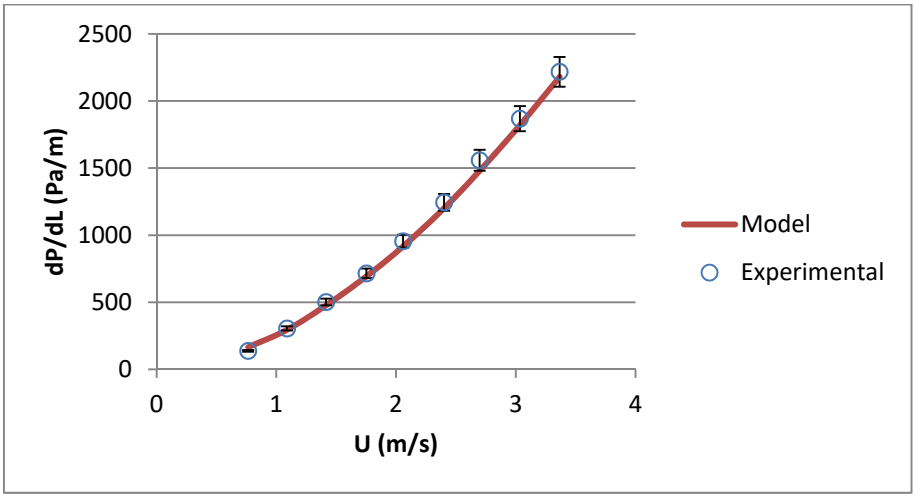

Figure 3. Comparison of measured and predicted pressure gradient without inner pipe rotation

After setting up all the assumptions and constant values, the results are obtained within a reasonable accuracy when it is compared with experimental data. Uncertainty analysis is used for determining the experimental uncertainties corresponding to experimental data. General uncertainty analysis using the Taylor series method is used. The previous study of Ulker et al. [21] is presented that the maximum uncertainty error for determining pressure gradient is around 5%. That means that the correlation has developed with a 95% level of confidence. Fig. 3 shows predicted and measured data for pressure gradient in fully eccentric annulus at room temperature without inner pipe rotation.

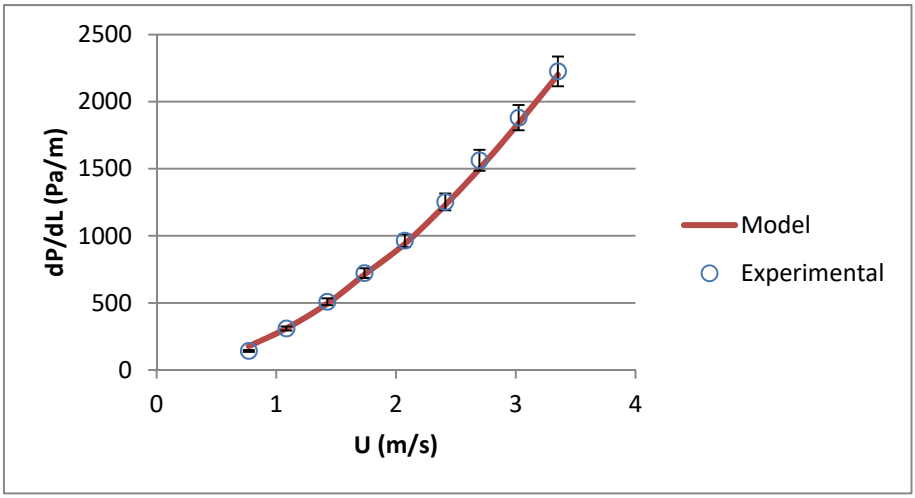

Figure 4. Comparison of measured and predicted pressure gradient for 30 rpm inner pipe rotation

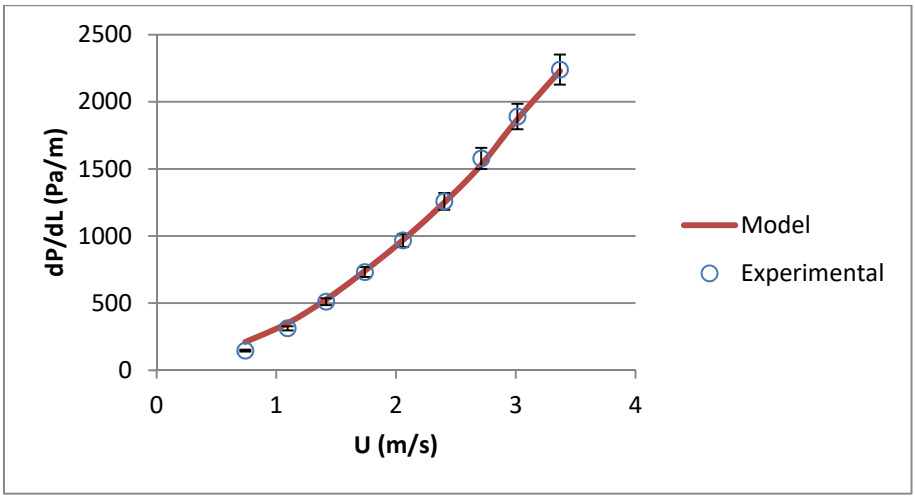

Figure 5. Comparison of measured and predicted pressure gradient for 60 rpm inner pipe rotation

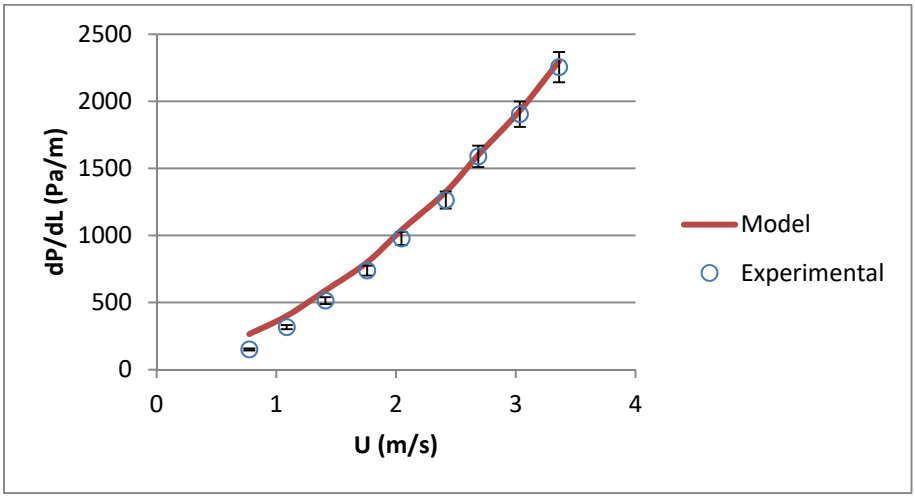

Figure 6. Comparison of measured and predicted pressure gradient for 90 rpm inner pipe rotation

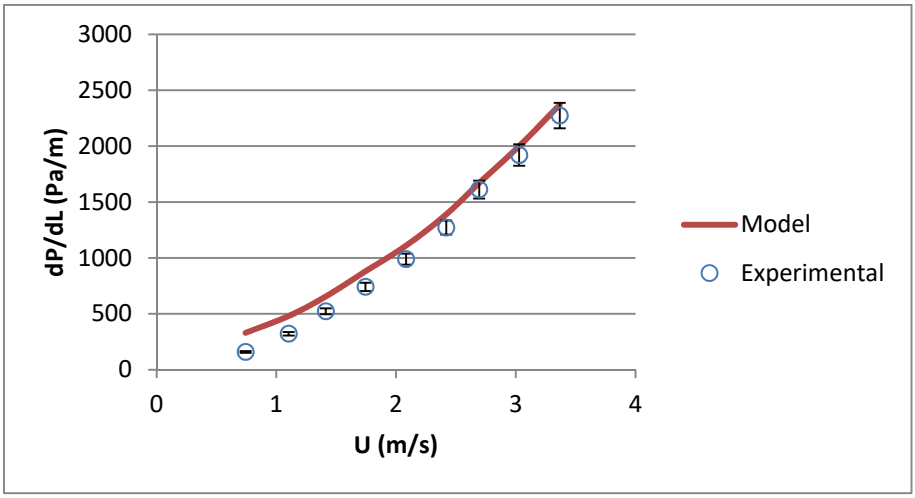

Figure 7. Comparison of measured and predicted pressure gradient for 120 rpm inner pipe rotation

The proposed model predicted the pressure gradient within 5.3% error margin. This shows the model has good accuracy. From now on, rotation effects can be included and compared. Figs. 4-7 show the pressure gradient for different inner pipe rotation rates.

When the Figs. 4-7 are analyzed, it can be concluded that the model can predict better pressure gradient at higher velocities. At lower velocities and high inner pipe rotation rate,

the model prediction performance is deteriorating. The reason is the wobbling effect of the inner pipe due to concentric ends. The axial velocity couldn't overcome this effect at lower velocities. Therefore, the discrepancy between the results arises.

The proposed mechanistic model gives reasonably close values with respect to experimental measurements. To have better insight, the performance of the methods is measured by calculating Average Absolute Percent Error (AAPE) and the result shows that pressure gradient for Newtonian fluid flow in fully eccentric annulus without inner pipe rotation and at room temperature can be predicted within a 5.3% error margin by using the semi-analytical method. However, the error increases as the effect of pipe rotation take part in the flow. Nevertheless, the model can determine a pressure gradient up to 14% error margin for all cases.

5. CONCLUSION

In the present study, two different methods are used to solve Navier-Stokes equations including inner pipe rotation effects and turbulent flow. The equation is primarily discretisized by the semi-analytical method via the central difference approximation and solved analytically in each iteration by freezing the non-linear terms. Even though the non-linear terms are frozen in each iteration, the fixed terms are renewed by the previous solution in each step. In other words, pressure gradient and the turbulent viscosity are solved sequentially. The results of the semi-analytical method are confirmed by a well-known "Newton-Raphson method". Although the former is computationally expensive, this numerical technique may allow solving challenging problems in a semi-analytical way. Additionally, the semi-analytical method predicts pressure gradient successfully. A mechanistic model is developed using the semi-analytical method for fully developed turbulent flow through eccentric annulus including inner pipe rotation. When the developed mechanistic model is compared with experimental measurements, it gives reasonably good agreement. Results show that without rotation, the developed model can determine pressure gradient within a 5.3% error margin. However, the discrepancy between experimental and numerical results gets higher when inner pipe rotation plays role in the system. Nevertheless, the model can determine pressure gradient within 14% error margin for all cases.

Symbols

$\boldsymbol{A}$ = van Driest's damping constant (-)

$\boldsymbol{c}$ = Concentric radial clearence (m)

$\boldsymbol{H}$ = Half width of the slot (m)

$\boldsymbol{l_m}$ = Mixing length (m)

$\boldsymbol{P}$ = Pressure (Pa)

$\boldsymbol{r_i}$ = Inner pipe radius (m)

$\boldsymbol{r_o}$ = Outer pipe radius (m)

t = Time (s)

u, v, w = Velocity components in cartesian coordinate (m s^{-1})

$\bar{u}, \bar{v}, \bar{w}$ = Mean velocity components (m s^{-1})

$\acute{u}, \acute{v}, \acute{w}$ = Fluctuating velocity components (m s^{-1})

ε = Eccentricity

ω = Pipe rotation speed (rad s^{-1})

ρ = Density (kg m^{-3})

τ_{ij} = Stress tensor (Pa)

ν = Kinematic viscosity (m^2 s^{-1})

θ = Angle (rad)

μ = Dynamic viscosity (Pa s)

μ_t = Turbulent viscosity (Pa s)

κ = von Karman constant (-)

References

[1] Deissler, R. G. (1954). Analysis of turbulent heat transfer, mass transfer, and friction in smooth tubes at high Prandtl and Schmidt numbers.

[2] Deissler, R. G., & Taylor, M. F. (1955). Analysis of fully developed turbulent heat transfer and flow in an annulus with various eccentricities. NACA Tech. Note 3451.

[3] Wolffe, R. A., & Clump, C. W. (1963). The maximum velocity locus for axial turbulent flow in an eccentric annulus. AIChE Journal, 9(3), 424-425.

[4] Heyda, J. F. (1959). A Green's function solution for the case of laminar incompressible flow between non-concentric circular cylinders. Journal of the Franklin Institute, 267(1), 25-34.

[5] Jonsson, V. K., & Sparrow, E. M. (1965). Results of laminar flow analysis and turbulent flow experiments for eccentric annular ducts. AIChE Journal, 11(6), 1143-1145.

[6] Jonsson, V. K., & Sparrow, E. M. (1966). Experiments on turbulent-flow phenomena in eccentric annular ducts. Journal of Fluid Mechanics, 25(01), 65-86.

[7] Rehme, K. (1973). Simple method of predicting friction factors of turbulent flow in non-circular channels. International Journal of Heat and Mass Transfer, 16(5), 933-950.

[8] Kacker, S. C. (1973). Some aspects of fully developed turbulent flow in non-circular ducts. Journal of Fluid Mechanics, 57(03), 583-602.

[9] Usui, H., & Tsuruta, K. (1980). Analysis of fully developed turbulent flow in an eccentric annulus. Journal of Chemical Engineering of Japan, 13(6), 445-450.

[10] Tosun, I. (1984). Axial laminar flow in an eccentric annulus: an approximate solution. AIChE journal, 30(5), 877-878.

[11] Özgen, C., & Tosun, I. (1987). Application of geometric inversion to the eccentric annulus system. AIChE journal, 33(11), 1903-1907.

[12] Uner, D., Ozgen, C., & Tosun, I. (1988). An approximate solution for non-Newtonian flow in eccentric annuli. Industrial & engineering chemistry research, 27(4), 698-701.

[13] Ogino, F., Sakano, T., & Mizushina, T. (1987). Momentum and heat transfers from fully developed turbulent flow in an eccentric annulus to inner and outer tube walls. Heat and Mass Transfer, 21(2), 87-93.

[14] Haciislamoglu, M., & Langlinais, J. (1990). Non-Newtonian flow in eccentric annuli. Transactions of the ASME. Journal of Energy Resources Technology, 112(3), 163-169.

[15] Nouri, J. M., Umur, H., & Whitelaw, J. H. (1993). Flow of Newtonian and non-Newtonian fluids in concentric and eccentric annuli. Journal of Fluid Mechanics, 253, 617-641.

[16] Nouri, J. M., & Whitelaw, J. H. (1994). Flow of Newtonian and non-Newtonian fluids in a concentric annulus with rotation of the inner cylinder. Transactions-American Society Of Mechanical Engineers Journal Of Fluids Engineering, 116, 821-821.

[17] Erge, O., Ozbayoglu, M. E., Miska, S. Z., Yu, M., Takach, N., Saasen, A., & May, R. (2014). Effect of drillstring deflection and rotary speed on annular frictional pressure losses. Journal of Energy Resources Technology, 136(4), 042909.

[18] Mossa, M. (2006). Resistance coefficient in a smooth concentric annular pipe. Journal of Hydraulic Research, 44(6), 832-840.

[19] Erge, O., Vajargah, A. K., Ozbayoglu, M. E., & van Oort, E. (2016, March). Improved ECD Prediction and Management in Horizontal and Extended Reach Wells with Eccentric Drillstrings. In IADC/SPE Drilling Conference and Exhibition. Society of Petroleum Engineers.

[20] Rushd, S., Shazed, A. R., Faiz, T., Kelessidis, V., Hassan, I. G., & Rahman, A. (2017, March). CFD Simulation of Pressure Losses in Eccentric Horizontal Wells. In SPE Middle East Oil & Gas Show and Conference. Society of Petroleum Engineers.

[21] Ulker, E., Sorgun, M., Solmus, I., & Karadeniz, Z. H. (2017). Determination of Newtonian Fluid Flow Behavior Including Temperature Effects in Fully Eccentric Annulus. Journal of Energy Resources Technology, 139(4),04200.

[22] Bird, R. Byron, Warren E. Stewart, and Edwin N. Lightfoot (2002) Transport phenomena. John Wiley & Sons.

[23] Erge, O., Vajargah, A. K., Ozbayoglu, M. E., & Van Oort, E. (2015). Frictional pressure loss of drilling fluids in a fully eccentric annulus. Journal of Natural Gas Science and Engineering, 26, 1119-1129.

[24] Azouz, I., & Shirazi, S. A. (1998). Evaluation of several turbulence models for turbulent flow in concentric and eccentric annuli. Journal of energy resources technology, 120(4), 268-275.

[25] Iyoho, Aniekan W., and Jamal J. Azar. (1981) An accurate slot-flow model for non-Newtonian fluid flow through eccentric annuli, Society of Petroleum Engineers Journal 21.05: 565-572.

[26] Vidts, P. De and White, R. E.(1992) A semi-analytical solution method for linear partial differential equations. Computers & Chemical Engineering, 16(10-11): 1007-1009

[27] Sheikholeslami M, Ganji D. D. (2017) Applications of Nanofluid for Heat Transfer Enhancement. Elsevier.

Teknik Dergi, 2018 8515-8535, Paper 510

Experimental Study Concerning Iron Wire Fiber Reinforced Asphalt Concrete

Sevil KÖFTECİ[1]

ABSTRACT

The usability of low-cost iron wire fiber for reinforcement of hot asphalt mixtures was investigated with experiments in this study. Five mixtures having different fiber content of 1%, 3%, 5%, 7%, 9% and control mixtures were prepared. Characteristic properties of bitumen, aggregate and iron wire used in the mixtures were determined by thermogravimetric analysis (TGA), conventional bitumen tests, conventional aggregate tests, and metal tensile tests. After optimum bitumen rate was determined Marshall Stability Test, Cantabro Tests were performed in order to measure the performance of the mixtures. Additionally, moisture susceptibility of samples was determined with indirect tensile strength test. As a result of indirect tensile strength tests, indirect tensile strength (St) and indirect tensile strength ratio (ITSR) values were calculated. The results of the investigations indicate that the addition of low-cost iron fiber in the amount of 1%-3% improved performance of asphalt mixtures. When the used fiber rate was increased over 3%, clustering created by fibers was observed through stereo-microscope observations. Consequently, air voids were increased and bitumen-aggregate interaction decreased. Increasing fiber ratio especially, at 7-9 percent caused compressing, durability and stability problems in the mixture.

Keywords: Reinforced asphalt concrete, iron wire fiber, Marshall stability, moisture susceptibility.

INTRODUCTION

A large rate of transportation activities in the world are performed through highways. Asphalt mixtures are the most widely used construction material in road building throughout the world. Bitumen and aggregates used in asphalt mixtures are sensitive materials especially against repetitive traffic loads and temperature. Therefore, highway pavements deteriorate before their preplanned service life. Primary means to avoid this deterioration is to enhance the structural properties of the mixture by using additives. Additives can be introduced into asphalt pavements using two methods. Polymer-based additives can be applied to the bitumen / mixture [1] or fibers can be added to the mixture.

Note:
- This paper has been received on November 08, 2017 and accepted for publication by the Editorial Board on April 17, 2018.
- Discussions on this paper will be accepted by September 30, 2018.
- DOI: 10.18400/tekderg.350135

1 Akdeniz University, Department of Civil Engineering, Antalya, Turkey - skofteci@akdeniz.edu.tr

Fiber additives have been used to improve properties of the composite materials for many years. Fibers such as steel fiber, polymer fiber, natural fiber etc. are frequently used for the reinforcement of concrete and mortars, and there are various studies regarding this particular topic in related literature [2-4]. Fibers are usually used in Stone Mastic Asphalt (SMA) which has a gap-graded configuration and porous asphalt which has an open-graded configuration, in order to prevent draining of bitumen between aggregates [5, 6]. However, in recent years, as well as concrete, in order to improve resistance to cracking and rutting of the asphalt mixtures, fibers have been generally utilized as additional constituents. Some fibers have higher tensile strength as related to asphalt mixtures, thus it was observed that fibers have the potential to improve cohesion and tensile strength of bituminous mixes [7].

A wide variety of fiber types has been used in asphalt mixtures, including cellulose, mineral, synthetic polymer, and glass fibers, as well as some less common fiber types. Recycled fiber materials-such as newsprint, carpet fibers, and recycled tire fibers-have also been used [8]. There are numerous studies in the literature regarding strengthening of asphalt concrete with fibers. [9-11]. Guo [12] used a steel fiber in order to improve the mechanical properties of asphalt concrete. In this article, analyzing the test results such as rutting test, low temperature bending test, freeze-thaw splitting test and comparing stability of mixtures in high temperature, anti-cracking performance in low temperature and comparing water stability of steel fiber asphalt concrete with ordinary asphalt concrete, it is concluded that adding steel fibers into asphalt concrete can significantly improve the performance of the road surface. Al-Ridha et al [13] conducted a study on the effect of steel fibers on the performance of hot mix asphalt with 5% asphalt content at different temperatures and compaction levels. According to the test results, it is recommended use of steel fibers in the layers that are under the surface layer, such as the binder course, in the amount that is less than or equal to 0.2%. Garcia et al [14] investigated the use of steel wool fibers in dense asphalt concrete to improve mechanical properties. Additionally, fibers (steel wool) distribution and their effect on the porosity and electrical conductivity of asphalt mixtures was investigated. Experimentally obtained results indicated that short and thick fibers disperse very well in mixtures. The study recommended that fiber content in the asphalt mixture must be 6% or higher in order to attain satisfying results. Serin et al. [15] examined the effect of fibers in asphalt concrete mixtures. The study concluded that fiber additions can be used in the binder course of flexible pavements because of its positive impact on stability. Based on the results, it is recommended to use fiber 0.75% in weights in order to obtain best results.

In the current study, due to the high costs of steel fibers, use of low-cost iron wire is currently being considered as asphalt concrete additive. For this purpose, Marshall Stability (MS) test, Cantabro test and Indirect Tensile Strength Test (ITS) were performed. Iron fiber was obtained from the building site at the Akdeniz University campus. Depending on the results of these experiments, impacts and usability of low-cost iron fiber in hot mix asphalt were investigated regarding stability, raveling, flexibility as well as moisture susceptibility effects.

2. MATERIALS AND METHODS

2.1. Materials

2.1.1. Bitumen

The bitumen 50/70 penetration grade was obtained from Aliağa/İzmir Refinery of the Turkish Petroleum Refineries Corporation (TUPRAS). Conventional bitumen tests on the aged and unaged bitumen such as penetration, softening point etc and thermogravimetric analysis (TGA) were performed in order to determine the properties of the bitumen. Temperature-dependent deterioration of bitumen binder used in the study was determined by thermogravimetric analysis (TGA) method. This temperature value was calculated by using the proportional reduction in weight. In the TGA test, reduction of weight proportions was measured under nitrogen atmosphere at 10 ^{0}C/min heating rate. While the test was performed, temperature range was measured in the range of 250 ^{0}C to 600 ^{0}C. Figure 1 shows the TGA test results.

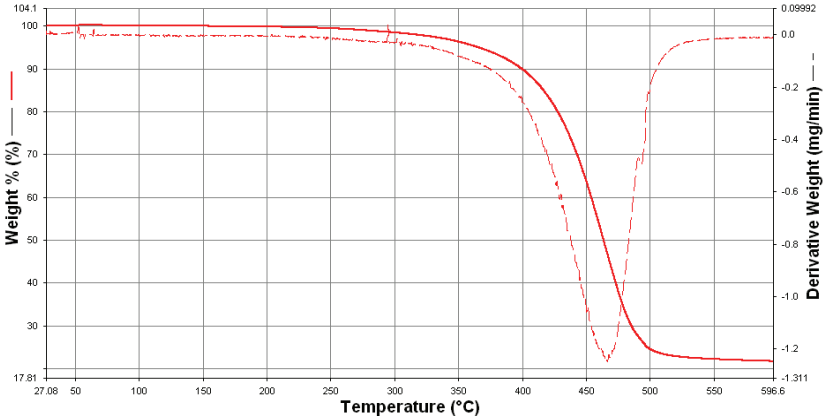

Figure 1. TGA result of bitumen used in the study

Table 1. Characteristic properties of the bitumen

Test	Specification	Results	Specification limits
Penetration (25 ºC; 0.1mm)	TS EN 1426	64	50-70
Softening point ºC;)	TS EN 1427	490C	46-54
Penetration index(PI)	-	-0,88	-
Ductility (25 C0;5 cm/min)	TS 119	>100	-
Flash point, 0C (Cleveland open cup)	TS ISO 2592	298 0C	230 (min)
Thin Film Oven Test (TFOT) (163 0C; 5h)	TS EN 12607-2		
Change of mass (%)		0.04	0.5 (max)
Change of softening point (ºC;)	TS EN 1427	2,2	9 (max)
Retained penetration (%)	TS EN 1426	56	50 (min)
Specific gravity	TS 1087	1.033	-

With increasing temperature, weight was not affected until 240 ^{0}C. After this temperature, weight decreased with increasing temperature. This meant that the bitumen binder started to deteriorate. Reduction of the total weight was determined as 78 %. Table 1 gives a summary of the results and their conformity with the relevant test methods of conventional tests performed on the 50/70 penetration grade bitumen.

2.1.2. Aggregates

Limestone aggregates were used for the preparation of samples. Aggregates were obtained from the quarries around Antalya. Limestone aggregates are generally used in Antalya for making of bituminous hot mixtures. In order to determine aggregate properties, aggregate tests were performed on coarse as well as fine aggregates and fillers. Results of tests were evaluated according to various specifications which are stated in the Turkish Highway Specifications 2013 [16]. Table 2 gives a summary of the results and their conformity with the relevant test methods of aggregates.

Table 2. Characteristic properties of the limestone aggregates

Aggregate type	Test	Specification	Results	Specification limits
Coarse aggergate	Volume specific gravity	ASTM C127	2,693	-
	Apparent specific gravity	ASTM C127	2,710	-
	Water absorption (%)	TS EN 1097/6	0,28	≤2,5
	Los angeles abrasion (%)	AASHTO T96	22,40	≤30
	Micro-Deval abrasion (%)	TS EN 1097-1	18,24	≤25
	Soundess of aggregate by use of Magnesiun Sulfate (%)	TS EN 1367-2	10,22	≤18
	Flakiness index (%)	BS 812	13,07	≤30
	Stripping resistance, (%)	TS EN 12697-11	85	≥60
Fine aggregate	Volume specific gravity (g/cm3)	ASTM C127	2,44	-
	Apparent specific gravity	ASTM C127	2,72	-
	Water absorption (%)	TS EN 1097/6	0,43	≤2,5
	Plasticity index (%)	TE 1900-1	N.P.	-
	Methylene blue, (g/kg)	TS EN 933-9	1,5	≤1,5
Filler	Apparent specific gravity	ASTM C127	2,69	-

Aggregates were brought to the laboratory in four groups. Mixture ratios were calculated according to binder course specifications based on the Turkish Highway Specifications 2013. Table 3 shows the mixture ratios used for mixture gradation.

Table 3. Mixture raitos

Sieve size	Mixture ratio
25 mm. - 19 mm.	26
19 mm.- 12,5 mm.	16
12,5 mm. – 4,75 mm.	20
< 4 mm.	38

Gradation of aggregates is very important for the design of mixtures. In order to prepare Marshall samples, aggregates were mixed by using the grading curve in Fig. 2.

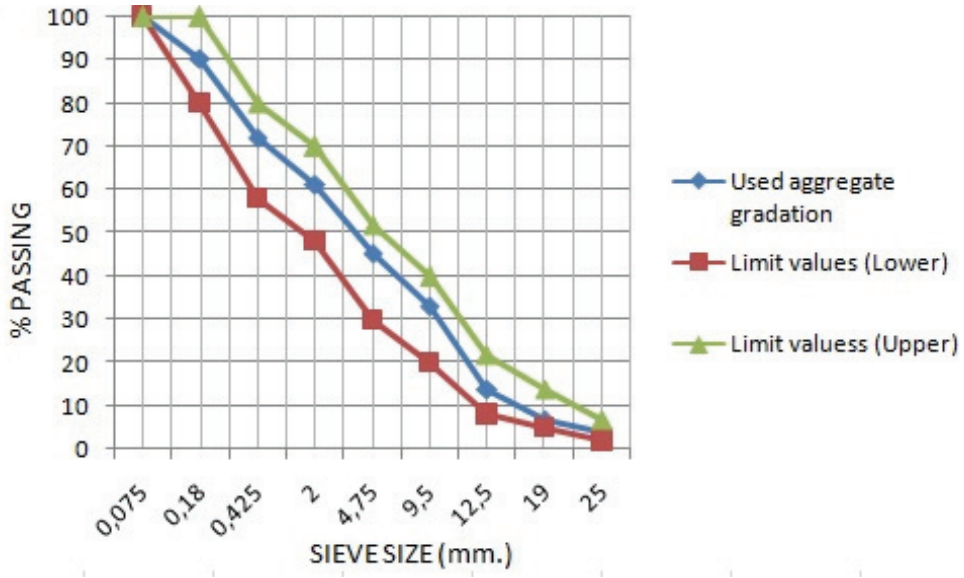

Figure 2. Aggregate grading curve

2.1.3. Iron Fiber

In this study, low-cost iron fiber which has the smallest diameter used in the construction industry was used. To this end, building site in the university was visited and iron wires were taken from the site in the shape of wire rolls. These iron fibers are very cheap and it can be found easily at every construction site. They are not specially produced steel fibers. In the road pavement laboratory, each wire coil was cut using hoof pliers. Length of wires varies in the range of 6 to 10 mm. Diameter of wires measured 1 mm. In the experiments, especially for the preparation of each sample, it was paid attention to the use of the fibers of approximately the same length. Fig 3 shows the wires used in the study.

Figure 3. Wire roll and cut iron pieces

In order to determine the strength of the iron fiber, metal tensile test was performed. According to test results, maximum stress and maximum strain values were measured as 444.599 N/mm^2 and 44.76% respectively. In view of values obtained from metal tensile tests, it can be said that iron fiber showed good performance in terms of strength. Figure 4 shows the metal tensile test results.

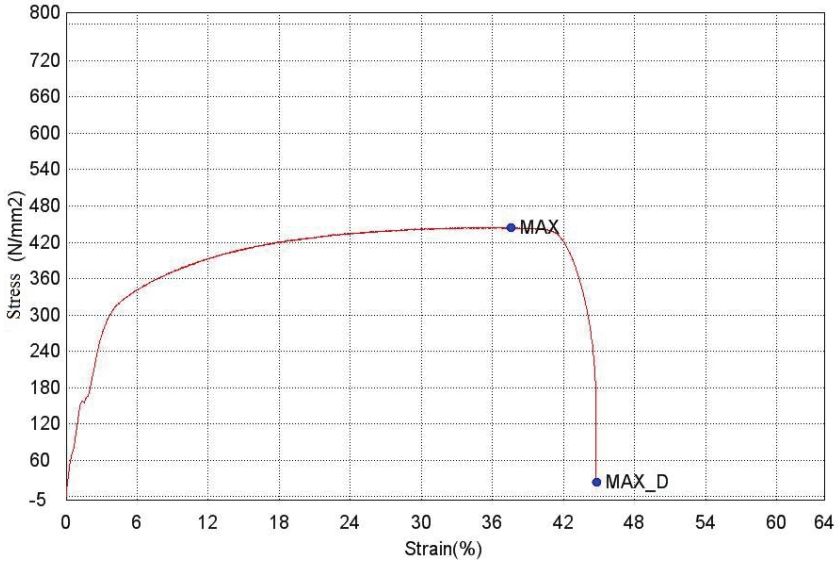

Figure 4. Curve of stress versus strain for iron fiber

2.2. Methods

2.2.1. Determination of Optimum Bitumen Content

In this study, the optimum bitumen content was determined using the Marshall mix design method described in AASHTO T 245-97. Mixtures with limestone aggregates weighing 1150 g. and 50/70 penetration bitumen were prepared for six different bitumen content

(3.0%, 3.50%, 4.0%, 4.50%, 5.0% and 5.50%). The sum total of the samples prepared for determination of optimum bitumen content was 18 (3 x 6). In the experiments, aggregates were heated at about 165 ^{0}C and bitumen was heated at about 150 ^{0}C. Both of them were heated at different ovens. Then they were introduced into the mixer and mixed for 120 seconds. The temperature of the mixture must be a minimum of 140 ^{0}C. For this reason, the temperature of the mixture was controlled continuously by using infrared thermometer during mixing. Prepared hot mixtures were placed in steel molds and compacted using Marshall compactor in order to obtain Marshall samples. Table 4 shows the hot mix asphalt design criteria for binder course according to the Turkish Highway Construction Specifications 2013.

Table 4. Hot mix asphalt design criterias

Features	Binder course		Specification
	Min.	Max.	
The number of blows to be applied making briquettes	75		TS EN 121697-30
Marshall stability, Kg	750	-	TS EN 121697-34
Voids volume, %	4	6	TS EN 121697-8
Voids filled with bitumen, %	60	75	TS EN 121697-8
Voids between mineral aggregates, %	13	15	TS EN 121697-8
Flow, mm (10-2inch)	2(8)	4(16)	TS EN 121697-34
Filler/Bitumen ratio	-	1,4	-
Bitumen (Weight percent)	3,5	6,5	TS EN 121697-1
ITSR ratio (% Min)	80		AASHTO T2 83

In the next step 18 samples were tested using the Marshall Stability Test machine. This test should be performed at 60 ^{0}C. To ensure this condition, samples were kept in a water bath at 60 ^{0}C for 40 minutes. Then samples were broken with a machine and Marshall stability, as well as Marshall flow values, were measured. Using these values, eight curves were plotted. These values were obtained from the curves; Bulk specific gravity (Dp) versus bitumen content, Marshall stability versus bitumen content; Marshall flow versus bitumen contents; percentage of air void (Vh)versus bitumen content; percentage of void filled with bitumen (V.F.A.) versus bitumen content; percentage of void in mineral aggregates versus bitumen content. Figure 5 shows the curves which are used for determining optimum bitumen content.

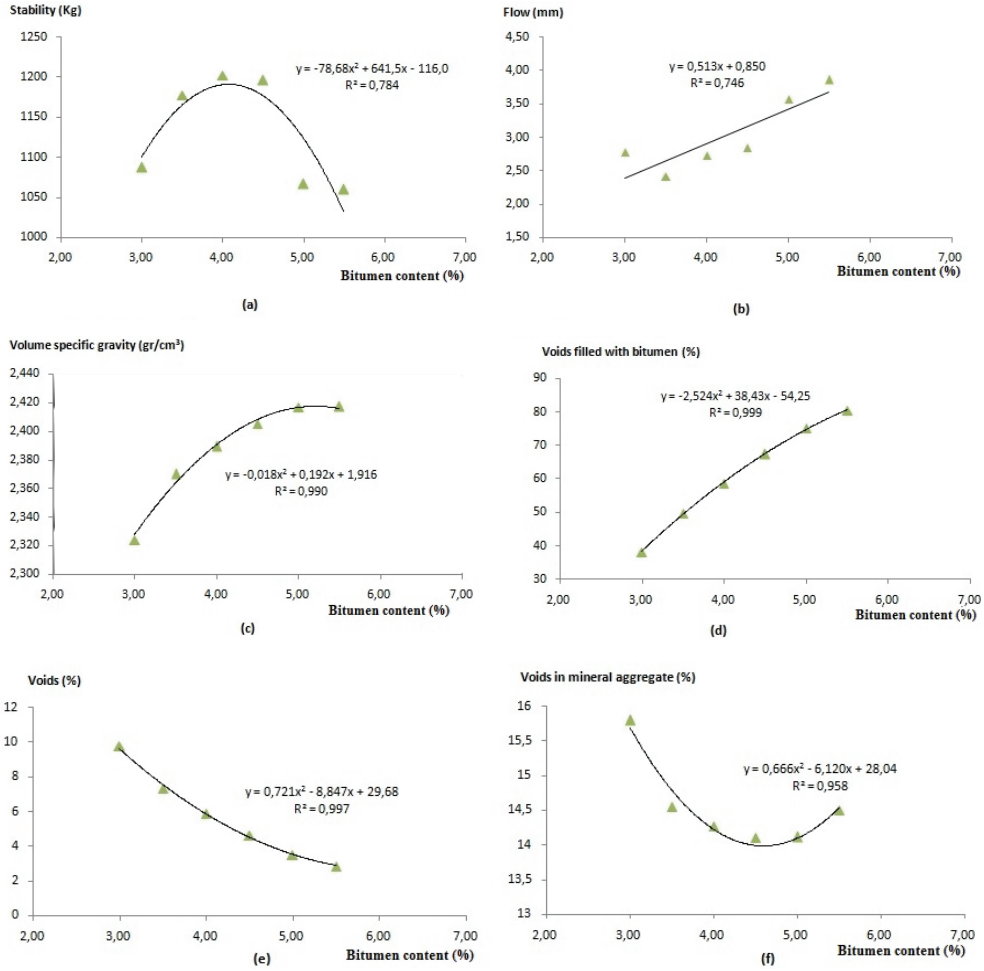

Figure 5. Graphs prepared according to bitumen content.

The optimum bitumen content was determined by taking into consideration four values which are obtained from the above curves. First value was determined from the stability curve which corresponds to maximum stability (a). The second value was obtained from volume specific gravity curve which corresponds to maximum volume specific gravity value (b). The third value was obtained from the voids graph (e). According to hot mix asphalt design criteria (seen from Table 4), the percentage of air voids should be between 4-6 % for the binder course. For this reason, average value of these limits was calculated and bitumen content corresponding to this value was determined. The last value was obtained from voids filled with bitumen graph (d). According to Table 4, the percentage of voids filled with bitumen should be between 60-75 % for the binder course. Average value of these limits was calculated and bitumen content corresponding to this value was determined. Considering these values, optimum bitumen content was calculated as follows:

$$\frac{4{,}10 + 5{,}0 + 4{,}2 + 4{,}3}{4} = 4{,}40$$

2.2.2. Preparation of Asphalt Mixtures Reinforced With Low-Cost Iron Wires

After optimum bitumen ratio was determined, iron fibers were added in different ratios (1%, 2%, 5%, 7%, 9%) by weight of the aggregates (1150) g. during mixing aggregates and bitumen. The samples used in the study were coded as below:

Control mix + 0% IWR – "CMIX"

Control mix + 1% IWR - "MIX-1-IWR"

Control mix + 3% IWR - "MIX-3-IWR"

Control mix + 5% IWR - "MIX-5-IWR"

Control mix + 7% IWR - "MIX-7-IWR"

Control mix + 9% IWR - "MIX-9-IWR"

2.2.3. Marshall Stability Test

After samples were prepared, weights of each sample in air and water, as well as heights for three-points were measured. By using these values and the other parameters such as bitumen and aggregate specific gravity, air voids (V_h), voids in mineral aggregate (VMA) and voids filled with bitumen (V_f) for each sample was drawn. Void in the bituminous hot mixture (V_h) is a small air gap between aggregates coated with bitumen. This value used in order to obtain durable pavements. V_h was calculated according to the following equation:

$$V_h = \frac{D_T - D_P}{D_T} x100 \quad (1)$$

where $D_p$is the volume the specific gravity of compacted mixture, D_T is the max. specific gravity of the uncompacted mixture. V_f represents the thickness of the bitumen film. The following equation was used to calculate V_f [17]:

$$V_f = \frac{VMA - V_h}{VMA} x100 \quad (2)$$

where VMA represents the voids in mineral aggregates, V_h indicates voids in the bituminous mixture. VMA is defined as gaps between aggregates in compacted hot mixtures. In other words, VMA includes the air voids and V_f (not absorbed). VMA proportion is very important in order to determine adequate film asphalt film thickness around each aggregate grain. This value is closely related to the durability and stability of mixtures. VMA was calculated as follows [17]:

$$VMA = 100 - \frac{D_p}{G_{sb}} x \frac{100}{100 + W_a} x100 \quad (3)$$

where D_p is the volume specific gravity of the compacted mixture, G_{sb} is the volume specific gravity of the aggregates, W_a is the bitumen ratio. Strength and flow values were determined by using a fully automatic Marshall stability test machine. The strength of the mixture is measured in terms of Marshall stability value. Compressive loading was implemented on the Marshall sample at a loading rate of just about 51 mm/min. until sample brakes. This test is performed at 60 ^{0}C which represents an favorable temperature according to specifications. The flow value shows the flexibility properties of the hot mixtures. This value measured by the change in diameter of the sample from the start of the loading until the stability values begin to decrease. Both stability and flow values are determined by using the Marshall stability device.

Marshall Quotient (MQ) represents the ratio of load to deformation. This value can be used to give an indication of the mixture's stiffness. This value is usually used by European agencies and is also known as the Marshall rigidity [18]. MQ which is well known as a form of pseudo stiffness is recognized as a measure resistance of materials to shear stresses, permanent deformation and hence rutting [19]. Arabani and Tahami [20] investigated the use of rice husk ash as modifier in asphalt mixture and calculated MQ, as well as rutting parameter (G*/Sin δ), were G* is the complex modulus and Sin δ is the phase angle of pure and modified samples. The study concluded that MQ can be using as an indicator of rutting resistance of the asphalt mixture. Gibreil and Feng [21] examined the effects of high-density polyethylene and crumb rubber powder as modifiers on properties of hot mix asphalt. Results showed that samples of which MQ values were calculated higher than the others showed higher resistance to rutting. The type of gradation significantly affects the validity of the MQ results. Conventional dense graded mixes normally combine high stability with low flow values and hence high MQ values, indicating a high stiffness mix with a greater ability to spread the applied load and resist creep deformation [22]. Tayfur et al.[23] evaluated the rutting performance of asphalt mixtures containing polymer modifiers by using MQ values and other performance tests. Results showed that Marshall Quotient may not be a good indicator of measuring permanent deformation for stone mastic asphalt mixtures. Similarly, Sengul et al. [24] evaluated the BS modified stone mastic asphalt pavement performance. They stated after MQ evaluation that MQ may not be a good indicator of measuring permanent deformation for stone mastic asphalt mixtures.

2.2.4. Cantabro Test

Asphalt mixtures are subjected to wearing effects continuously due to traffic loads. For this reason, mass loss of pavements occur. The most common method for determination of mass loss is the cantabro test. Cantabro test is usually used for the OGFC (Open-Graded Friction Courses) mixtures such as porous asphalt [25-27]. However, there are numerous studies in the literature which are related to usage of these methods for dense gradations [28-32]. In this study, cantabro test was carried out according to the Turkish standard TS EN 12697-17. In this test, Marshall samples of different types of mixtures were tested by using the Los Angeles drum. During the test, weights of samples were measured (M_1). Then samples were placed

in the drum without steel spheres. The drum was rotated 300 times with a speed of 30-33 rpm. Finally, weights of damaged samples were measured again (M_2). The following equation was used to calculate the percentage of mass loss (K):

$$K = 100 \text{ x } \frac{M_1 - M_2}{M_1} \quad (4)$$

In this study, cantabro test was performed on aged and unaged samples. In order to prepare aged samples, samples were placed in the forced draft oven at 60 ^{0}C for seven days. Unaged samples were kept at room temperature. Then both groups of samples were tested according to the procedure described above.

2.2.5. Indirect Tensile Strength Test and Moisture Sensitivity

Moisture-induced damage in asphalt mixtures, better known as stripping, is one of the primary causes of distress in the asphalt pavement layers [33]. For this reason, moisture susceptibility of the samples was investigated. The moisture susceptibility of the samples at optimum asphalt content was prepared and evaluated according to AASHTO T283. The results of these tests are the indirect tensile strength (St) and the indirect tensile strength ratio (ITSR). Mixtures were prepared for each additive percentage. Maximum theoretical specific weight, bulk specific gravity and volume values of each sample were calculated. Samples were divided into two groups according to average air void and defined as unconditioned and conditioned. Unconditioned samples were placed in sealed plastic bags and they were kept at room temperature. Conditioned samples were saturated with water by use of a vacuum desicator to obtain 70%-80% saturated samples. Then, they were wrapped with stretch film and they were placed in plastic bags with 10 ml. water. In the next step, conditioned samples were placed in a deep freezer at (-18) ^{0}C for 16 hours. After 16 hours, conditioned samples were immersed in a water bath at 60 ^{0}C and plastic bags were taken out from samples instantly. After 24 hours, plastic bags were taken out from the unconditioned samples and both conditioned and unconditioned samples were kept in a water bath at 25 ^{0}C for 2 hours. Finally, all samples were broken vertically at a loading rate of just about 51 mm/min with Marshall tester to determine indirect tensile strength values (P). Diameters (D) and heights (T) of samples were measured. The units of determined values were converted from kg to kg/cm^2 by using Eq5. ITSR was calculated by using Eq6 St_1 and St_2 are the arithmetic mean of indirect tensile strength values of unconditioned and conditioned samples respectively.

$$S_t = \frac{2.P}{\pi.T.D} \quad (5)$$

$$ITSR = \frac{S_{t2}}{S_{t1}} \quad (6)$$

3. RESULTS

3.1. Marshall Stability Test Results

The stability values determined following stability tests are shown in Figure 6. These values were obtained for control and reinforced samples which were prepared using iron wire of 1%, 3%, 5%, 7% and 9%. Marshall stability values of all samples were measured higher than 750 kg which is the lower limit value according to the Turkish Highway Construction Specifications 2013. Fig. 6 indicates that the stability of mixtures increased with increasing additive content initially.

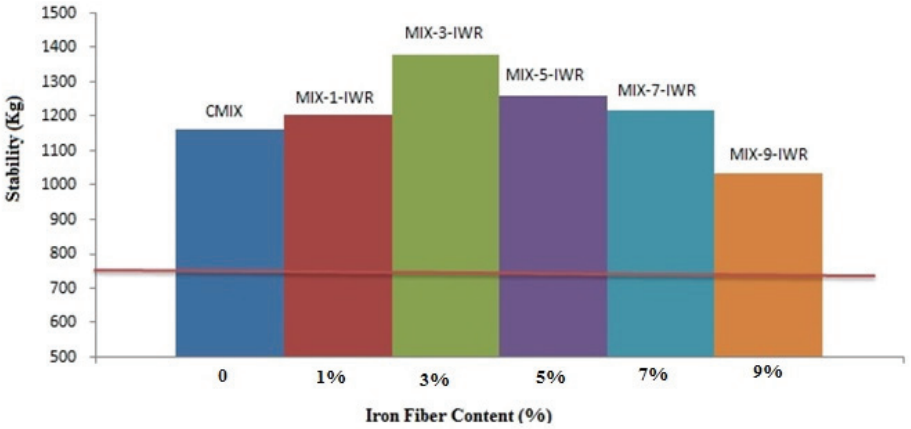

Figure 6. Stability values for each fiber content used in the experimental study

Maximum stability was obtained at 3% fiber content. Then stability values decreased. When the underlying reason is questioned, it can be seen that fibers may not distribute homogeneously in the mixture. Generally, applied loads are taken by the aggregate mass by means of contact points in Marshall samples. Because fibers created clustering in the mixture, contact between aggregate particles may be lost, and hence the stability of mixtures decreased at high fiber contents. In order to observe distribution fibers in the mixture, stereo images of mixtures were taken. According to Figure 7, it can be stated that all fibers were not dispersed in the mixture homogeneously at high fiber rates especially. Undistributed images of fibers in the mixture supports these conclusions. But these images also show us that, iron fibers in the mixtures worked properly without exhibiting any segregation and/or agglomeration from the mixture.

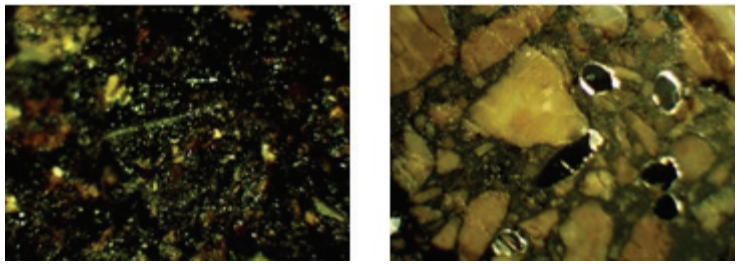

Figure 7. Stereo microscope image analysis results of mixtures prepared with iron fiber

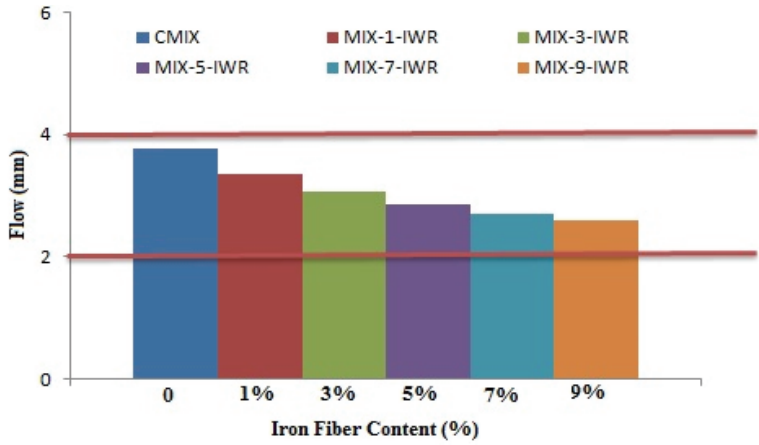

Figure 8. Flow values for each fiber percent used in the experimental study

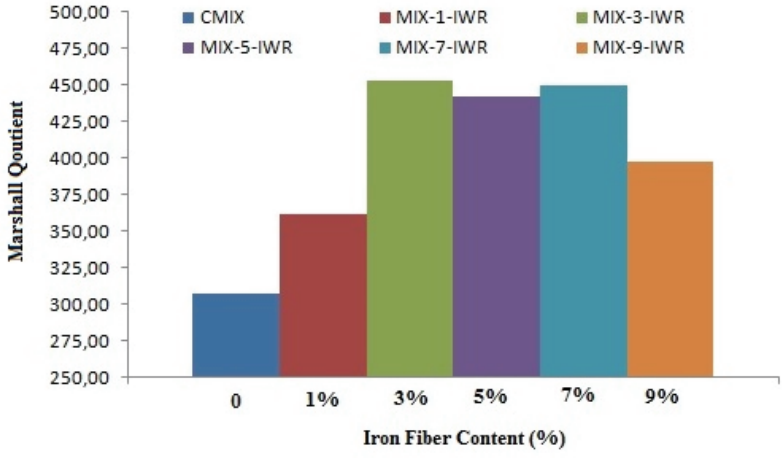

Figure 9. Marshall Quotient for each fiber percent used in the experimental study

The flexibility of mixtures was measured in terms of flow value. Figure 8 shows the flow values. When flow values were examined, it was observed that with increasing amounts of fiber, flow values decreased. This means that, as the amount of the fiber increased, the mixture became less flexible owing to the stiffness of fibers. Nevertheless, flow values were measured between required specification ranges of 2 to 4 mm.

MQ values were determined by using the ratio of stability to deformation value of mixture. The results obtained calculating MQ are shown in Figure 9.

According to Figure 9, it is evident that use of iron wire fiber as an additive in the mixture improved the MQ values. The iron wire fiber addition at the rate of 3% raised MQ value of control mixture from 306, 98 kg/mm to 452, 34 kg/mm which is almost equal to 1,5 times the MQ of the control mixture. It can be said that, adding at the rate of 3% provides rigidity, so it provides better strength against permanent deformation. This means that the mixtures gained additional stiffness with the addition of iron fibers. When the fiber contents were increased above 7%, fragility was observed in the samples. Obtained MQ results, supports the MQ approach with dense gradation mixtures as explained above.

Figure 10 shows the air voids values of samples. According to the Turkish Highway Construction Specifications 2013, air void amount should be within the range of 4% to 6% for the binder course. An evaluation of Fig 10 indicated that, with the exception of the MIX-5-IWR, MIX-7-IWR, and MIX-9-IWR, other samples were measured between required specification ranges. Too much air voids would result in low durability of the mixture, i.e. the performance would become worse. However, increasing air void value is important for pavements design in hot regions where the asphalt is suspected to flushing and bleeding. Increased void ratio can be a solution for these problems. It is important that, air voids should be within the specification limit values. As can be seen from Fig 10 the air void values increased with increasing amounts of iron fiber. The increase in air void values means that compressing the mixtures becomes more difficult with increasing fiber content.

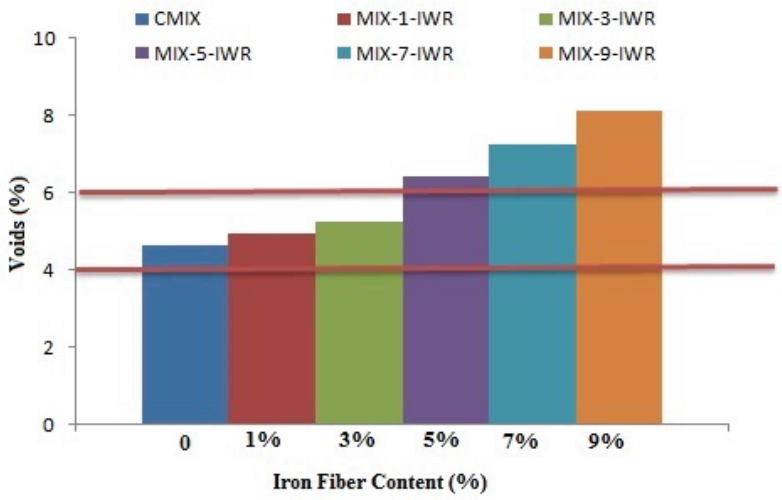

Figure 10. Air void values for each fiber percent used in the experimental study

Increasing the additive content decreases V_f values as shown in Fig 11. All samples were prepared with the same bitumen content. When fiber content was increased in the mixtures, voids filled with bitumen decreases because the amount of the bitumen in the mixture becomes insufficient.

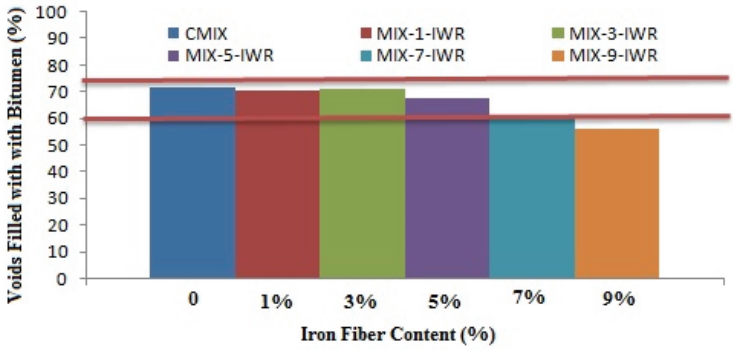

Figure 11. Voids filled with bitumen values for each fiber percent used in the study

In order to obtain enough durable and stable mixtures, VMA value should be within the range of 13% to 15% for binder course according to the specification. According to Figure 12, it can be said that VMA values of samples except for the MIX-5-IWR, MIX-7-IWR and MIX-9-IWR were determined between required specification ranges. This means mixtures with 5%, 7% and 9% iron wire content require an uneconomical amount of binder which may cause stability problems. The decrease in stability value supports this conclusion.

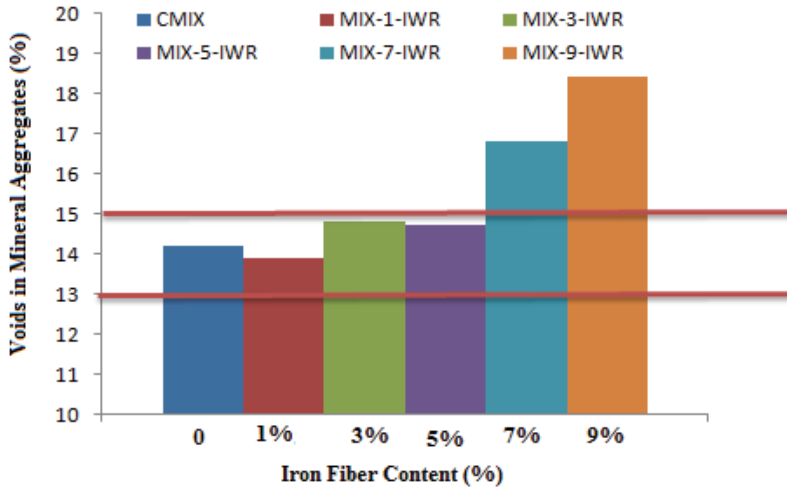

Figure 12. Voids between mineral aggregate values for each fiber percent used in the study

3.2. Cantabro Test Results

Cantabro tests were performed on aged and unaged samples for evaluating the quality of the bitumen/aggregate bond. Figure 13 shows the results of the tests. According to Figure 13, it can be said that the unaged samples exhibit lower mass loss during tests. This was expected since the samples were battered as a result of the aging process. This figure indicates that, at higher percentages of additive for both aged and unaged samples, mass loss values were significantly increased. However, when the mass loss values of unaged samples are examined, it will be seen that these values obtained for the samples defined as MIX-1-IWR, MIX-3-IWR and MIX-5-IWR correspond to rather low mass losses comparable to those obtained for the samples defined as MIX-7-IWR and MIX-9-IWR. Moreover, the similar situation was observed for the aged samples with the exception of MIX-1-IWR.

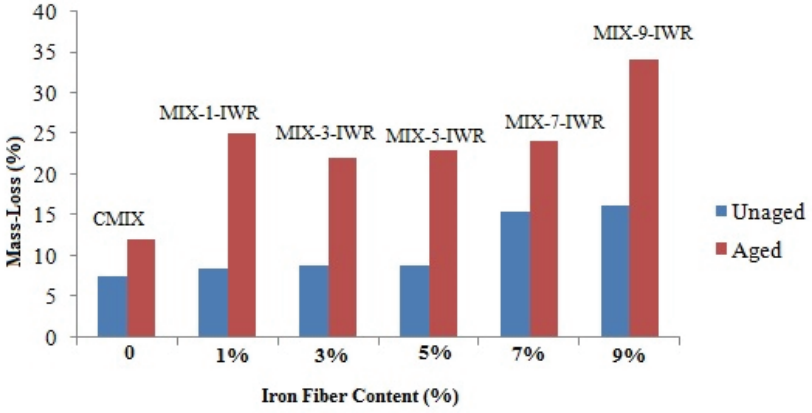

Figure 13. Mass-Loss values for each fiber percent used in the experimental study

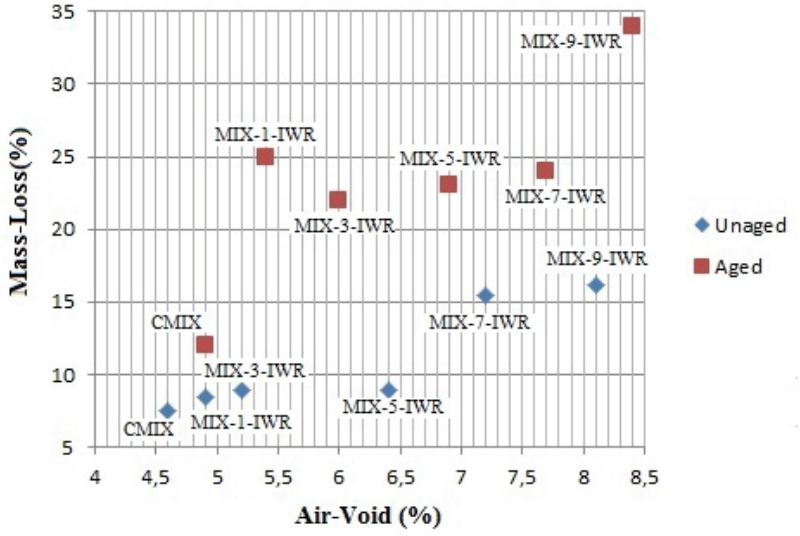

Figure 14. Change of mass loss according to air void for each fiber content

In order to better evaluate the influence of the air voids in the wear resistance of each sample, the air void-mass loss graph for the aged and unaged samples was drawn. This graph is given in Figure 14. According to Figure 14, it can be said that mass loss increases with the increase of air void content in the mixture. This means that gaps between aggregates caused decrease of the bond between bitumen and aggregate.

3.3. Moisture Susceptibility

In order to evaluate performance of low-cost iron wires iron reinforced asphalt mixtures in regards to moisture susceptibility, S_t and ITSR values were determined. Figure 15 shows the average S_t values for three samples at 25 ^{0}C for both wet and dry groups at optimum bitumen content for each additive input. Both dry and wet S_t values remained approximately the same up to 5% additive content. At higher percentages of additive, the S_t values decreased gradually. Maximum dry average S_t value was obtained with 5% additive while max. wet average S_t value was obtained from control samples. The higher this parameter, the more resistant is the sample against vertical loads. This means that, due to the air voids increased with increasing amount of fiber, gaps between aggregates of saturated samples were filled with water. Also, because samples were in the freeze-thaw cycle during the test, this water caused weakening of samples against loading.

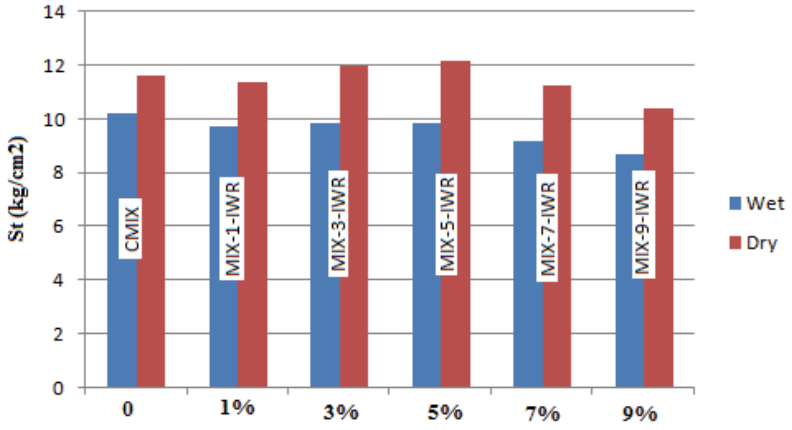

Figure15. S_t values for the each additive content

Moisture susceptibilities of each additive percentage were determined according to ITSR values, as shown in Fig 16. According to the Turkish Highway Construction Specifications 2013, the minimum ITSR value should be 80%. As seen in Fig 16, all samples provide this limit. However, control samples showed most resistance against moisture damage. ITSR value of these samples calculated as 88,02%. So, when the ITSR values examined, one can see that fiber additives could not improve the moisture susceptibility of the mixtures.

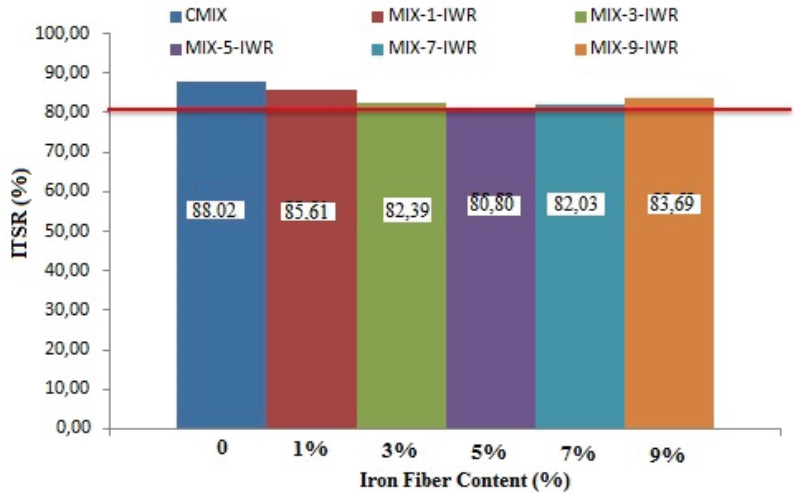

Figure 16. ITSR values for the each additive content

4. CONCLUSIONS

The asphalt mixture should be strengthened especially for heavy traffic conditions. Using low-cost iron fibers instead of other expensive reinforcing additives in the asphalt mixture presents a benefit to the community from an economic point of view. The aim of this study is to determine properties of the reinforced asphalt mixtures with low-cost iron fiber.

The optimum bitumen content for the mixtures was determined as 4.40% by weight of aggregate. Marshall stability test results showed that stability values increased up to 3% by additive. Using additive more than 3% in the mixture affected the samples adversely. When the reason of decreasing stability especially at high ratios was investigated by using stereomicroscope, it was seen that fibers were not distributed in the mixture homogeneously and that they created clustering. Although all samples were prepared with the same number of blows in the Marshall compactor, it was observed that mixtures showed less flexibility with increasing amount of fiber by reason of clustering. Measured flow values support this conclusion. Compressing the mixtures becames more difficult as well especially at high fiber ratios. Air void values were increased at high fiber ratios and consequently, samples required an uneconomical amount of binder which could cause stability problems. Additionally, air void values at samples with more than 5% additive exceed specification limits. Such a high rate air void in the mixture caused durability problems of mixtures as well. Cantabro test was performed in order to evaluate bitumen-aggregate bond for aged and unaged samples. Mass-loss percent of aged samples were measured higher than unaged samples. The Indirect tensile strength values of both wet and dry samples remained approximately the same up to 5% additive. Using additive higher than 5 percent led to a sudden and dramatic increase in indirect tensile strength values. On the other hand, although indirect tensile strength value of samples calculated higher than 80% which is the specified limit, fiber additives could not improve the moisture susceptibility of the mixtures at all.

When all of these results are considered together, it can be concluded that in strengthening of asphalt concrete with the low-cost iron fibers, best results were obtained at the rate of 3% additive. In addition, it should be explained that, adding of steel fibers to surface layers of flexible pavements may cause discomfort for drivers and they reduce safety on the road, which may cause accidents, therefore, it is recommended to use it in the below the surface layers such as the binder course. In view of improving stability effect of fiber on a mixture, further research is needed to determine the stability results of either stone mastic asphalt mixture strengthed with iron wire fiber or dense graded asphalt mixture strengthened with the powder form of iron wire. Because of stone mastic asphalt has a gap-graded gradation; high air voids caused by fibers may not cause compressive strength problems in the mixture.

References

[1] Ahmedzade P.,The investigation and comparison effects of SBS and SBS with new reactive terpolymer on the rheological properties of bitumen, Construction and Building Materials 2013; 38: 285-291

[2] Emon, M.A.B., Manzur, T., Yazdani, N., "Improving performance of light weight concrete with brick chips using low-cost steel wire fiber", Construction and Building Materials 106 (2016), 575–583.

[3] Facconi, L., Minelli, F., Plizzari, G.," Steel fiber reinforced self-compacting concrete thin slabs – Experimental study and verification against Model Code 2010 provisions", Engineering Structures 122 (2016), 226–237

[4] Caratelli A., Imperatore, S., Meda, A., Rinaldi, Z., "Punching shear behavior of lightweight fiber reinforced concrete slabs", Composites Part B 99 (2016), 257-265

[5] Putman, B.J., Amirkhanian, S.N., "Utilization of waste fibers in stone matrix asphalt mixtures", Resources, Conservation and Recycling 42 (2004) 265–274

[6] Wu, S., Liu, G., Mo, L., Chen, Z., Ye, Q. "Effect of fiber types on relevant properties of porous asphalt" Transactions of Nonferrous Metals Society of China, 16(2006): 791-795

[7] Abtahi, S.M., Sheikhzadeh, M., Hejazi, S.M., "Fiber-reinforced asphalt-concrete – A review", Construction and Building Materials 24 (2010) 871–877

[8] Transportation Research Board (TRB):NCHRP Synthesis Report 475, "Fiber Additives in Asphalt Mixtures", 2015, Washington D.C.

[9] Park, P., El-Tawil S., Park, S., Naman, A., "Cracking resistance of fiber reinforced asphalt concrete at -20 ^{0}C", Construction and Building Materials 81 (2015), 47–57

[10] Fazaelli, H., Samin, Y., Pirnoun, A., Dabiri, A.S., "Laboratory and field evaluation of the warm fiber reinforced high performance asphalt mixtures (case study Karaj – Chaloos Road)", Construction and Building Materials 122 (2016) 273–283

[11] Ferotti, G., Pasquini, E., Canestrari, F., "Experimental characterization of high-performance fiber-reinforced cold mix asphalt mixtures", Construction and Building Materials 57 (2014) 117–125

[12] Guo, J.F., "The Effect of Steel Fiber on the Road Performence of Asphalt Concrete", Applied Mechanics and Materials, 584-586 (2014), 1342-1345

[13] Al-Ridha A.S.D., HAmeed, A., Ibrahim, S.K., "Effect of steel Fiber on the Performance of Hot Mix Asphalt with Different Temperaturesand Compaction", Australian Journal of Basic and Applied Sciences, 8(6) ,2014: 123-132

[14] Garcia, A., Norambuena-Contreras, J., Parti, M.N., Schuetz, P., "Uniformity and mechanical properties of dense asphalt concrete with steel wool fibers", Construction and Building Materials 43 (2013) 107–117

[15] Serin, S., Morova, N., Saltan, M., Terzi, S., "Investigation of usability of steel fibers in asphalt concrete mixtures", Construction and Building Materials, 36(2016), 238-244

[16] General Directorate of of Highways,"Highway Construction Specifications", Ankara, General Directorate of Highway Press, 2013 (in Turkish)

[17] General Directorate of of Highways, "Bituminous mixtures laboratory manual", Ankara, Turkey, General Directorate of Highway Press, 2012 (in Turkish).

[18] Lavin, P. (2003), "Asphalt pavements: A practical guide to design, production and maintenance for engineers and architecs", CRC Press.

[19] Whiteoak D, The Shell bitumen handbook, UK: Shell Bitumen; 1991.

[20] Arabani, M., Tahami, S.A.," Assessment of mechanical properties of rice husk ash modified asphalt mixture", Construction and Building Materials, 149 (2017), 350-358

[21] Gibreil, H.A.A., Feng, C.P., "Effects of high-density polyethylene and crumb rubber powder as modifiers on properties of hot mix asphalt", Construction and Building Materials 142 (2017) 101–108

[22] Zoorob, S.E., Suparma, L.B., "Laboratory design and investigation of the properties of continuously graded Asphaltic concrete containing recycled plastics aggregate replacement (Plastiphalt)", Cement & Concrete Composites 22 (2000) 233-242

[23] Tayfur, S., Ozen, H., Aksoy, A., "Investigation of rutting performance of asphalt mixtures containing polymer modifiers", Construction and Building Materials 21 (2007) 328–337.

[24] Sengul C.E., Oruc, S., Iskender, E., Aksoy, A., "Evaluation of SBS modified stone mastic asphalt pavement performance", Construction and Building Materials 41 (2013) 777–783

[25] Arrieta, V.S., Maquilon, J.E.C., "Resistance to degradation or cohesion loss in Cantabro test on specimens of porous asphalt friction courses.", XVIII Panamerican Conference of Traffic and Transportation Engineering and Logistics (PANAM 2014), Procedia - Social and Behavioral Sciences 162 (2014) 290 – 299

[26] Shirini, B., Imaninasab, R., "Performance evaluation of rubberized and SBS modified porous asphalt mixtures", Construction and Building Materials 107 (2016), 165–171

[27] Chiu, C., "Use of ground tire rubber in asphalt pavements: Field trial and evaluation in Taiwan", Resources, Conservation and Recycling 52 (2008) , 522–532

[28] Celauro, C., Bernardo, C. Gabriele, B., "Production of innovative, recycled and high-performance asphalt for road pavements", Resources, Conservation and Recycling 54 (2010), 337–347

[29] Lin, J., Guo, P., Wan, L., Wu, S., "Laboratory investigation of rejuvenator seal materials on performances of asphalt mixtures", Construction and Building Materials 37 (2012,) 41–45

[30] Colonna P, Berloco N., Ranieri V., Shuler S.T., "Application of Bottom Ash for Pavement Binder Course", SIIV - 5th International Congress - Sustainability of Road Infrastructures, Procedia - Social and Behavioral Sciences 53 (2012), 962 – 972

[31] Pereira, S.M.S., Oliveira, J.R.M., Freitas, E.F., Machado, P., "Mechanical performance of asphalt mixtures produced with cork or rubber granulates as aggregate partial substitutes", Construction and Building Materials 41 (2013), 209–215

[32] Contreras, J.N., Gaecia, A., "Self-healing of asphalt mixture by microwave and induction heating", Materials and Design 106 (2016), 404–414

[33] Liang R.Y., "Refine AASHTO T283 Resistance of compacted bituminous mixture to moisture induced damage for Superpave " , U.S. Department of Transportation Federal Highway Administration Report, Report No: FHWA/OH-2008/1, 2008

[34] Tapkın, S., "The effect of polypropylene fibers on asphalt performance", Building and Environment 43 (2008) 1065–1071

Teknik Dergi, 2018 8537-8561, Paper 511

A Method for Determination of Accident Probability in the Construction Industry

Senem BİLİR[1]
G. Emre GÜRCANLI[2]

ABSTRACT

Safety issues within the construction industry have been an area of concern in almost every country. In this paper, an objective and quantitative accident probability calculation approach is proposed using 623 actual construction accidents that resulted in 681 casualties between the years 2000 and 2013. Of these accidents, the first five account for 84.1% of all fatalities and 85.4% of all injuries. In total, five construction jobs (excavation, reinforced concrete work, masonry, plastering and painting, and roof work) were the focus of the study, as they account for 70.8% of all occurrences. Probability values were calculated by using the Poisson distribution, in which accident rates and exposure values were used as distribution parameters. In an industry where accidents are recorded according to non-specific standards, it is very difficult to represent the probability of accidents within a known distribution model. The proposed approach in this paper provides an objective method to obtain probabilities by using the Poisson distribution for construction accidents.

Keywords: Construction safety, accident probability, exposure, man-hour values, Poisson distribution, risk assessment.

Abbreviations:

BLS: Bureau of Labor Statistics

CFOI: Census of Fatal Occupational Injuries

ILO: International Labour Organization

OSHA: Occupational Health and Safety Administration

SSI: Social Security Institution

Note:
- This paper has been received on December 07, 2017 and accepted for publication by the Editorial Board on May 16, 2018.
- Discussions on this paper will be accepted by September 30, 2018.

• DOI: 10.18400/tekderg.363613

1 Technical University of Istanbul, Dep. of Civil Engineering, İstanbul, Turkey - sbilir@itu.edu.tr
2 Technical University of Istanbul, Dep. of Civil Engineering, İstanbul, Turkey - gurcanlig@itu.edu.tr

1. INTRODUCTION

In many developing countries, the construction industry has a great influence on both the economy and also social policies. However, one of its most significant factors is the high number of fatalities that it suffers. These are due to the characteristics of the industry, such as its contingent forms of contracting, the difficulty in coordinating subcontractors and trade contractors, the existence of different types of jobs on a single site, an uneducated/untrained workforce, and the risks that arise from the content of the construction projects themselves [1].

Table 1. Incidence rates for fatal accidents in the construction industries of 17 countries [5].

Country	2008	2009	2010	2011	2012	2013	2014	2015	2016
Austria	11.7		8.7	5.3	11.3	10.9	6.1	4.1	7.2
Belgium		10	10.4	8.8	6.5	9.5			
Croatia		7.5	12.2	13.7	11.7	5.4		8.7	11.6
Bulgaria	19.4	12.7	15.2	11.9	7.3	13.1	13.9	12	13.6
Hong Kong. China		81	47	19	42	47	46	45	
Czech Republic		7.7	8.6	11.1	8.3	9.6	11.7	12.4	
Israel					24.8		23.1	24.8	
Poland	14.7	13.4	13	11.2	9.2		6.8	8.3	
Romania	32	24	32.1	16.4	14.3	12	14.9	10.3	11.8
Spain	10	9	8.5	8.6	6.6	6.2	8.2	7.7	5.1
Ukraine						14.5	17.6	20.3	
Norway		6.1	5	5.8	3.6	4.3			
Portugal						14.6	15.6		
Switzerland				7.9		24.6	23.8	1.7	
Turkey	36.4	35.3	32.1	29.8	13.2	27.4	22.1	6.8	13.4
United Kingdom		1.8	2.3	2.3		1.9		2	
United States		9.9	9.5	9.1	9.5	9.7	9.8		

F: Fatalities; I: Injuries. Ratios are one per 100,000 insured workers.

Occupational accidents also have a negative impact on the industry in terms of reduced productivity and lost working days. According to the Census of Fatal Occupational Injuries (CFOI) 2013 report, 828 fatalities occurred in the construction industry of the United States of America (the highest number of deaths among all industries), and this sector ranks fourth in terms of fatal accident rates per 100,000 full-time workers [2]. Accident statistics in developing countries reveal that implementation of laws and regulations, as well as prevention techniques, fall short in their attempts to mitigate or abate hazards on construction

sites. The figures show that the majority of fatalities occurred on projects undertaken by small or medium sized enterprises. These companies do not implement adequate safety rules or management procedures, and the workers in those companies lack the training to carry out these practices [3,4].

As revealed in Table 1, the fatality rates of developing countries are higher than those of developed countries. The table compares the construction industries of seventeen countries [5].

Based on the Social Security Institution (SSI) data set for the years 2000 to 2016, the annual average number of employees is 18,840,449. 1,283,756 of these work in the construction industry [6]. The average share of the industry with regard total employment has reached 7.7% (see Table 2), and this represents a 20-year high [7].

Table 2. 2000 - 2016 Occupational accident statistics of the SSI [6].

Year	Employment of construction industry and its share (%) in total workforce	Total permanent disabilities due to occupational accidents	Permanent disabilities in construction industry and their share (%) in total	Total fatal accidents for all industries	Number of Fatal construction accidents and their share (%) in total
2000	761452 (3.5)	1818	399 (21.9)	1173	379 (32.3)
2001	681882 (3.2)	2183	517 (23.7)	1008	341 (33.8)
2002	713629 (3.3)	1820	439 (24.1)	872	319 (62.6)
2003	685902 (3.2)	1421	354 (24.9)	810	274 (32.8)
2004	752136 (3.8)	1693	345 (20.4)	841	263 (31.3)
2005	933498 (4.7)	1639	322 (19.6)	1072	290 (27.1)
2006	1185723 (5.8)	2267	425 (18.7)	1592	397 (24.9)
2007	1247970 (6)	1550	361 (23.3)	1043	359 (34.4)
2008	1238888 (5.8)	1452	373 (25.7)	865	297 (34.3)
2009	1227698 (5.8)	1668	282 (16.9)	1171	156 (13.3)
2010	1431000 (6.3)	1976	319 (16.1)	1434	475 (33.1)
2011	1581000 (7)	2093	405 (19.4)	1700	570 (33.5)
2012	1789487 (15)	2036	563 (27.7)	744	256 (34.4)
2013	1849942 (14.8)	1660	459 (27.7)	1360	521 (38.3)
2014	1875929 (14.2)	1421	404 (28.4)	1626	501 (30.8)
2015	1980630 (14.1)	3433	979 (28.5)	1252	473 (37.8)
2016	1887099 (13.7)	4447	1450 (32.6)	1405	496 (35.3)
Ave	1283756.8 (7.7)	2033.9	493.9 (23.5)	1174.6	374.5 (32.1)

The most striking fact that can be perceived from Table 2 is that over the period from 2000 to 2016, the average number of fatal occupational accidents is 1174; whereas in the Turkish construction industry the average number of fatal occupational accidents is 374 [6]. Although, the Turkish construction industry accounts for 7.7% of total employment, it accounts for 32.1% of fatal occupational accidents. Gurcanli and Mungen (2013) reported official figures that showed that there were 1700 fatal occupational accidents in Turkey in 2011, and that 570 of them occurred in the construction industry [8]. This means that approximately every one out of three occupational accident fatalities occur in the construction industry, and for this reason, it has a reputation for being the most dangerous industry in Turkey.

Current occupational health and safety legislation (Health and Safety Law No:6311 and related regulations) requires employers to implement safety measures as well as safety management systems in Turkey more strictly. However, the level of conscientiousness in the industry is unsatisfactory, and safety is perceived as an extra cost and unnecessary expenditure. For this reason, the industry has acquired a reputation of being one of the most hazardous when it is compared with other industrial branches. In recent years, huge construction projects have been implemented, improving the level of conscientiousness and the quality of safety promotion techniques. However, the subcontracting system and related problems such as the coordination and training of subcontractors still exist and the majority of the victims of fatal accidents are employees of these subcontractors.

Hazard analysis and applicable risk assessment methods are considered to be prominent elements of an effective safety system and on-site prevention practices. Each element of any risk assessment technique should be established by using experience, historical data and numerical methods. Common risk assessment techniques such as L Matrix and Fine Kinney depend on the personal opinions and experiences of the practitioners on-site. However, the professionals who apply risk assessment techniques have not often benefited from being trained by a scientific approach. Accident likelihood or accident probability is one of the fundamental parameters for risk assessment methods, and the knowledge of how to calculate or assess this parameter is an important issue.

This study proposes an objective probability calculation method which focuses on construction activities in conventional construction projects by using accident rates and worker exposure levels in order to implement easy and effective risk assessment specifically for construction sites. Moreover, the authors argue that the findings can be used by decision makers, safety experts, project planners and site engineers as well as academicians for safety-inherent project planning at all stages of a construction project, from pre-design to post-construction.

2. LITERATURE RESEARCH

Health and safety in the construction industry has been discussed in several studies, but it is still a hot topic due to the number of fatalities and the effects of new technologies and construction methods [9-21]. New hazards and risks require applicable risk assessment methodologies or the adaptation of older ones by changing/improving the elements within those methods. Accident probability is one of the most important parameters for evaluating the level of risk on construction sites. For instance, Van Nunen et al. (2016) argue that

accident probability, and the possible loss in terms of decision making while resolving risks and uncertainties, could have adverse results [22]. Jocelyn et al. (2016) presented a quantitative risk estimation methodology using the probability parameter to prevent machinery-related accidents [23]. Wang et al. (2017) examined railway system safety and the concept of system risk using the catastrophe theory [24]. The authors used a fault tree in order to calculate the probability of dangerous phenomena in their study. In addition, there is a great deal of research that focuses on the determination of accident probability or likelihood in the construction industry. For instance, Brauer (1994) classified the likelihood parameters as: frequent, probable, occasional, remote, and improbable [25]. Lee and Halpin (2003) determined seven safety factors (including the experience of workers, skills, behavior, training, etc.) through consultation with 35 experts with an average of 24 years of work experience [26]. The three most critical safety factors were determined to be: education, supervision and preplanning, and by using these factors they estimated accident probabilities using a fuzzy logic-based analysis. Moreover, Jannadi ve Almishari (2003) calculated probability by conducting four pre-analyses [27]. The authors developed the RAM software for risk assessment. In order to designate accident probability with RAM, users were asked to define the tools and equipment, materials, and chemicals to be used in a given activity. In addition to these probability parameters, other problems can be encountered in the workplace, and users were asked to list the personal protective equipment provided to the employees. As a result of these questions, RAM was able to calculate the probabilities of accidents. Furthermore, Hallowell and Gambatese (2009) proposed an activity-based total risk quantification of concrete formwork in their research [28]. The authors utilized a risk quantification method that was proffered formerly by Jannadi and Almishari (2003) and Baradan and Usmen (2006) [9-27]. They accepted accident frequency as an accident probability parameter. Hallowell and Gambatese (2009) first decided on the frequency scale, and then set sub-activities of concrete formwork by using field observations [28]. In order to assign frequency values to the sub-activities involved in concrete formwork erection and striking, the opinions of 15 experts were taken using a 3-step Delphi method. The accident frequencies garnered from this data are shown in Table 3. Not only Hallowell and Gambatese (2009), but also Sun et al. (2008) have accepted accident frequency as representative of accident probability in their studies of risk estimation [29].

Mitropoulos and Namboodiri rejected the tradition of identifying risk as a function of probability and severity [30]. They developed a task demand assessment in order to calculate the risk of a given activity by using the risk factors involved in it. The resulting task demand scores provide insight into the likelihood of risk and the difficulty of the selected activities. The authors claimed that if the task demand factors increase, the likelihood of accident increase correspondingly.

On the other hand, after 2008 the U.S. Bureau of Labor Statistics (BLS) started to calculate fatal accident rates according to the working hours of full-time employees as shown in Equ.1 [31].

$$\text{Fatal Accident Rate} = (N / EH) * 200{,}000{,}000 \quad (1)$$

N: number of fatal accidents; EH: total working hours of all employees within the calendar year; 200,000,000: total working hours, which was obtained by assuming that 100,000 employees work 40 hours per week for 50 weeks. In accordance with this rate, the accident

likelihoods within industries can be easily compared according to years, states, age groups, gender etc.

Table 3. Accident frequency scale of Hallowell and Gambatese (2009)

Man-hour per accident	Accident Frequency
> 100,000,000	1
10,000,000-100,000,000	2
1,000,000-10,000,000	3
100,000-1,000,000	4
10.000-100.000	5
1,000-10.000	6
100-1,000	7
10-100	8
1-10	9
0.1-1	10

If the literature is analyzed in detail, it can be seen that there are different risk assessment approaches (and/or calculations) that can be made according to different assumptions, and that this leads to a great variety of accident probability and likelihood definitions. The literature review for this study reveals that there is no strict definition of accident probability or likelihood, and that there are many gaps to fill for construction industry-specific risk assessment approaches and probability calculations.

3. METHODOLOGY

The construction industry is a project-based type of activity and each project is unique during its planning and construction phase. However, despite their differences, the main construction activities within each project are very similar – for example formwork, scaffolding, or roofing for residential building projects; or excavation, piling, and drainage for infrastructure projects. If construction activities are examined in detail, the similarities in their method of construction and the related safety risks may be observed. Therefore, an activity-based methodology was chosen for the calculation of probability parameters in this study. This was done to provide more generalized results. In the literature, there are many studies concerning construction safety [11, 21, 28, 32, 33, 34, 35] that use an activity-based approach. In this research, actual accident data was used in order to remove all subjectivity from the study. For this purpose, 623 expert witness reports from construction accidents (with a total of 681 casualties) that were submitted to the criminal and labor courts between 2000 and 2013 were analyzed (Figure 1). These expert witness reports were submitted for the construction accidents from all over the Turkey. The most common types of accidents, and the most prevalent activities in which these accidents occur, were identified. Within the scope

of the study, instead of focusing on all construction activities, five main construction activities (excavation, reinforced concrete work, masonry, plastering and painting, and roof work) were analyzed due to their disproportionate share of accidents. These activities accounted for 482 of the total 681 cases (both fatal and non-fatal), a share of 70.8% [36].

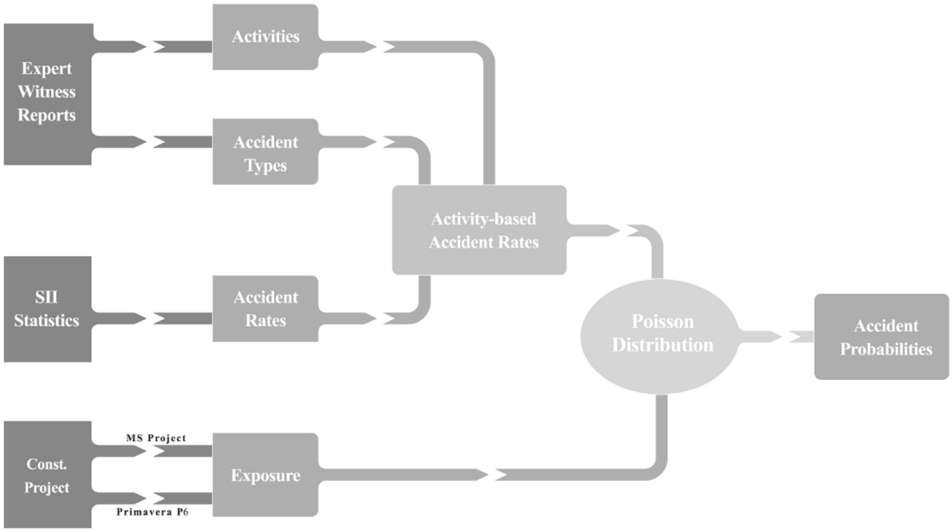

Figure 1. Graphical representation of the methodology

In addition, the "occupational accidents and diseases statistics" published between 2000 and 2013 by the SSI were examined and combined with the results obtained from the expert witness reports. From these analyses, activity-based and accident type-based accident frequencies were obtained as an outcome. The exposure values for construction activities (i.e. man hour values) were also taken from the work schedules and planning tables of twenty traditional construction projects.

Accident probabilities were calculated using the Poisson distribution model by taking into account accident rates and exposure values [37]. In the construction industry, where accidents are recorded according to a non-specific standard, it is very difficult to represent the probability of accidents within a known distribution model, but thanks to this approach, it was possible to provide an objective method to obtain accident probabilities using the Poisson distribution.

3.1. Determining Activity-Based Accident Rates

The accident rates were calculated using the data from the SSI accident statistics and expert witness reports in order to prevent subjectivity in this study. The first step is to focus on the most frequent accidents types obtained from these expert reports.

Most frequent accident types

In this study, occupational accidents between the years 2000 and 2013 were used. Although, legislative amendments were added after the year 2003 in order to comply with European Union standards, the utilization of new construction technologies and methods in huge projects have been carried out in Turkey since 2000. The time interval is therefore considered to be suitable for the purpose of this research study [38].

Table 4. Fatal and non-fatal construction accidents obtained from expert witness reports

Accident Type	Fatality	Fatality (%)	Injury	Injury (%)	Total	Total (%)
Fall from height	278	59.3	118	55.7	396	58.1
Struck by flying/falling object	42	9	23	10.8	65	9.5
Building/Structure collapse	30	6.4	21	9.9	51	7.5
Contact with electricity	28	6	11	5.2	39	5.7
Cave-ins	16	3.4	8	3.8	24	3.5
Other	15	3.2	9	4.2	24	3.5
Struck by a moving vehicle	14	3	1	0.5	15	2.2
Struck by moving part of a vehicle	12	2.6	6	2.8	18	2.6
Explosives Accidents	12	2.6	3	1.4	15	2.2
Equipment roll over accidents	11	2.3	1	0.5	12	1.8
Traffic Accidents	7	1.5	6	2.8	13	1.9
Hazards due to machine and tool usage	4	0.9	5	2.4	9	1.3
Total	469		212		681	

The classification of the accident types were the first step, and in this respect, both the OSHA (1971/97) and ILO (1998) accident classification databases were used [39,40]. Using the accident classification schemes in these databases, 12 accident types were identified as the most frequent. Following this, 623 expert witness reports were analyzed. These were based on the accident type classification, and 681 accident cases were obtained from these reports (Table 4).

In Table 4, the number of the most frequent accidents and their percentages are shown. Fall from height, struck by flying/falling object, building/structure collapse, contact with electricity and cave-ins appear as the five most frequent accidents. It can be also seen that these five accident types constitute a very significant share of the total, accounting for 84.1%

of fatalities and 85.4% of injuries. Although, there are several activities in any construction project, it is reasonable to determine the most critical activities based on the occurrence of accidents and then to concentrate only on these critical activities to reach more generalized results. Therefore, within the scope of this study the first five accident types and the most common construction activities were chosen.

Most hazardous activities

Gurcanli and Mungen (2013) analyzed 1,117 expert witness reports of construction accidents in Turkey between the years 1972 and 2008, and noted the activities of any casualty at the time of each accident [8]. However, further analyses were required in order to determine the accident types. For this reason, all expert witness reports were reviewed and the roles of the casualties at the time of each accident were obtained. This gave an insight leading to determination of the most hazardous construction activities.

Additionally, "Fall from height" which ranks first, and which accounts for 59.3% of fatalities, was examined in detail due to the possibility of its occurrence in many different activities on construction sites [41]. Similar attention was given to the other frequent accidents, and their sub-types (fall near the edge of a slab, fall into a hole and so on) were identified. Furthermore, this analysis revealed the activities of the casualties. As a result, the most hazardous construction areas were determined as being: excavation, reinforced concrete work, masonry, plastering and painting, and roof work.

Risk analysis of most hazardous activities

Risk analysis was needed to specify the risks of the five activities. The accident types that are given in Table 4 may not be observed in each of the five activities. For example, during roof works it is very unlikely to observe traffic accidents. Therefore, accident types were distributed to activities by considering the nature of the activity in Table 5. Assuming there are no safety measures on construction sites, the most common accidents were assigned to the most hazardous activities.

Accident concentration

Accident concentration is a term that has been generally used for presenting the intensity of traffic accidents encountered in states, provinces or zones [42,43,44]. However, in this study the term "accident concentration" was used for the number of accidents in each activity. Concentration values were needed in order to calculate the activity-based and accident type-based accident frequencies. Therefore, the 623 expert witness reports were examined again and accident concentrations were determined by taking into consideration the five selected construction activities and th

It can be said that the most hazardous risks of excavation work are cave-ins, being struck by a moving vehicle, being struck by flying/falling object, being struck by moving part of a vehicle, and traffic accidents (see Table 6). Figure 2 demonstrates the distribution of 9 different risks that exist in excavation work and also the accident concentration of each one.

Table 5. The most hazardous construction activities and their risks

Activity Number	Activity Name	Risk Number	Risk Code	Risks
1	Excavation	1	R05	Cave-ins
		2	R01	Fall from height
		3	R02	Struck by flying/falling object
		4	R03	Building/Structure collapse
		5	R04	Contact with electricity
		6	R07	Struck by a moving vehicle
		7	R10	Equipment roll over accidents
		8	R12	Traffic Accidents
		9	R11	Struck by moving part of a vehicle
2	Reinforced Concrete	1	R01	Fall from height
		2	R02	Struck by flying/falling object
		3	R06	Other
		4	R03	Building/Structure collapse
		5	R09	Hazards due to machine and tool usage
		6	R04	Contact with electricity
		7	R11	Struck by moving part of a vehicle
		8	R07	Struck by a moving vehicle
3	Masonry	1	R01	Fall from height
		2	R07	Struck by a moving vehicle
		3	R02	Struck by flying/falling object
		4	R06	Other
4	Plastering & Painting	1	R01	Fall from height
		2	R02	Struck by flying/falling object
		3	R06	Other
		4	R07	Struck by a moving vehicle
		5	R09	Hazards due to machine and tool usage
5	Roof Works	1	R01	Fall from height
		2	R02	Struck by flying/falling object
		3	R06	Other
		4	R07	Struck by a moving vehicle

Table 6. Accident concentration of excavation work

Activity Number	Activity	Risk Number	Risk Code	Risk Name	Number of Fatalities	Number of Injuries	Accident Concentration
1	Excavation	1	R05	Cave-ins	10	3	13
		2	R01	Fall from height	3	1	4
		3	R02	Struck by flying/falling object	5	5	10
		4	R03	Building/Structure collapse	2	1	3
		5	R04	Contact with electricity	3	1	4
		6	R07	Struck by a moving vehicle	8	3	11
		7	R10	Equipment roll over accidents	3	1	4
		8	R12	Traffic Accidents	2	4	6
		9	R11	Struck by moving part of a vehicle	7	1	8
				Total	43	20	63

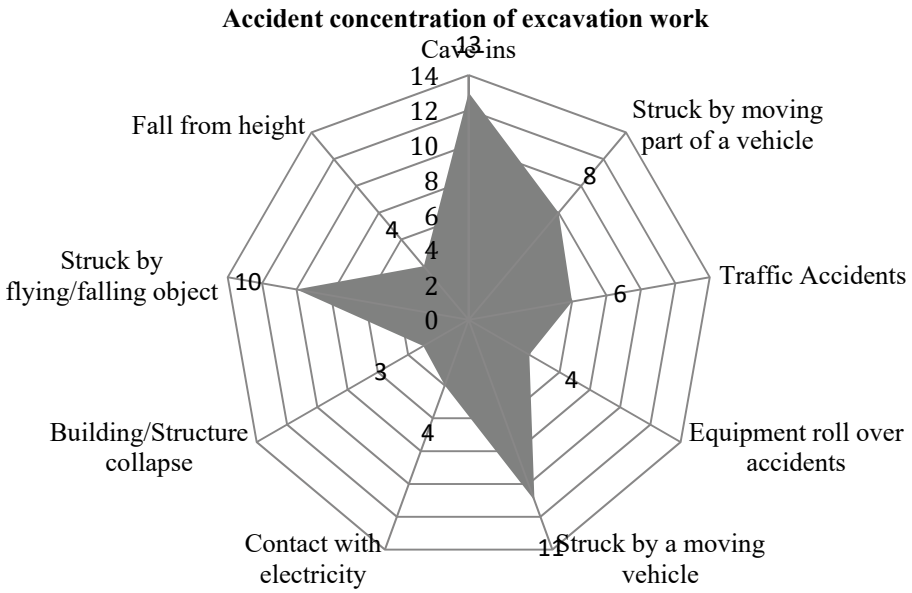

Figure 2. Accident concentration of excavation works

As previously mentioned, the number of victims of the five selected activities (excavation, reinforced concrete works, masonry, plastering and painting, and roof works) constitute 70.8% of all accidents (681) in the expert witness reports database (Table 7). Furthermore, this ratio is important for accident rate calculation of total occupational accidents in Turkey. Since it is impossible to investigate the expert witness reports of all occupational accidents, this ratio was used to estimate the number of accidents that fall within the scope of this work.

Table 7. Accident concentrations of determined construction activities

Activity Name	Number of fatalities	Number of injuries	Total number	Ratio of total number of accidents (%)
Excavation	43	20	63	9
Reinforced Concrete	110	34	144	21.1
Plastering&Painting	60	49	109	16
Masonry	62	27	89	13.1
Roof	65	12	77	11.3
Total	340	142	482	70.8

Accident rates

For the calculation of the Accident Rate parameter, the "Work Place and Employee Statistics" and the "Occupational Accident Statistics" archives of the Turkish SSI were analyzed. From these, construction industry employment data, the number of accidents resulting in permanent injuries and the number of fatal accidents were obtained for the years between 2000 and 2013.

Based on the SSI data, it could be assumed that construction workers work 45 h/wk (this is the maximum legal limit but it is often exceeded) and 50 wk/yr. While calculating the average accident rate for the 13 years under discussion, first the total working hour for the construction industry was calculated for each year. Since the accident concentration of the five selected construction activities constitutes 70.8% of all construction accidents according to the expert witness reports, 70.8% of SSI accidents data was calculated for each year. After dividing the number of accidents by the work volume, the accident rates for each year were obtained. An average of 13 years was used as the "accident rate" in the activity-based and accident type-based accident rate calculations. The average accident rate was found to be 2.26×10^{-7} accidents per 100,000 hours construction work for the five activities (Table 8).

The distribution of accidents among the five activities were utilized in order to obtain the activity-based and accident type-based accident rate values. Table 9 shows the fatalities, injuries and total accident numbers and ratios for the five activities.

Table 8. Accident rates of the construction industry of Turkey between 2000 and 2013

Year	Const. industry employment	Number of perm. disability	Number of fatality	Number of accident	70,8% of number of accidents	Weekly work hour (h)	Annual work (wk)	Annual work volume (man-hour / yr)	Accident rates for 5 jobs (annual number of accidents / total work volume)
2000	761,452	399	379	778	551	45	50	1,713,267,000	3.22E-07
2001	681,882	517	341	858	607	45	50	1,534,234,500	3.96E-07
2002	713,629	439	319	758	537	45	50	1,605,665,250	3.34E-07
2003	685,902	354	274	628	445	45	50	1,543,279,500	2.88E-07
2004	752,136	345	263	608	430	45	50	1,692,306,000	2.54E-07
2005	933,498	322	290	612	433	45	50	2,100,370,500	2.06E-07
2006	1,185,723	425	397	822	582	45	50	2,667,876,750	2.18E-07
2007	1,247,970	361	359	720	510	45	50	2,807,932,500	1.82E-07
2008	1,238,888	373	297	670	474	45	50	2,787,498,000	1.70E-07
2009	1,227,698	282	156	438	310	45	50	2,762,320,500	1.12E-07
2010	1,431,000	319	475	794	562	45	50	3,219,750,000	1.75E-07
2011	1,581,000	405	570	975	690	45	50	3,557,250,000	1.94E-07
2012	1,789,487	563	256	819	580	45	50	4,026,345,750	1.44E-07
2013	1,849,942	459	521	980	694	45	50	4,162,369,500	1.67E-07
Σ		5,563	4,897	10,46	7,406			Ave:	2.26E-07

Table 9. Distribution of accidents between five construction activities

Activity	Number of Fatalities	Ratio of Fatalities (%)	Number of Injuries	Ratio Of Injuries (%)	Total number of accidents	Ratio of Total Number of Accidents (%)
Excavation	43	12.6	20	14.1	63	13.1
Reinforced Concrete	110	32.4	34	23.9	144	29.9
Plastering &Painting	60	17.6	49	34.5	109	22.6
Masonry	62	18.2	27	19	89	18.5
Roof	65	19.1	12	8.5	77	16
Total	340	1	142	1	482	1

By examining the distribution (or share of each job) in Table 9, Table 10 can easily be worked out. First, the ratio of each activity across the total number of accidents is calculated (third column). It can be seen that the most hazardous activity is reinforced concrete work with a ratio of 0.229. The values for plastering and painting, masonry, roof work and excavation are 0.226, 0.185, 0.160 and 0.131 respectively. Secondly, the accident rates for the five construction activities are calculated and given in the fourth column. For instance, the activity-based accident rate for excavation work was found to be 2.95×10^{-8} (accident/work-hours). This accident rate was distributed across risk categories according to their ratios and the accident type-based rates for each risk category in excavation work were calculated in the last column. The accident rates of reinforced concrete work (6.747E-08), masonry (4.170E-08), plastering and painting (5.107E-08) and roof work (3.608E-08) were obtained using the same work outs. The accident probabilities can therefore be calculated with the help of these accident rates.

3.2. Calculating Activity-Based Exposures

In the literature, exposure values are either not included (i.e. in L Matrix) or are used as constant values for all risks [27, 45]. However, it is crucial to establish a conceptual framework for the exposure parameter, which is based on man-hour values extracted from the project schedule to eliminate subjectivity in risk assessment. Unfortunately, there are few studies in the literature suggesting that the exposure parameter can be obtained from the man-hour values for use in establishing a linkage between construction scheduling, planning and risk assessment [28,32]. For instance, Mitropoulos and Namboodiri (2011) suggest exposure as a percentage of the duration that a worker is exposed to the relevant hazard [30]. In addition, Gangolles et al. (2010) determined exposure as depending on drawings and the bill of quantities for 90 risk types [11].

Table 10. Accident rates of five construction activities

Activity Name	Average Accident Rate for 5 Activities	Ratio of Activity to Total Number of Accidents (%)	Accident Rate of Activity	Risk Number	Risk Code	Risk Name	Number of Accidents for Activity	Ratio of Accidents for Activity	Rate of Accidents for Activity
Excavation	2.26E-07	0.131	2.95E-08	1	R05	Cave-ins	13	0.206	6.09E-09
				2	R01	Fall from height	4	0.063	1.87E-09
				3	R02	Struck by flying/falling object	10	0.159	4.69E-09
				4	R03	Building/Structure collapse	3	0.048	1.41E-09
				5	R04	Contact with electricity	4	0.063	1.87E-09
				6	R07	Struck by a moving vehicle	11	0.175	5.15E-09
				7	R10	Equipment accidents (Roll over etc.)	4	0.063	1.87E-09
				8	R12	Traffic accidents	6	0.095	2.81E-09
				9	R11	Struck by moving part of a vehicle	8	0.127	3.75E-09
Reinforced Concrete	2.26E-07	0.299	6.75E-08	1	R01	Fall from height	90	0.625	4.217E-08
				2	R02	Struck by flying/falling object	20	0.139	9.371E-09
				3	R06	Other	6	0.042	2.811E-09
				4	R03	Building/Structure collapse	13	0.090	6.091E-09
				5	R09	Hazards due to machine and tool usage	1	0.007	4.686E-10
				6	R04	Contact with electricity	4	0.028	1.874E-09
				7	R11	Struck by moving part of a vehicle	8	0.056	3.749E-09
				8	R07	Struck by a moving vehicle	2	0.014	9.371E-10
Masonry	2.26E-07	0.185	4.17E-08	1	R01	Fall from height	49	0.551	2.296E-08
				2	R07	Struck by a moving vehicle	7	0.079	3.280E-09
				3	R02	Struck by flying/falling object	21	0.236	9.840E-09
				4	R06	Other	12	0.135	5.623E-09
Plastering & Painting	2.26E-07	0.226	5.11E-08	1	R01	Fall from height	83	0.761	3.889E-08
				2	R02	Struck by flying/falling object	14	0.128	6.560E-09
				3	R06	Other	6	0.055	2.811E-09
				4	R07	Struck by a moving vehicle	5	0.046	2.343E-09
				5	R09	Hazards due to machine and tool usage	1	0.009	4.686E-10
Roof Works	2.26E-07	0.160	3.61E-08	1	R01	Fall from height	59	0.766	2.765E-08
				2	R02	Struck by flying/falling object	9	0.117	4.217E-09
				3	R06	Other	4	0.052	1.874E-09
				4	R07	Struck by a moving vehicle	5	0.065	2.343E-09

While determining exposure values, the project schedules and planning tables of 20 traditional construction projects in the Istanbul province were examined. These project schedules and planning tables were analyzed in detail with the aid of Primavera P6 and MS Project software [46,47]. After ensuring the accuracy of the data, the exposure values of the five selected activities were determined for 20 construction projects. The exposure values were calculated as follows:

$$E_i = H \times N_i \quad (1)$$

where E_i denotes the exposure of the activity, H represents daily working hours and N_i corresponds to the number of workers involved in that activity. The daily working hours was taken to be nine hours (the same as the daily working hours of the SSI) and the number of workers were taken from the project planning tables. Since exposures were calculated on a daily basis, data regarding the total duration of the work is not required. Table 11 illustrates how the exposure values were calculated.

Table 11. Calculation of exposure for foundation excavation in Project 1

Sub-activity name	Activity type	Risk Code	Risk Name	Accident Rate	Duration of activity (day)	Daily working hour (h)	Number of worker	Exposure
Foundation Excavation	Excavation	R05	Cave-ins	6.09E-09	15	9	8	72
		R01	Fall from height	1.87E-09	15	9	8	72
		R02	Struck by flying/falling object	4.69E-09	15	9	8	72
		R03	Building/Structure collapse	1.41E-09	15	9	8	72
		R04	Contact with electricity	1.87E-09	15	9	8	72
		R07	Struck by a moving vehicle	5.15E-09	15	9	8	72
		R10	Equipment accidents (Roll over etc.)	1.87E-09	15	9	8	72
		R12	Traffic accidents	2.81E-09	15	9	8	72
		R11	Struck by moving part of a vehicle	3.75E-09	15	9	8	72

3.3. Calculating Activity-Based Accident Probabilities

Due to the characteristics of the construction industry, such as the uniqueness of each project, the difficulty to establish time series for accidents and their project-based character (as opposed to process-based), and so on, it is difficult to use the concept of "probability". Since the distribution of occurrences (or accidents) do not fit within probabilistic distributions, in

many safety studies "accident likelihood" was often preferred and used instead of "accident probability" [12,32,33].

On the other hand, the utilization of "likelihood" has some disadvantages. For example, in an activity that has 1,000 man-hours work and accident frequency rate of 0.002 (accident/work-hours), the accident likelihood will be calculated as 2 (accident frequency x exposure). This means that in a 1,000 man-hours of work, 2 occupational accidents will take place. However, occupational accidents are random events, and it would be wrong to give an exact number of accidents for a given activity. Therefore, it is important that the accident occurrence rate of the construction industry is represented as a probability function.

For this study, the Poisson distribution model was used to calculate accident probability. The Poisson distribution is a discrete probability distribution that can be used to calculate the probability of a number of event occurrences for a specific time. In order to utilize the Poisson distribution for a data set, two prerequisites are required [48]:

(1) Events should have a known and constant occurrence rate

(2) Events should be independent

For the construction industry, occupational accidents are independent events. Moreover, the rates of occupational accident occurrences can be calculated using the calculation method proposed in this study. Therefore, the Poisson distribution may be selected as a suitable model for the expression of accident occurrence probabilities.

In the Poisson distribution, the probability of k times the occurrence of an event can be calculated from equation 2:

$$Pr(X = k) = \frac{\lambda^k e^{-\lambda}}{k!} \quad (2)$$

where λ= AR x E (Accident Rate x Exposure), and k: number of accidents. It is possible to determine the probability of the occurrence of an accident 0,1,2,…,n times by using the Poisson distribution. If the same example is used in the likelihood approach (an activity that has 1,000 man-hours of work and where the accident frequency rate is 0.002 accident/work-hours) and is expressed with the Poisson distribution, 0,1,2,…, the n times accident occurrence probability can be calculated as shown in Figure 3.

As shown in Figure 3, the probability of zero accidents is less than 0.15, the probability of 1 or 2 accidents are between 0.25 – 0.3 for an activity that has 1000 man-hours of work. The probability of 3 or 4 accidents in a single construction job is relatively high and cannot be ignored for further analyses. However, the probability of five or more accidents are quite low. Although the accident likelihood was calculated as being 2, the accident probabilities of 0, 1, 2, 3 and 4 accidents were considerably higher for the same example. For this reason, the accident probability as calculated by using the Poisson distribution, offers a broader perspective to implement risk assessments for safety professionals or on-site practitioners.

In the proposed accident probability approach, it was assumed that risk assessment will be performed during the planning stage. This allows a zero accident target to be set during the project duration. Therefore, the probability of having zero accidents was calculated and it

was subtracted from 1 in order to calculate the total probability of accident occurrences (1 - P(X=0)).

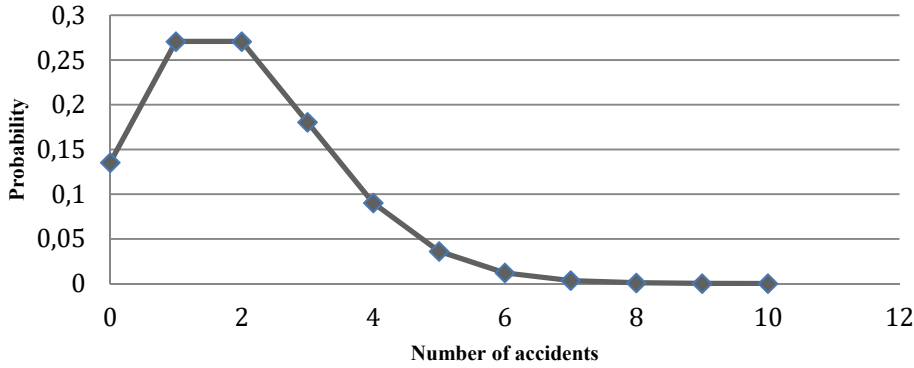

Figure 3. Accident probabilities in the Poisson distribution

Table 12. Accident probability calculation for foundation excavation activity in Project 1

Sub-activity name	Risk code	Risk name	Accident rate	Exposure	Accident Rate x Exposure	Accident probability	Accident probability x 1.000.000
						Σ	**2,13**
Foundation excavation	R05	Cave-ins	6.09E-09	72	4.40E-07	4.00E-07	0.44
	R01	Fall from height	1.87E-09	72	1.30E-07	1.00E-07	0.14
	R02	Struck by flying / falling object	4.69E-09	72	3.40E-07	3.00E-07	0.34
	R03	Building / Structure collapse	1.41E-09	72	1.00E-07	1.00E-07	0.1
	R04	Contact with electricity	1.87E-09	72	1.30E-07	1.00E-07	0.14
	R07	Struck by a moving vehicle	5.15E-09	72	3.70E-07	4.00E-07	0.37
	R10	Equipment roll over accidents	1.87E-09	72	1.30E-07	1.00E-07	0.14
	R12	Traffic Accidents	2.81E-09	72	2.00E-07	2.00E-07	0.2
	R11	Struck by moving part of a vehicle	3.75E-09	72	2.70E-07	3.00E-07	0.27

As an example, the calculation of accident probability of the foundation excavation work of Project 1 is given in Table 12. In Project 1, eight workers were assigned to foundation excavation, and with a 9-hour working day, the exposure value was calculated to be 72 man-hours. Similar calculations were made for the other construction activities and sub-activities. Since the resulting probabilities are relatively small, each probability value was multiplied by 1,000,000 in order for it to be more easily understood. The total accident probability of the foundation excavation of Project 1 was calculated to be 2.125, in other words this figure represents the total probability of all accidents which may occur during foundation excavation work. Similarly, the probabilities of any sub-activities in excavation, reinforced concrete work, masonry, plastering and painting and roof work can be calculated for a traditional construction project (see Table 12). This approach allows an easy way of calculating the total accident probability of a sub-activity (of any construction job) as well as providing a tool to highlight the most hazardous accident that may occur in a given activity.

4. RESULTS

If the flow of the method is similarly followed, probability calculation tables can be prepared and total accident probabilities can be found. As an example, there are eight different sub-work items in Project 1, and their probabilities are given in Table 13. There are 55 sub-activities in Project 1, but within the scope of this paper only the first 8 items are being given as examples. It can be seen that the total accident probability value in the first row (2.13) comes from the probability calculations depicted in Table 12. For all other sub-activities, similar calculations were made and are collected in this table.

Although some sub-activities belong to the same main activity, their probabilities were calculated differently due to their different exposure values (see Table 13). Decision makers and safety experts can use these probability values while preparing lists of project work items according to their significance. Additionally, these calculated probabilities can be used, together with accident severity, in any on-site risk assessment application.

It is also worth mentioning that the accident rates given here can be considered accurate because they were calculated using actual accident data from expert witness reports and SSI statistics. Likewise, the exposure values of the five selected activities were calculated on a daily basis from actual project planning tables using man-hour values. Hence, the probabilities were calculated using accident rates and exposures which are reliable and precise.

Since the calculation tables use man-hour values and a well established work breakdown structure of all construction jobs, the proposed methodology requires a continuous collaboration between planning departments and safety professionals. Information regarding scope changes, usage of free or total floats, changes in schedule or methods of construction should be immediately given to the safety experts. For instance, the assignment of more workers to a construction project to decrease the duration (in other words, a way of "crashing") will result in an increase of exposure. Since exposure is an indispensable parameter for accident probability calculations, such deviations should not alter the probability calculation approach. Using our Poisson distribution approach, accident probabilities are always expressed between 0 and 1 which eliminates the need for scaling, no matter the size of the exposure value.

Table 13. Total accident probability calculations for 8 sub-work items in Project 1

#	Sub-activity name	Activity name	Beginning	Ending	Exposure	Total Accident Probability
1	Foundation excavation	Excavation	8.05.06	24.05.06	72	**2.13**
2	Lean concrete	Reinforcement Concrete	25.05.06	26.05.06	27	1.82
3	Cement coating	Reinforcement Concrete	2.06.06	2.06.06	63	4.26
4	Foundation formwork	Reinforcement Concrete	9.06.06	9.06.06	81	5.47
5	Foundation reinforcement	Reinforcement Concrete	10.06.06	22.06.06	108	7.27
6	Foundation concrete	Reinforcement Concrete	23.06.06	24.06.06	72	4.85
7	Basement shear wall formwork	Reinforcement Concrete	28.06.06	3.07.06	81	5.47
8	Basement shear wall reinforcement	Reinforcement Concrete	4.07.06	8.07.06	90	6.07

The presented probability approach was applied across all sub-activities of the 20 construction projects and reasonable results were obtained in all cases. Thanks to this approach, hazardous sub-work items can be listed from the highest to the lowest accident probability on a daily basis. The primary purpose of this study is to suggest a new and objective approach to estimate the accident probability parameter for risk assessment within the construction industry. Therefore, actual accident values were analyzed several times to determine the most frequent accident types and the most hazardous work-items, as well as a risk analysis of the most hazardous activities and accident concentrations.

Following this, the accident rates for construction work items and certain accident types, such as fall from height; cave-ins and so on were calculated. Similarly, with sufficient past data, the overall probabilities of all sub-work items in a project can be calculated. The combination of a solid and consistent accident probability parameter that includes exposure as well as severity for any approach toward risk assessment will provide reliable risk scores for decision makers, safety professionals and construction managers to plan and manage projects by taking health and safety into account. It is hoped that safety experts, project planners, site engineers and academicians (for further research) can easily use the probability approach developed for this study. As previously mentioned, the majority of former approaches for the assessment of risks on construction sites determined “accident probability” through expert opinion. Calculating the probability of an accident without the need for personal experiences and opinions, in other words calculating it in an objective manner, is an important feature of this approach. In addition, project planners can compare the accident probabilities of different

construction projects at the same time and manage their own resource planning (and/or resource levelling) according to results of these comparisons.

Supplementary to these contributions, it may be argued that, especially for practitioners on-site, using probability scores in advance may allow a greater focus on project scheduling, man-hour figures, amount of resources assigned for construction activities and budget limitations as well as on the workforce. Moreover, thanks to the risk analysis of the most hazardous activities prepared in this study, safety experts do not need to repeatedly analyze the activities with the highest risks for every project. Furthermore, safety professionals who wish to use the presented probability approach will only require the exposure values of their projects, and these figures can be easily adapted for any country that has sufficient past accident data and similar industry characteristics. It is thought that the proposed approach, in general, provides:

- Objective assessment of the past accident data,
- Utilization of man-hour values through the aid of the planning department to reach exposure values,
- Guidance on how to use real project schedules for risk estimation for safety professionals.

5. CONCLUSION

In this study 623 expert witness reports for accidents that occurred between 2000 and 2013 were analyzed in detail. Similarly, occupational accident statistics by the SSI were analyzed and accident concentrations for excavation, reinforced concrete work, masonry, plastering and painting and roof work were provided, and the most frequent accident types for these activities were obtained. Since, all data was obtained from real cases, this study accurately represents the accident rates and applicable probability values. Because the activities under examination are used in various construction works, the probability approach presented in this research study can be used for other construction projects. Accident probabilities were calculated using the Poisson distribution, and by adapting the accident probability values to risk assessment methods it is possible to provide more objective and realistic risk assessments.

In this study, the data which was used as a starting point to analyze accidents in the construction industry were taken from official statistics as well as expert witness reports submitted to the Turkish criminal and labor courts. Other countries can also use these accident rates in their own risk assessments or adapt the presented method to their countries' construction industry.

Acknowledgement

This work is supported by the Coordination of Scientific Research Projects of Istanbul Technical University (BAP-ITU) under the project no. 38168.

References

[1] Zou, P., X.,W., Sunindijo, R., Y., 2013. Skills for managing safety risk, implementing safety task, and developing positive safety climate in construction project. Automation in Construction, 34, 92-100.

[2] CFOI. Census of Fatal Occupational Injuries Report, 2013.<http://www.bls.gov/iif/oshcfoi1.htm> (retrieved 12.05.14).

[3] Loosemore, M., Andonakis, N., 2007. Barriers to implementing OHS reforms – the experience of small subcontractors in the Australian construction industry. International Journal of Project Management 25, 579–588.

[4] Yi, J.-s., Kim Y.-w., Kim K.-a., Koo B. 2012. A suggested color scheme for reducing perception-related accidents on construction work sites. Accident Analysis and Prevention, 48, 185-192.

[5] ILO. International Labour Organization, Statistics and Database, LABORSTA, Occupational Injuries. <http://www.ilo.org/ilostat/faces/home/statisticaldata/data_by_subject?_adf.ctrl-state=vchypfgka_4&_afrLoop=598083992046714> (retrieved 06.04.2014)

[6] SSI. Social Security Institution Occupational Accidents Statistics Report, 2012. 10.12.2013. Retrieved from http://www.isteguvenlik.tc/SGK2012IsKazaIstatistik.pdf (in Turkish).

[7] Gurcanli E., Bilir S., Sevim M., 2015. Activity Based Risk Assessment And Safety Cost Estimation For Residential Building Construction Projects. Safety Science, 2015, 80, 1–12, DOI: 10.1016/j.ssci.2015.07.002.

[8] Gurcanli G.E., Mungen U., 2013. Analysis of construction accidents in turkey and responsible parties. National Industrial Health, 51 (6), 581-595.

[9] Baradan, S., and Usmen, M. A. 2006. Comparative injury and fatality risk analysis of building trades. J. Constr. Eng. Manage., 132(5), 533–539.

[10] Gnoni, M. G., Saleh, J. H., 2017. Near-miss management systems and observability-in-depth: Handling safety incidents and accident precursors in light of safety principles. Safety Science, 91, 154-167.

[11] Gangolells, M., Casals, M., Forcada, N., Roca, X. and Fuertes, A. 2010. Mitigating construction safety risks using prevention through design. Journal of Safety Research, Vol. 41, 107-122.

[12] Gurcanli G.E., Mungen U., 2009. An occupational safety risk analysis method at construction sites using fuzzy sets. International J. of Industrial Ergonomics 39(2), 371-387.

[13] Hallowell, M. 2011. Risk-Based Framework for Safety Investment in Construction Organizations. J. Constr. Eng. Manage., 137(8), 592–599.

[14] Irumba R., 2014. Spatial analysis of construction accidents in Kampala, Uganda. Safety Science. 64. 109-120.

[15] Park, C. S., Kim, H. J., 2012. A framework for construction safety management and visualization system. Automation in Construction 33, 95–103.

[16] Raviv, R., Fishbain, B., Shapira, A., 2017a. Analyzing risk factors in crane-related near-miss and accident reports. Safety Science, 91, 192-205.

[17] Raviv, R., Fishbain, B., Shapira, A., 2017b. AHP-based analysis of the risk potential of safety incidents: Case study of cranes in the construction industry. Safety Science, 91, 298-309.

[18] Zhang, S., Sulankivi, K., Kiviniemi, M., Romo, I., Eastman, C. M., Teizer, J., 2015. BIM-based fall hazard identification and prevention in construction safety planning. Safety Science, 72, 31-45.

[19] Zwetsloot, G.I.H.M., Kines, P., Wybo, J.L., Ruotsala, R., Drupsteen, L., Bezemer, R. A., 2017. Zero Accident Vision based strategies in organisations: Innovative perspectives. Safety Science, 91, 260-268.

[20] Tozer, K , Celik, T , Gurcanli, G . (2018). Classification of Construction Accidents in Northern Cyprus. Teknik Dergi, 29 (2), 8295-8316. DOI: 10.18400/tekderg.325546

[21] Baradan, S , Akboga, O , Cetinkaya, U , Usmen, M . (2016). Ege Bölgesindeki İnşaat İş Kazalarının Sıklık ve Çapraz Tablolama Analizleri. Teknik Dergi, 27 (1), 7345-7370.

[22] Van Nunen, K., Reniers, G., Ponnet, K., Cozzani, V., 2016. Major accident prevention decision-making: A large-scale survey-based analysis. Safety Science, 88, 242-250.

[23] Jocelyn, S., Chinniah, Y., Ouali, M., S., 2016. Contribution of dynamic experience feedback to the quantitative estimation of risks for preventing accidents: A proposed methodology for machinery safety. Safety Science, 88, 64-75.

[24] Wang, Y., Weidmann, U., A., Wang, W., 2017. Using catastrophe theory to describe railway system safety and discuss system risk concept. Safety Science, 91, 269-285.

[25] Brauer, R. L. 1994. Risk management and assessment. Safety and health for engineers, Van Nostrand Reinhold, New York, 543–572.

[26] Lee, S., and Halpin, D. 2003. Predictive tool for estimating accident risk. J. Constr. Eng. Manage., 129(4), 431–436.

[27] Jannadi, O., and Almishari, S. 2003. Risk assessment in construction. J. Constr. Eng. Manage., 129(5), 492–500.

[28] Hallowell, M. and Gambatese, J. 2009. Activity-Based Safety Risk Quantification for Concrete Formwork Construction. J. Constr. Eng. Manage., 135(10), 990–998.

[29] Sun, Y., Fang, D., Wang, S., Dai, M., and Lv, X. 2008. Safety risk identification and assessment for Beijing Olympic venues construction."J. Manage. Eng., 24(1), 40–47.

[30] Mitropoulos, P., Namboodiri M., 2011. New method for measuring the safety risk of construction activities: task demand assessment. J. of Constr. Eng and Manage., 137(1), 30-38.

[31] BLS. Bureau of Labor Statistics. 2013. <http://www.bls.gov/iif/#data> (retrieved 25.06.13).

[32] Casanovas, M. M., Armengou,J., Ramos, G. 2014. Occupational risk ındex for assessment of risk in construction work by activity. Journal of Construction Engineering and Management,Vol. 140, pp.04013035-1-04013035-9.

[33] Woodruff, J. M. 2005. Consequence and likelihood in risk estimation: A matter of balance in UK health and safety risk assessment practice. Safety Science, 43(5), 345-353.

[34] Birgönül, M. T., & Dikmen, İ. (1996). İnşaat projelerinin risk yönetimi. İMO teknik Dergi, 7(4), 1305-1326.

[35] Erginel, N., & TOPTANCI, Ş. (2017). Is Kazası Verilerinin Olasılık Dağılımları İle Modellenmesi. Mühendislik Bilimleri ve Tasarım Dergisi, 5(SI), 201-212.

[36] Bilir, S. (2015). An Activity Based Occupational Safety Risk Assessment Method Integated to The Project Schedule In Construction Projects. (Doctoral dissertation, Institude of Science and Technology).

[37] Bilir, S., & Gurcanli, G. E. (2016). A Method to Calculate the Accident Probabilities in Construction Industry Using a Poisson Distribution Model. In Advances in Safety Management and Human Factors (pp. 513-523). Springer, Cham.

[38] OSHA. 1971/97. Recording and reporting occupational injuries and illness. Regulations, Part 1904, Occupational Safety and Health Administration, U.S. Departmant of Labor, Washington, D.C.

[39] ILO. 1998. Meeting of Experts on Labour Statistics. Report MELSOI/1998/1, Geneva. Ingstad, O. and Bodsberg, L., 1989. CRIOP: A Scenario - Method for Evaluation of the Offshore Control Centre. SINTEF, Report No. STF75 A89028, Trondheim.

[40] Zhang, S., Teizer, J., Lee, J. K., Eastman, C. M., Venugopal, M., 2013. Building information modelling (BIM) and safety: automatic safety checking of construction models and schedules. Automation in Construction, 29,183-195.

[41] Borsos, A, Cafiso, S., D'Agostino, C., Miletics, D., 2016. Comparison of Italian and Hungarian black spot ranking. Transportation Research Procedia, 14, 2148 – 2157.

[42] Cafisoa, S.,Di Silvestroa, G., Di Guardoa, G., 2012. Application of Highway Safety Manual to Italian divided multilane highways. Procedia - Social and Behavioral Sciences 53, 911 – 920.

[43] Van Geelen, H., Volckaert, A., Sarrazin, R., Janssens, I., 2016. Evolutionary approach of accident concentration zones. Transportation Research Procedia, 14, 3332 – 3341.

[44] Fine, W. T., & Kinney, W. D. 1971. Mathematical evaluation for controlling hazards. Journal of Safety Research, 3(4), 157−166.

[45] Primavera P6 Software, 2013. <http://www.oracle.com/us/products/applications/primavera/p6-professional-project-management/overview/index.html> (retrieved 04.02.13).

[46] MS Project, 2013. <https://products.office.com/en/project/project-and-portfolio-management-software> (retrieved 07.01.13).

[47] Kjellen, U., Preventation of accidents through experience feedback. London.GBR: CRC Press, 2000.

[48] Statistics – The Poisson Distribution. 02.07.2015. Retrieved from <https://www.umass.edu/wsp/resources/poisson/>

TEKNİK DERGİ MANUSCRIPT DRAFTING RULES

1. The whole manuscript (text, charts, equations, drawings etc.) should be arranged in Word and submitted in ready to print format. The article should be typed on A4 (210 x 297 mm) size paper using 10 pt (main title 15 pt) Times New Roman font, single spacing. Margins should be 40 mm on the left and right sides and 52.5 mm at the top and bottom of the page.
2. Including drawings and tables, articles should not exceed 25 pages, technical notes 6 pages.
3. The manuscript, along with a hardcopy, must be electronically sent (CD or e-mail attachment).
4. The text must be written in a clear and understandable language, conform to the grammar rules. Third singular person and passive tense must be used, and no inverted sentences should be contained.
5. Title must be short (10 words maximum) and clear, and reflect the content of the paper.
6. Sections should be arranged as: (i) abstract and keywords, (ii) title, abstract and keywords in the other language, (iii) main text, (iv) symbols, (v) acknowledgements (if required) and (vi) references.
7. Both abstracts should briefly describe the object, scope, method and conclusions of the work and should not exceed 100 words. If necessary, abstracts may be re-written without consulting the author. At least three keywords must be given. Titles, abstracts and keywords must be fitted in the first page leaving ten line space at the bottom of the first page and the main text must start in the second page.
8. Section and sub-section titles must be numbered complying with the standard TS1212.
9. Symbols must conform to the international rules; each symbol must be defined where it appears first, additionally, a list of symbols must be given in alphabetic order (first Latin, then Greek alphabets) at the end of the text (before References).
10. Equations must be numbered and these numbers must be shown in brackets at the end of the line.
11. Tables, drawings and photographs must be placed inside the text, each one should have a number and title and titles should be written above the tables and below the drawings and photographs.
12. Only SI units must be used in the manuscripts.
13. Quotes must be given in inverted commas and the source must be indicated with a reference number.
14. Acknowledgement must be short and mention the people/ institutions contributed or assisted the study.
15. References must be numbered (in brackets) in the text referring to the reference list arranged in the order of appearance in the text. References must include the following information:

    If the reference is an article: Author's surname, his/her initials, other authors, full title of the article, name of the journal, volume, issue, starting and ending pages, year of publication.

    Example : Naghdi, P. M., Kalnins, A., On Vibrations of Elastic Spherical Shells. J. Appl. Mech., 29, 65-72, 1962.

    If the reference is a book: Author's surname, his/her initials, other authors, title of the book, volume number, editor if available, place of publication, year of publication.

    Example : Kraus. H., Thin Elastic Shells, New York. Wiley, 1967.

    If the reference is a conference paper: Author's surname, his/her initials, other authors, title of the paper, title of the conference, location and year.

    If the source is a thesis: Author's surname, his/her initials, thesis title, level, university, year.

    If the source is a report: Author's surname, his/her initials, other authors, title of the report, type, number, institution it is submitted to, publication place, year.
16. Discussions to an article published in Teknik Dergi should not exceed two pages, must briefly express the addressed points, must criticize the content, not the author and must be written in a polite language. Authors' closing remarks must also follow the above rules.
17. A separate note should accompany the manuscript. The note should include, (i) authors' names, business and home addresses and phone numbers, (ii) brief resumes of the authors and (iii) a statement "I declare in honesty that this article is the product of a genuinely original study and that a similar version of the article has not been previously published anywhere else" signed by all authors.

CONTENTS

ISSN: 1300-3453